SHARPNESS-AWARE MACHINE UNLEARNING

Haoran Tang
Department of Computer Science
Purdue University
thr@purdue.edu

Rajiv Khanna
Department of Computer Science
Purdue University
rajivak@purdue.edu

ABSTRACT

We characterize the effectiveness of Sharpness-aware minimization (SAM) under machine unlearning scheme, where unlearning forget signals interferes with learning retain signals. While previous work prove that SAM improves generalization with noise memorization prevention, we show that SAM abandons such denoising property when fitting the forget set, leading to altered generalization depending on signal strength. We further characterize the signal surplus of SAM in the order of signal strength, which enables learning from less retain signals to maintain model performance and putting more weight on unlearning the forget set. Empirical studies show that SAM outperforms SGD with relaxed requirement for retain signals and can enhance various unlearning methods either as pretrain or unlearn algorithm. Motivated by our refined characterization of SAM unlearning and observing that overfitting can benefit more stringent sample-specific unlearning, we propose Sharp MinMax, which splits the model into two to learn retain signals with SAM and unlearn forget signals with sharpness maximization, achieving best performance. Extensive experiments show that SAM enhances unlearning across varying difficulties measured by memorization, yielding decreased feature entanglement between retain and forget sets, stronger resistance to membership inference attacks, and a flatter loss landscape. Our observations generalize to more noised data, different optimizers, and different architectures.

1 INTRODUCTION

Deep neural networks have grown so large and complex that retraining a model from scratch to forget even a few samples has become impractically costly in both computation and energy. This challenge has catalyzed the study of machine unlearning: methods that efficiently remove the influence of specific training data without full retraining, aiming to forget designated examples while preserving overall performance. Numerous unlearning strategies have been explored – from influence-based updates that subtract a data point's contribution (Izzo et al., 2021), to fine-tuning with targeted weight sparsification (Jia et al., 2023), to joint optimization approaches that explicitly balance "retain" vs. "forget" objectives by gradient ascent/descent on different data subsets (Kurmanji et al., 2023). However, a fundamental understanding of what makes unlearning effective remains elusive. Key questions persist: How should we trade off forgetting unwanted data versus retaining accuracy on the rest? How do different training algorithms influence unlearning dynamics? Why are some samples inherently harder to forget than others? In practice, the lack of principled answers has led to ad-hoc hyperparameter tuning and unpredictable behavior across tasks. In particular, when a model is simultaneously fed with conflicting retain and forget signals, these signals can interfere and even cancel out during training, hampering the unlearning process (Kurmanji et al., 2023). To date, there are few robust solutions to mitigate this interference, underscoring the need for a deeper theoretical foundation for machine unlearning.

Recent advances in learning theory and optimization hint at possible directions to tackle these issues. First, a signal-versus-noise perspective has provided new insight into model behavior: for example, Chen et al. (2023) formalize how networks learn meaningful patterns while ignoring or memorizing label noise, and Zhao et al. (2024) empirically identify factors that make certain data points harder to forget. Particularly relevant is the Sharpness-Aware Minimization (SAM) method (Foret et al., 2020) that has been shown to seek flatter loss minima and thereby dramatically reduce memorization of noisy data, leading to improved generalization in noisy-label settings (Chen et al., 2023).

These observations suggest that a model's ability to distinguish true signal from noise may be key to effective unlearning. An optimizer that naturally suppresses memorization of noise might also be better suited for forgetting specific examples when required. To investigate this hypothesis, we quantify each sample's memorization level using established metrics (Feldman, 2020; Feldman & Zhang, 2020), allowing us to rank the "forget set" by difficulty. This enables a controlled study of how different optimization algorithms perform when asked to forget data that the model has learned to varying extents.

We present a comprehensive theoretical and empirical study of machine unlearning through the combined lens of signal-noise decomposition and sharpness-aware optimization. We focus on the challenging scenario where both retain and forget samples are present in each training batch with mixed objectives, and we compare standard Stochastic Gradient Descent (SGD) to SAM in this context. Building on recent theoretical frameworks for ReLU networks (Kou et al., 2023), we derive rigorous results for a two-layer CNN that characterize the unlearning process under each optimizer. Our analysis yields several striking findings. (1) SAM's noise suppression can break down under unlearning: we prove that when tasked with intentionally forgetting a set of samples (treated as "noise"), SAM is forced by objective to abandon its usual denoising behavior – effectively overfitting to the forget set nearly as much as SGD does. This result challenges the expectation that flatter-minima methods would inherently excel at unlearning. (2) We establish formal guidelines for balancing retain vs. forget objectives: in particular, we derive the minimum retain-weighting factor α needed to prevent catastrophic forgetting of the kept data. Our theory shows that SAM can accomplish successful unlearning with a significantly smaller retain weight α than SGD, meaning SAM tolerates a stronger forgetting signal without sacrificing retained accuracy. In the regime of benign overfitting (where the model fits even noisy data without large generalization error), we quantify the gap in required α between SAM and SGD and prove it scales on the order of $O(\sqrt{d/n})$ (with d the model dimension and n the training set size). (3) Perhaps most surprisingly, our findings call for a re-examination of overfitting in unlearning. Contrary to conventional wisdom, we show that deliberate overfitting – in a controlled way that limits its impact on the rest of the data – can enhance the complete removal of those samples. This insight is especially relevant in stringent privacy or copyright scenarios, suggesting that the strict avoidance of overfitting may not always be optimal.

Our contributions can be summarized as follows:

Theoretical Framework: We introduce a rigorous analytical framework for machine unlearning based on signal-noise decomposition. This framework explicitly models the interplay between retain and forget signals. Using this lens, we analyze the behaviors of SGD versus SAM and prove that SAM's denoising advantage "shuts off" on forget data: when SAM is asked to unlearn labeled noise, it ends up overfitting to the forget set almost as much as SGD.

Balancing Retain vs. Forget Objectives: We derive provable guidelines for balancing the retain/forget trade-off. In particular, we identify the minimal value of the weighting ratio parameter α that guarantees sufficient retention of knowledge. We show that SAM requires a strictly smaller α than SGD to achieve effective unlearning. In the regime of benign overfitting for both the optimizers, we analytically bound the difference in required α on the order of $O(\sqrt{d/n})$.

Empirical Validation: Through extensive experiments on CIFAR-100 and ImageNet datasets, we validate our theoretical insights. We demonstrate that incorporating SAM into state-of-the-art unlearning methods consistently boosts forgetting efficacy while better preserving accuracy on the remaining data. Models optimized with SAM yield flatter loss landscapes and reduced entanglement between retained and forgotten samples, corroborating our theory that SAM distinguishes signal from noise better. We also observe that SAM-trained models are less vulnerable to membership inference attacks to forget set, indicating improved unlearning.

Novel Unlearning Algorithm: Finally, inspired by our analysis, we propose Sharp MinMax, a new unlearning approach that decouples the retain and forget objectives. Sharp MinMax splits the model into two cooperative parts: one is trained with SAM on the retained data, while the other performs sharpness maximization on the forget data to intentionally overfit those samples to ensure forgottenness. This design mitigates interference between retain and forget signals. Sharp MinMax achieves state-of-the-art unlearning performance in our experiments, especially on challenging high-memorization forget sets, where it significantly outperforms existing techniques in completely erasing the target data's influence.

2 PRELIMINARIES

2.1 DATA AND MODEL CONSTRUCTION

We construct a practical learning scenario which distinguishes between useful and unrelated signals from inputs. Similar constructions have been adopted in previous work (Kou et al., 2023; Chen et al., 2023) with rich notation. For convenience, we summarize a table of notation in App. C. Consider learning binary classification with label $y \in \{\pm 1\}$ using a two-layer CNN on image training data set $\mathcal{S} = \{(\mathbf{x}_i, y_i)\}_{i\in[n]} \sim \mathcal{D}$. Each image consists of P patches and assign randomly one of them as the signal $y_i\boldsymbol{\varphi}$ for label y_i and the universal signal vector $\boldsymbol{\varphi} \in \mathbb{R}^d$, and represent other patches by the noise vector $\boldsymbol{\xi}_i \in \mathbb{R}^d \sim \mathcal{N}(\mathbf{0}, \sigma_p^2\mathbf{I})$. Thus, each input image is vectorized as $\mathbf{x}_i = [\boldsymbol{\xi}_i, ..., y_i\boldsymbol{\varphi}, ..., \boldsymbol{\xi}_i] \in \mathbb{R}^{P\times d}$, where $y_i\boldsymbol{\varphi}$ can appear at any position.

The second layer of CNN is fixed as $\pm 1/m$ respectively for m convolutional filters. The two-classes network can be expressed as $f(\mathbf{W}, \mathbf{x}) = f_{+1}(\mathbf{W}_{+1}, \mathbf{x}) - f_{-1}(\mathbf{W}_{-1}, \mathbf{x})$, where

$$f_j(\mathbf{W}_j, \mathbf{x}) = \frac{1}{m}\sum_{r=1}^{m}\sum_{p=1}^{P}\sigma(\langle \mathbf{w}_{j,r}, \mathbf{x}\rangle) = \frac{1}{m}\sum_{r=1}^{m}\sigma(\langle \mathbf{w}_{j,r}, y\boldsymbol{\varphi}\rangle) + (P-1)\sigma(\langle \mathbf{w}_{j,r}, \boldsymbol{\xi}\rangle). \quad (1)$$

Here σ denotes ReLU activation, $\mathbf{w}_{j,r} \in \mathbb{R}^d$ denotes the weight for the r-th filter, and $\mathbf{W}_j$ is the collection of model weights for $j = \pm 1$. We train this CNN with cross-entropy loss $\mathcal{L}(\mathbf{W}, \mathcal{S})$. Denote $\mathbf{w}_{j,r}^{(t,b)}$ for $j \in \{\pm 1\}, r \in [m]$ the convolutional filter at the b-batch of t-th epoch of SGD. We decompose the weight update into learning signal and noise coefficients $\kappa_{j,r}^{(t,b)}, \zeta_{j,r,i}^{(t,b)}$ for learning the signal and the noise respectively, such that

$$\mathbf{w}_{j,r}^{(t,b)} = \mathbf{w}_{j,r}^{(0,0)} + j\cdot\kappa_{j,r}^{(t,b)}\cdot\boldsymbol{\varphi}\|\boldsymbol{\varphi}\|_2^{-2} + (P-1)^{-1}\sum_{i=1}^{n}\zeta_{j,r,i}^{(t,b)}\cdot\boldsymbol{\xi}_i\|\boldsymbol{\xi}_i\|_2^{-2}, \quad (2)$$

where the learning goal is to increase $\kappa_{j,r}^{(t,b)}$ and decrease $\zeta_{j,r,i}^{(t,b)}$. This construction also extends to multiclass classification considering one vs. all setting with K binary classification problems. For readability, we abbreviate subscript j, r and replace superscript (t, b) with time vector $\mathbf{t}$ in following sections, and leave full notation to proofs in the Appendix.

2.2 SIGNAL-TO-NOISE UNLEARNING

Given a pretrained model $f_{\mathcal{A}}^{T_1}$ by algorithm $\mathcal{A}$ for T_1 epochs on $\mathcal{S}$, machine unlearning aims to eliminate the influence of forget set $\mathcal{F} \subseteq \mathcal{S}$ to the model training, while maintain generalizability to unseen data without compromising performance on the remaining retain set $\mathcal{R} = \mathcal{S} \setminus \mathcal{F}$. Denote the unlearned model as $f_{\mathcal{U}}^{T_2}$ by unlearning algorithm $\mathcal{U}$, which is initialized as $f_{\mathcal{A}}^{T_1}$ and unlearned for T_2 epochs. We consider unlearning a small portion of $\mathcal{S}$ with much less expense than retraining the model from scratch on $\mathcal{R}$, so $|\mathcal{F}| < |\mathcal{R}|$ and $T_2 < T_1$.

Random Label (RL) (Graves et al., 2021) aims to unlearn by finetuning on $\mathcal{S}$ but with $\mathcal{F}$'s labels randomly flipped in each epoch. It naturally fits into our setup as label-flipped $\mathcal{F}$ become the noise, and motivates us to investigate unlearning algorithms under the same theoretical framework. The gradient update of $\kappa^{\mathbf{t}}$ and $\zeta_i^{\mathbf{t}}$ of class j can be expressed as

$$\begin{aligned}\kappa^{\mathbf{t}+\mathbf{1}} &= \kappa^{\mathbf{t}} - \frac{\eta\|\boldsymbol{\varphi}\|_2^2}{Bm}\left[\sum_{i\in\mathcal{I}_{\mathbf{t}}^{\mathcal{R}}}\ell_i'^{\mathbf{t}}\sigma'(\langle \mathbf{w}^{\mathbf{t}}, \widehat{y}_i\boldsymbol{\varphi}\rangle) - \sum_{i\in\mathcal{I}_{\mathbf{t}}^{\mathcal{F}}}\ell_i'^{\mathbf{t}}\sigma'(\langle \mathbf{w}^{\mathbf{t}}, \widehat{y}_i\boldsymbol{\varphi}\rangle)\right], \\ \zeta_i^{\mathbf{t}+\mathbf{1}} &= \zeta_i^{\mathbf{t}} - \frac{\eta(P-1)^2\|\boldsymbol{\xi}_i\|_2^2}{Bm}\cdot\ell_i'^{\mathbf{t}}\sigma'(\langle \mathbf{w}^{\mathbf{t}}, \boldsymbol{\xi}_i\rangle)\cdot\mathrm{sgn}(y_i = j),\end{aligned} \quad (3)$$

where B, η denote the batch size and learning rate, $\mathrm{sgn}(\cdot)$ denotes ± 1 sign function, $\mathcal{I}_{\mathbf{t}}^{\mathcal{R}}$ and $\mathcal{I}_{\mathbf{t}}^{\mathcal{F}}$ denote batch samples from $\mathcal{R}$ and $\mathcal{F}$ at $\mathbf{t}$, respectively. In each iteration, $\mathcal{I}_{\mathbf{t}}^{\mathcal{F}}$ aims to erase its signal in $\kappa^{\mathbf{t}}$, while $\boldsymbol{\xi}_i$ reinforces or decreases $\zeta_i^{\mathbf{t}}$ update depending on label agreement.

Negative Gradient (NegGrad) (Kurmanji et al., 2023) unlearns $\mathcal{F}$ using gradient ascent while gradient-descending on $\mathcal{R}$. Unlike RL or other $\mathcal{U}$ that aim at random guessing, ascent-based unlearning encourages misclassification by its objective:

$$\mathcal{L}_{\text{NegGrad}}(\mathbf{W}, \mathcal{R}, \mathcal{F}) = \frac{1}{|\mathcal{R}|}\sum_{i\in\mathcal{R}}\alpha\ell\left(y_i f\left(\mathbf{W}, \mathbf{x}_i\right)\right) - \frac{1}{|\mathcal{F}|}\sum_{i\in\mathcal{F}}(1-\alpha)\ell\left(y_i f\left(\mathbf{W}, \mathbf{x}_i\right)\right). \quad (4)$$

Minimizing $\mathcal{L}_{\text{NegGrad}}$ induces competing gradients, canceling each other during κ, ζ update. α serves as a weight coefficient that accounts for the size imbalance between $\mathcal{R}$ and $\mathcal{F}$. To synchronously optimize the model with retain and forget samples, we draw B samples from both subsets each batch and train for $|\mathcal{R}|/B$ batches. Thus, forget samples' signals are relatively enlarged by a fraction of $|\mathcal{R}|/|\mathcal{F}|$ due to repetition. Heuristically, $\alpha \propto |\mathcal{R}|/(|\mathcal{F}| + |\mathcal{R}|)$.

2.3 Denoising Property of SAM

Sharpness-Aware Minimization (SAM) (Foret et al., 2020) aims to minimize a perturbed empirical loss at the worst point in the neighborhood of $\mathbf{W}$, solving the following optimization problem:

$$\min_{\mathbf{W}} \mathcal{L}(\mathbf{W}, \mathcal{S}) + \left[\max_{\widehat{\epsilon}} \mathcal{L}(\mathbf{W} + \widehat{\boldsymbol{\epsilon}}, \mathcal{S}) - \mathcal{L}(\mathbf{W}, \mathcal{S}) \right], \tag{5}$$

for a controlled perturbation $\widehat{\boldsymbol{\epsilon}}$. It ensures a uniformly low training loss and avoids sharp landscape. While both SGD and SAM learn a sufficient signal with $\kappa^{T_1} = \Omega(1)$ after T_1 epochs, Chen et al. (2023) prove that SAM outperforms SGD by noise suppression and SAM upper bounds $\zeta_i^{T_1}$ by $O(1)$ while SGD is dimension dependent $O(\log d)$. The key difference stems from the noise memorization prevention of SAM. Given the perturbation term $\widehat{\boldsymbol{\epsilon}}^{\mathbf{t}}$ in SAM for class j:

$$\widehat{\boldsymbol{\epsilon}}^{\mathbf{t}} = \frac{\tau}{m} \sum_{i \in \mathcal{I}_{\mathbf{t}}} \sum_{p \in [P]} \ell_i'^{\mathbf{t}} j \cdot y_i \sigma'(\langle \mathbf{w}^{\mathbf{t}}, \mathbf{x}_{i,p} \rangle) \mathbf{x}_{i,p} \cdot \left\| \nabla_{\mathbf{W}} \mathcal{L}(\mathbf{W}^{\mathbf{t}}, \mathcal{I}_{\mathbf{t}}) \right\|_F^{-1}, \tag{6}$$

consider ReLU activation at any fixed iterate $\mathbf{w}^{\mathbf{t}}$ for SGD: $\langle \mathbf{w}^{\mathbf{t}}, \boldsymbol{\xi}_k \rangle \geq 0$ vs. SAM:$\langle \mathbf{w}^{\mathbf{t}} + \widehat{\boldsymbol{\epsilon}}^{\mathbf{t}}, \boldsymbol{\xi}_k \rangle$ for $k \in \mathcal{I}_{\mathbf{t}}, j = y_k$. SAM's $\langle \mathbf{w}^{\mathbf{t}} + \widehat{\boldsymbol{\epsilon}}^{\mathbf{t}}, \boldsymbol{\xi}_k \rangle$ expands to $\langle \mathbf{w}^{\mathbf{t}}, \boldsymbol{\xi}_k \rangle + \langle \widehat{\boldsymbol{\epsilon}}^{\mathbf{t}}, \boldsymbol{\xi}_k \rangle$, where $\langle \widehat{\boldsymbol{\epsilon}}^{\mathbf{t}}, \boldsymbol{\xi}_k \rangle$ is proven to be sufficiently negative to cancel $\langle \mathbf{w}^{\mathbf{t}}, \boldsymbol{\xi}_k \rangle$ by selecting a proper τ, thus deactivating the noise (Chen et al., 2023). This effectively prevents SAM from learning from the noise which would lead to harmful overfitting for SGD. We are curious about whether SAM improves unlearning: a flatter landscape can make learning easier, then it should make unlearning easier too despite a reverse sign. But is it a simple adaptation, and can we straightforwardly extend previous theories and findings to develop unlearning algorithms?

3 Sharpness-Aware Unlearning

We first show that the SAM's noise memorization prevention in Sec. 2.3 does not fully hold when SAM is used with NegGrad for gradient ascent on $\mathcal{F}$. Specifically, SAM overfits to forget signals as much as SGD, while maintaining its denoising property on $\mathcal{R}$. Based on this result, we derive refined test error bounds for SGD and SAM under NegGrad and characterize the different α thresholding between SGD and SAM for unlearning. Although SAM continues to improve unlearning and maintain generalizability, the altered activation patterns and unlearning behaviors are not captured by previous works, as SAM is forced to fit forget signals (viewed as noise) by NegGrad objective. This leads to divergent behaviors on $\mathcal{R}$ and $\mathcal{F}$, which can be of independent interest.

3.1 NegGrad Revisited

Unlike RL, the mutual interference between $\mathcal{F}$ and $\mathcal{R}$ under NegGrad additionally affects ζ update. The update rules for $\kappa^{\mathbf{t}}$ and $\zeta^{\mathbf{t}}$ under NegGrad now become:

$$\begin{aligned} \kappa^{\mathbf{t}+\mathbf{1}} &= \kappa^{\mathbf{t}} - \frac{\eta \|\boldsymbol{\varphi}\|_2^2}{Bm} \left[\alpha \sum_{i \in \mathcal{I}_{\mathbf{t}}^{\mathcal{R}}} \nabla_{\boldsymbol{\varphi}_i} - (1-\alpha) \sum_{i \in \mathcal{I}_{\mathbf{t}}^{\mathcal{F}}} \nabla_{\boldsymbol{\varphi}_i} \right], \\ \zeta^{\mathbf{t}+\mathbf{1}} &= \zeta^{\mathbf{t}} - \frac{\eta (P-1)^2}{Bm} \left[\alpha \sum_{i \in \mathcal{I}_{\mathbf{t}}^{\mathcal{R}}} \nabla_{\boldsymbol{\xi}_i} - (1-\alpha) \sum_{i \in \mathcal{I}_{\mathbf{t}}^{\mathcal{F}}} \nabla_{\boldsymbol{\xi}_i} \right], \end{aligned} \tag{7}$$

where $\nabla_{\boldsymbol{\varphi}_i} = \ell_i'^{\mathbf{t}} \sigma'(\langle \mathbf{w}^{\mathbf{t}} + \delta, y_i \boldsymbol{\varphi} \rangle)$, $\nabla_{\boldsymbol{\xi}_i} = \text{sgn}(y_i = j) \|\boldsymbol{\xi}_i\|_2^2 \ell_i'^{\mathbf{t}} \sigma'(\langle \mathbf{w}^{\mathbf{t}} + \delta, \boldsymbol{\xi}_i \rangle)$, and $\delta = \widehat{\boldsymbol{\epsilon}}^{\mathbf{t}}$ for SAM and 0 for SGD. In plain words, a retain sample of class j causes a decrease in ζ_j, discouraging memorizing noise for the correct class, while another retain sample of class $-j$ causes an increase in ζ_j, encouraging w_j to use $\boldsymbol{\xi}_i$ to distinguish class j from $-j$. Conversely, a sample $i \in \mathcal{F}$ of class j, which we want to predict $-j$ in ascent-based unlearning, will increase ζ_j and encourage w_j to use noise $\boldsymbol{\xi}_i$ in a way that harms class j, and vice versa. Similar intuition also applies to κ. The interference in ζ update will alter SAM's behaviors towards forget signals as summarized in Lemma 3.1.

Lemma 3.1 *(Noise memorization of $\mathcal{F}$ by SAM under NegGrad). Under the NegGrad scheme and the Assumption D.1 holds, for class j we have that if for SGD: $\langle \mathbf{w}^{\mathbf{t}}, \boldsymbol{\xi}_k \rangle \geq 0, k \in \mathcal{I}_{\mathbf{t}}^{\mathcal{R}}$ and $j = y_k$, then for SAM: $\langle \mathbf{w}^{\mathbf{t}} + \widehat{\boldsymbol{\epsilon}}^{\mathbf{t}}, \boldsymbol{\xi}_k \rangle < 0$. However, if for SGD: $\langle \mathbf{w}^{\mathbf{t}}, \boldsymbol{\xi}_k \rangle \geq 0, k \in \mathcal{I}_{\mathbf{t}}^{\mathcal{F}}$ and $j = y_k$, then for SAM: $\langle \mathbf{w}^{\mathbf{t}} + \widehat{\boldsymbol{\epsilon}}^{\mathbf{t}}, \boldsymbol{\xi}_k \rangle > 0$.*

See proof in App. D.2. Because the activation patterns on $\mathcal{I}_{\mathbf{t}}^{\mathcal{R}}$ and $\mathcal{I}_{\mathbf{t}}^{\mathcal{F}}$ diverge, SAM continues to suppress noise memorization and leverage its sharpness-aware updates when fitting $\mathcal{R}$, but "falls back" to SGD-like behavior on $\mathcal{F}$. This split yields two distinct sets of bounds on κ and ζ for $\mathcal{R}$ and $\mathcal{F}$, which lead to separate test errors shown in App. D.1 and D.2. However, given a pretrained model $f_{\mathcal{A}}^{T_1}$ with $\kappa^{T_1} > 0$ to start unlearning, **as long as retain signals weighted by α dominate, the signal strength will remain sufficient and continue to grow**. This is shown in Chen et al. (2023) when the signal strength is saturated at $T < T_1$. We can thus choose α threshold based on this principle. With proper forget-retain size ratio, results in Chen et al. (2023) still hold: SGD's test error converges when signal strength is sufficient, but can't be upper bounded otherwise; SAM's test error converges either way. β serves as a knob to control the convergence rate:

Theorem 3.2 *(SGD test error under NegGrad). Under Assumption D.1, for any $\epsilon > 0$ and $1 > \alpha \geq |\mathcal{R}|/(|\mathcal{F}| + |\mathcal{R}|) := \beta > 0.5$, then with probability at least $1 - \delta$, the training loss converges: $\mathcal{L}(\mathbf{W}^T, \mathcal{D}) \leq \epsilon$. Moreover, if $\|\boldsymbol{\varphi}\|_2 \geq C_1 d^{1/4} n^{-1/4} P \sigma_p$, we have the test error $\mathcal{L}^{test}(\mathbf{W}^T, \mathcal{D}) \leq \epsilon$. If $\|\boldsymbol{\varphi}\|_2 \leq C_3 d^{1/4} n^{-1/4} P \sigma_p$, we have $\lim_{\beta \to 1} \mathcal{L}^{test}(\mathbf{W}^{T_2}, \mathcal{D}) \geq 0.1$, and $\lim_{\beta \to 0.5} \mathcal{L}^{test}(\mathbf{W}^{T_2}, \mathcal{D}) \geq 0.05$.*

Theorem 3.3 *(SAM test error under NegGrad). Under Assumption D.1, for any $\epsilon > 0$ and $1 > \alpha \geq |\mathcal{R}|/(|\mathcal{F}| + |\mathcal{R}|) := \beta > 0.5$, choose $\tau = \Theta(\frac{m\sqrt{B}}{P\sigma_p\sqrt{d}})$. Then with probability at least $1 - \delta$, the training loss converges: $\mathcal{L}(\mathbf{W}^T, \mathcal{D}) \leq \epsilon$. Moreover, if $\|\boldsymbol{\varphi}\|_2 \geq C_1 d^{1/4} n^{-1/4} P \sigma_p$, we have $\lim_{\beta \to 1} \mathcal{L}^{test}(\mathbf{W}^T, \mathcal{D}) \leq \epsilon$. If $\Omega(1) \leq \|\boldsymbol{\varphi}\|_2 \leq C_3 d^{1/4} n^{-1/4} P \sigma_p$: we still have $\lim_{\beta \to 1} \mathcal{L}^{test}(\mathbf{W}^T, \mathcal{D}) \leq \epsilon$.*

See proofs in App. D.1 and D.2. Together, these theorems describe how SGD and SAM behave when retain signals dominate. For SAM, if $\|\boldsymbol{\varphi}\|_2 \leq C_3 d^{1/4} n^{-1/4} P \sigma_p$, it will suffer harmful overfitting to $\mathcal{F}$. However, as long as $\alpha \geq |\mathcal{R}|/(|\mathcal{F}| + |\mathcal{R}|)$ and $\|\boldsymbol{\varphi}\|_2 \geq \Omega(1)$, learning on $\mathcal{R}$ guarantees overall benign training and yields a bounded test error. Under the same condition, Corollary 3.3.1 concludes that while the signal coefficient continues to grow for both SGD and SAM, SGD's noise accumulation is loosely bounded by model dimension, while SAM's by $O(1)$:

Corollary 3.3.1 *(κ, ζ update under NegGrad). Under the NegGrad, if $\alpha \geq |\mathcal{R}|/(|\mathcal{F}| + |\mathcal{R}|)$, since $\kappa^{T_1} = \Omega(1)$, both SGD and SAM continue to grow. Given the learned ζ^{T_1}, SGD continues to overfit the noise with $O(\log d)$, while SAM overfit the noise from $\mathcal{F}$ with $O(\log d)$ and from $\mathcal{R}$ with $O(1)$.*

See proof in App. D.3. Finally, we characterize the differed choice of α for SGD and SAM as SAM learns signal more efficiently. We also reveal that α depends not only on forget-retain size ratio as commonly conjectured, but also on the signal strength, and thus the dimensionality of the problem:

Lemma 3.4 *(Signal-surplus of SAM under NegGrad). Under the NegGrad, for any $\boldsymbol{\varphi}$ where $\|\boldsymbol{\varphi}\|_2 \geq \Omega(1)$, SAM exhibits faster signal learning on $\mathcal{R}$: $\Delta_{epoch}^{SAM}\kappa / \Delta_{epoch}^{SGD}\kappa = \Theta(\|\boldsymbol{\varphi}\|_2^2)$.*

See proof in App. D.4. As a result, SAM relies on a more relaxed α threshold than SGD due to faster signal learning. For SGD to achieve the same signal learning performance as SAM, we need to scale up α^{SGD} to satisfy $\alpha^{\text{SGD}}/\alpha^{\text{SAM}} = \Theta(\|\boldsymbol{\varphi}\|_2^2)$. If $\|\boldsymbol{\varphi}\|_2 \geq C_1 d^{1/4} n^{-1/4} P \sigma_p$ and both SGD and SAM achieve benign overfitting, then given the extra signal learning from $\mathcal{R}$, SAM results in faster κ update and a surplus signal of $\Theta(d^{1/2}|\mathcal{R}|^{-1/2} P^2 \sigma_p^2)$ in each unlearning epoch.

3.2 Sharp MinMax

In Sec. 3.1, we showed that SAM is provably better on out of sample test errors under NegGrad, and we empirically verify that SAM achieves better unlearning performance in Sec. 4. But how does the refined characterization matter, given maintained test error conclusions? Jointly with empirical observations, the altered behaviors of SAM on $\mathcal{F}$ motivates new unlearning algorithms. Our

experiments show that SAM+NegGrad attains higher forget accuracy than SGD+NegGrad, forgetting less effectively. This finding forces us to reconsider the conventional view that overfitting is always detrimental: while overfitting indeed harms generalization, it may be beneficial when the goal is to remove specific samples from a model. Consequently, for abstract concept forgetting we continue to demand strong generalization; but for stringent scenarios—where exact sample removal is mandated by privacy or compliance constraints—a model's tendency to overfit can actually enhance its unlearning of those exact points. The divergent behaviors under SAM+NegGrad motivates the following new algorithm: we can split a portion of model parameters to purposefully overfit to $\mathcal{F}$, denoted as the forget model $\mathbf{W}_\mathcal{F}$, while leaving the rest as the retain model $\mathbf{W}_\mathcal{R}$ to maximally maintain the model utility by leveraging SAM purely on $\mathcal{R}$. Motivated by how SGD with sharper minima tends to forget better, we propose Sharp MinMax to intentionally optimize for sharper-than-SGD minima with the purpose of overfitting to forget signals for unlearning. Inspired by Kim et al. (2023), we leverage sharpness maximization on $\mathbf{W}_\mathcal{F}$:

$$\min_{\mathbf{W}_\mathcal{F}} \mathcal{L}(\mathbf{W}_\mathcal{F}, \mathcal{F}) - \left[\max_{\widehat{\boldsymbol{\epsilon}}} \mathcal{L}(\mathbf{W}_\mathcal{F} + \widehat{\boldsymbol{\epsilon}}, \mathcal{F}) - \mathcal{L}(\mathbf{W}_\mathcal{F}, \mathcal{F})\right], \tag{8}$$

resulting in a sharper landscape that harms the generalization by overfitting. We apply weight masking based on gradient magnitudes (Fan et al., 2023) to divide our model into $\mathbf{W}_\mathcal{R}, \mathbf{W}_\mathcal{F}$ during optimization. Specifically, we pass $\mathcal{F}$ to $f_\mathcal{A}$ once, accumulate gradients for each parameter, and check top parameters with smallest magnitudes cut off by a given percentage. We then apply SAM on $\mathbf{W}_\mathcal{R}$ and sharpness maximization on $\mathbf{W}_\mathcal{F}$. The retain model with SAM is already characterized by Chen et al. (2023), while $\mathbf{W}_\mathcal{F}$ requires a stronger signal strength than SGD to avoid harmful overfitting. See implementation details in App. E.2.

3.3 Quantifying Unlearning Difficulty with Memorization

We examine the effectiveness of unlearning $\mathcal{U}$ based on memorization, which sufficiently reveals the difficulty of unlearning (Zhao et al., 2024). Feldman & Zhang (2020) define the degree to which a sample is memorized by a pretraining $\mathcal{A}$ on example $(\mathbf{x}_i, y_i)$ from $\mathcal{S}$ as the memorization score:

$$\text{mem}(\mathcal{A}, \mathcal{S}, i) := \Pr_{f \leftarrow \mathcal{A}(\mathcal{S})}\left[f\left(\mathbf{W}, \mathbf{x}_i\right) = y_i\right] - \Pr_{f \leftarrow \mathcal{A}(\mathcal{S}\setminus i)}\left[f\left(\mathbf{W}, \mathbf{x}_i\right) = y_i\right], \tag{9}$$

where $\mathcal{S} \setminus i$ denotes $\mathcal{S}$ with the sample $(\mathbf{x}_i, y_i)$ removed. Samples of high-memorization scores can be atypical samples which model usually learns later in the training process after more updates to the model than typical ones. Thus unlearning them would be harder and may require more iterations of unlearning steps which may impact the model performance on the retain distribution. The converse is true for samples of low-memorization scores. We can hence construct $\mathcal{F}$ of varying unlearning difficulties based on memorization scores to comprehensively evaluate $\mathcal{U}$.

4 Empirical Study

We conduct major experiments on CIFAR-100 (Krizhevsky et al., 2009) and ImageNet-1K (Russakovsky et al., 2015) using ResNet-50 (He et al., 2016), and adopt pre-computed memorization scores for from Feldman & Zhang (2020) to generate $\mathcal{F}$ of different difficulties with $|\mathcal{F}| \approx 5\%|\mathcal{S}|$, denoted as $[\mathcal{F}_\text{high}, \mathcal{F}_\text{mid}, \mathcal{F}_\text{low}]$. For both pretraining and unlearning, we adopt SAM (Foret et al., 2020) with $\rho = 0.1$ and Adaptive SAM (ASAM) (Kwon et al., 2021) with $\rho = [0.1, 1.0]$. We ensure same optimal hyper-paprameters for each comparable [SGD,SAM] pair. See details in App. E.

Evaluation. We follow previous work (Triantafillou et al., 2024; Zhao et al., 2024) to measure the tug-of-war tradeoff between forgetting and retaining of $f_\mathcal{U}$ based on accuracy $\text{Acc}(\theta, \mathcal{D})$, with the retrained model $f_{\mathcal{A}(\mathcal{R})}$ as reference:

$$\begin{aligned}\text{ToW}(f_\mathcal{U}) =&(1 - (\text{Acc}(f_{\mathcal{A}(\mathcal{R})}, \mathcal{R}) - \text{Acc}(f_\mathcal{U}, \mathcal{R}))) \cdot (1 - (\text{Acc}(f_\mathcal{U}, \mathcal{F}) - \text{Acc}(f_{\mathcal{A}(\mathcal{R})}, \mathcal{F})))\\ &\cdot(1 - (\text{Acc}(f_{\mathcal{A}(\mathcal{R})}, \mathcal{D}_\text{test}) - \text{Acc}(f_\mathcal{U}, \mathcal{D}_\text{test}))), \text{ with test transforms on } \mathcal{R}, \mathcal{F}.\end{aligned} \tag{10}$$

Thus, we encourage high retain/test accuracies and low forget accuracy. Note that our ToW differs from that in previous work as we measure the raw accuracy difference instead of the absolute difference, because new unlearning methods that continue to fine-tune on $\mathcal{R}$ can outperform $f_{\mathcal{A}(\mathcal{R})}$ within a conventional unlearning time T_2. If using the absolute ToW, a higher test accuracy than $f_{\mathcal{A}(\mathcal{R})}$ will be penalized and the model performance cannot be properly measured.

Table 1: ToW(%) ↑ of unlearning on ImageNet-1K and CIFAR-100. For each $(\mathcal{U}, \mathcal{A})$ pair, we report ToW of each $\mathcal{F}$ and compute averages. SAM consistently improves current unlearning methods.

ImageNet	$\mathcal{A}$ =SGD				$\mathcal{A}$ =ASAM 0.1				$\mathcal{A}$ =ASAM 1.0				$\mathcal{A}$ =SAM 0.1			
Unlearn $\mathcal{U}$	High	Mid	Low	AVG	High	Mid	Low	AVG	High	Mid	Low	AVG	High	Mid	Low	AVG
NegGrad	78.764	84.199	88.515	83.826	78.426	83.93	86.651	83.002	78.522	83.929	89.947	84.133	78.03	84.176	88.839	83.682
+ASAM 0.1	78.52	84.113	89.188	83.94	78.366	84.07	89.098	83.845	78.762	84.267	90.579	84.536	78.083	84.062	89.973	84.039
+ASAM 1.0	78.966	83.389	92.174	**84.843**	78.975	83.358	91.843	**84.725**	78.027	83.326	92.772	**84.708**	77.762	83.284	92.617	**84.554**
+SAM 0.1	77.898	82.985	92.841	84.575	78.301	83.04	91.722	84.354	77.388	82.473	93.429	84.43	76.807	82.587	92.829	84.074
RL	74.598	86.617	86.714	82.643	74.857	86.462	86.192	82.504	74.317	86.813	87.630	82.92	74.055	86.715	88.594	83.121
+ASAM 1.0	74.951	85.581	91.069	**83.867**	75.221	85.473	90.425	**83.707**	73.950	85.393	91.516	**83.62**	73.579	85.494	91.74	**83.604**
SalUn	44.981	71.839	95.008	70.609	46.104	71.735	94.652	70.83	45.814	72.308	95.116	71.079	46.006	72.419	95.218	71.214
+ASAM 1.0	45.998	71.554	95.628	**71.06**	46.938	71.268	95.224	**71.143**	45.856	71.695	95.924	**71.158**	46.358	72.034	95.791	**71.394**

CIFAR100	$\mathcal{A}$ =SGD				$\mathcal{A}$ =ASAM 0.1				$\mathcal{A}$ =ASAM 1.0				$\mathcal{A}$ =SAM 0.1			
Unlearn $\mathcal{U}$	High	Mid	Low	AVG	High	Mid	Low	AVG	High	Mid	Low	AVG	High	Mid	Low	AVG
NegGrad	78.334	83.335	83.718	81.796	79.277	86.454	88.637	84.789	77.274	78.59	85.443	80.436	67.826	74.145	76.374	72.78
+ASAM 0.1	78.131	82.846	86.78	82.586	80.336	87.539	87.671	85.182	77.331	79.074	88.039	81.482	70.054	74.158	78.087	74.1
+ASAM 1.0	80.806	81.465	87.052	83.108	82.196	84.391	90.502	**85.696**	78.731	79.264	93.249	**83.748**	72.518	75.653	86.759	**78.31**
+SAM 0.1	81.331	75.059	94.151	**83.514**	82.86	77.94	94.179	84.993	74.704	70.898	95.898	80.5	65.080	66.089	95.078	75.416
L1-Sparse	63.448	68.686	53.991	62.042	63.699	72.775	60.34	65.605	61.252	68.197	61.47	63.64	65.258	71.941	59.014	65.404
+ASAM 1.0	66.903	75.554	58.967	**67.141**	66.213	77.119	66.697	**70.01**	65.117	73.754	62.517	**67.129**	63.051	74.556	65.117	**67.575**
SCRUB	58.418	76.125	12.708	49.084	67.163	79.09	10.823	52.359	57.816	73.176	58.483	63.158	43.246	68.433	17.368	43.016
+ASAM 1.0	50.313	73.353	97.631	**73.766**	60.515	80.204	97.508	**79.409**	48.569	73.09	97.776	**73.145**	18.137	61.618	97.933	**59.229**
RL	68.464	84.395	72.4	75.086	64.518	80.215	69.711	71.481	66.689	86.411	69.677	74.259	64.391	85.481	70.55	73.474
+ASAM 1.0	69.952	86.779	74.409	**77.047**	66.909	86.557	69.375	**74.280**	69.73	91.124	80.321	**80.392**	72.884	88.633	78.066	**79.861**
SalUn	69.926	83.056	71.73	74.904	66.541	83.377	71.95	73.956	67.355	89.768	79.095	78.739	69.671	90.495	75.281	78.482
+ASAM 1.0	73.268	92.225	88.175	**84.556**	71.426	89.182	86.13	**82.246**	67.715	93.401	89.289	**83.468**	70.933	92.914	86.477	**83.441**

Table 2: MIA (%) ↓ correctness to $\mathcal{F}$ on CIFAR-100. We enhance each $\mathcal{U}$ with ASAM 1.0 and observe consistent improvement.

	$\mathcal{A}$ =SGD				$\mathcal{A}$ =ASAM 0.1				$\mathcal{A}$ =ASAM 1.0				$\mathcal{A}$ =SAM 0.1			
Unlearn $\mathcal{U}$	High	Mid	Low	AVG	High	Mid	Low	AVG	High	Mid	Low	AVG	High	Mid	Low	AVG
L1-Sparse	94.733	63.233	8.6	55.522	94.933	61.367	4.0	53.433	93.833	62.067	5.8	53.9	92.867	60.033	5.033	52.644
+ASAM 1.0	94.267	58.5	5.5	**52.756**	94.3	57.3	3.6	**51.733**	93.633	56.033	3.9	**51.189**	93.8	59.333	3.8	**52.311**
SCRUB	55.433	18.6	32.6	35.544	64.733	23.1	71.633	53.155	54.767	16.133	9.833	26.911	39.3	9.833	56.3	35.144
+ASAM 1.0	46.467	14.867	0.1	**20.478**	57.367	22.633	0.167	**26.722**	44.7	14.567	0.2	**19.822**	14.433	2.333	0.2	**5.655**
RL	90.767	62.933	10.767	54.822	91.633	68.267	13.5	57.8	89.067	63.567	15.8	56.145	89.167	61.967	8.267	53.134
+ASAM 1.0	90.3	61.3	9.467	**53.689**	91.6	62.667	12.7	**55.656**	88.0	61.3	10.667	**53.322**	86.3	59.833	5.833	**50.655**
SalUn	83.433	59.233	7.333	50.0	84.533	59.1	11.167	51.6	79.3	54.667	8.8	47.589	81.467	53.133	6.867	47.156
+ASAM 1.0	79.1	51.833	4.5	**45.144**	81.7	54.167	6.633	**47.50**	74.967	49.5	4.2	**42.889**	75.633	47.667	4.067	**42.456**
NegGrad	86.933	37.233	2.167	42.111	88.867	40.2	1.733	43.60	82.167	32.1	1.8	38.689	74.667	36.967	3.433	38.356
+ASAM 1.0	84.5	30.1	0.733	**38.444**	85.6	30.1	0.7	**38.8**	81.233	24.533	0.533	**35.433**	73.967	20.733	0.366	**31.689**

4.1 SAM Consistently Outperforms with Better Tradeoff

We conduct unlearning with various unlearning algorithms $\mathcal{U}$ given different pretrained $f_{\mathcal{A}}$. Tab. 1 reports ToW scores of $\mathcal{U}$ on CIFAR-100 and ImageNet. We observe that SAM consistently improves all unlearning methods under different initializations $f_{\mathcal{A}}^{T_1}$, suggesting that **SAM can universally enhance prevailing** $\mathcal{U}$. While different $\mathcal{U}$ exhibit varied effectiveness to $[\mathcal{F}_{\text{high}}, \mathcal{F}_{\text{mid}}, \mathcal{F}_{\text{low}}]$, we observe that NegGrad achieves a better balance between three forget sets than other methods. We include detailed [retain, forget, test] accuracies, further analysis and demonstration of statistical significance in App. F. Upon close examination on those accuraices, we observe that despite SAM outperforms SGD by better retain and test accuracies and thus better ToW, SGD can oftentimes achieve lower forget accuracies. This aligns with our theoretical analysis where SGD overfits more to $\mathcal{F}$, and it also sparks our Sharp MinMax. Smaller experiments on CIFAR-10 and Tiny-ImageNet in App. G yield aligned conclusions.

MIA correctness. We report correctness rates of membership inference attack (MIA) to $\mathcal{F}$ on CIFAR-100 in Tab. 2. Lower correctness means better unlearning: forget samples behave more like samples that were never in $\mathcal{S}$. We find that **SAM consistently improves data privacy while unlearning more effectively**. Note that NegGrad achieves better MIA correctness than RL; this is because gradient ascent actively erases gradient signatures of $\mathcal{F}$ in the model. SCRUB (Kurmanji et al., 2023) with SAM achieves best MIA performance.

Relearning attacks. We also present relearning attack experiments to demonstrate SAM's unlearning robustness in App. G.5. We observe that SAM enhanced $\mathcal{U}$ are more resilient to relearning attacks with smaller increases. While not our main focus, these experiments highlight the robustness of our approach and encourage future works for deeper investigation into the role of loss landscape geometry for robust unlearning.

KL on margins. While ToW measures performance closeness between unlearned model and retrained model, Georgiev et al. (2024) propose to measure distribution closeness in output space with KL divergence on margins (KLoM). We evaluate NegGrad w/ SGD vs. w/ SAM on CIFAR-100 using KLoM means and 95%-percentiles (tails) in App. G.7, and observe similar conclusions: on KLoM means, SGD can outperform SAM on $\mathcal{F}$, but SAM achieves better closeness on $\mathcal{R}$, $\mathcal{D}_{\text{test}}$ and hence better KLoMs overall; on 95%-percentiles, SAM outperforms SGD for all settings, suggesting lower variance and better stability at tails. While SAM is not targeted to resolve data dependency issues in unlearning (Georgiev et al., 2024), it ameliorates them by its geometric properties as suggested by lower entanglement and better ToW and KLoM.

Our observations further generalize. We consider structured noise unlearning, where another source of noise is introduced during unlearning. We adopt the glass blur and snow effect from ImageNet-C (Hendrycks & Dietterich, 2019) to corrupt $\mathcal{R}$ and $\mathcal{F}$ of CIFAR-100, and unlearn with NegGrad and Sharp MinMax. We record experiment results in App. G.3, and observe consistent conclusions where SAM outperforms under both corruptions. We also experiment on ViT-Small (Dosovitskiy et al., 2020) with AdamW (Loshchilov & Hutter, 2017) on CIFAR-100 in App. G.4, with NegGrad and Sharp MinMax. We continue to observe promising improvement by adding SAM, with significant increase of ToW on Sharp MinMax. While we focus on studying the geometric properties of SAM rather than efficiency, we are the first to demonstrate how recent efficient SAM variants (specifically Momentum SAM (Becker et al., 2024)) can perform equivalently well as the original SAM with much less computation overhead in App. G.6.

4.2 Constrained Overfitting Benefits Unlearning

Table 3: ToW(%) ↑ of Sharp MinMax on ImageNet-1K and CIFAR-100. Comparing with Tab. 1, Sharp MinMax achieves new best ToW performance.

ImageNet	$\mathcal{A}$ =SGD				$\mathcal{A}$ =ASAM 0.1				$\mathcal{A}$ =ASAM 1.0				$\mathcal{A}$ =SAM 0.1			
Unlearn $\mathcal{U}$	High	Mid	Low	AVG	High	Mid	Low	AVG	High	Mid	Low	AVG	High	Mid	Low	AVG
SGD	73.357	80.881	86.334	80.191	73.418	80.784	84.378	79.527	73.103	81.105	86.402	80.204	73.052	80.913	85.517	79.827
ASAM 0.1	78.066	87.914	87.338	84.44	79.077	87.4	86.953	84.476	70.148	88.039	87.554	81.914	78.529	87.642	86.668	84.28
ASAM 1.0	86.658	87.345	89.694	**87.899**	86.166	87.192	89.138	**87.498**	86.915	87.27	90.142	88.109	86.272	87.076	90.064	**87.804**
SAM 0.1	86.463	86.755	90.005	87.741	85.511	86.635	89.852	87.333	86.849	86.722	91.111	**88.227**	85.712	86.486	90.207	87.468

CIFAR100	$\mathcal{A}$ =SGD				$\mathcal{A}$ =ASAM 0.1				$\mathcal{A}$ =ASAM 1.0				$\mathcal{A}$ =SAM 0.1			
Unlearn $\mathcal{U}$	High	Mid	Low	AVG	High	Mid	Low	AVG	High	Mid	Low	AVG	High	Mid	Low	AVG
SGD	70.7668	76.692	82.853	76.771	72.137	77.864	81.847	77.282	65.925	74.526	80.127	73.526	60.478	71.931	73.843	68.751
ASAM 0.1	78.895	96.027	83.473	86.132	84.968	96.451	82.883	88.101	81.825	93.786	87.151	87.587	72.897	80.104	86.659	79.887
ASAM 1.0	82.27	94.913	86.504	87.896	77.576	99.422	85.894	87.631	84.521	87.761	84.381	85.554	76.037	83.633	77.461	79.044
SAM 0.1	90.578	90.960	92.494	**91.344**	91.695	95.543	91.508	**92.915**	88.664	88.646	93.163	**90.158**	85.195	78.286	90.963	**84.814**

We present ToW of Sharp MinMax and compare to Tab. 1. Compared with NegGrad and other methods, Sharp MinMax further improves the unlearning capabilities across all settings by a noticeable margin, especially on $\mathcal{F}_{\text{high}}$, and SAM 0.1 achieves ToW > 0.9 for most settings on CIFAR-100. The effectiveness of Sharp MinMax assures our assumptions about overfitting for sample-specific unlearning, providing new insights for designing future unlearning algorithms. By constraining overfitting to only a small portion of model parameters which are most salient to $\mathcal{F}$, Sharp MinMax effectively boosts unlearning performance. In App. G.5, the impact of relearning attacks to Sharp MinMax is effectively limited to the sharp terrains as it makes retain and forget models geometrically distinct, so the robustness against relearning attacks as well as the model performance is retained.

4.3 Quantitative Analysis and Visualizations

Table 4: Entanglement ↓ between $\mathcal{F}$ and $\mathcal{R}$ of different memorization levels given models based on SGD and ASAM 1.0. While E_{Var} is hard to conclude a comparison between SGD and SAM across different $\mathcal{U}$, SAM shows less entanglement both before and after unlearning than SGD by E_{W_p}.

SGD	Variance E_{Var}				Wasserstein E_{W_p}				**SAM**	Variance E_{Var}				Wasserstein E_{W_p}			
Model	High	Mid	Low	AVG	High	Mid	Low	AVG	Model	High	Mid	Low	AVG	High	Mid	Low	AVG
Pretrained	30.5	95.28	32.39	52.72	59.58	66.3	63.13	63.0	Pretrained	29.56	88.43	28.91	**48.97**	55.86	61.74	59.84	**59.15**
-per class	2.5	6.71	2.51	**3.91**	51.21	57.11	59.64	55.99	-per class	2.88	6.66	2.71	4.08	45.45	49.88	52.46	**49.26**
NegGrad	18.87	37.16	22.12	**26.05**	51.24	52.99	56.12	53.45	NegGrad	17.78	37.49	24.47	26.58	49.87	52.36	54.93	**52.39**
-per class	0.56	1.8	2.69	**1.68**	35.22	46.91	55.93	46.02	-per class	0.66	2.03	2.88	1.86	36.42	44.71	50.83	**43.99**
MinMax	17.7	38.03	21.51	25.75	51.12	53.7	56.77	53.86	MinMax	16.35	32.07	20.75	**23.06**	51.26	51.8	55.08	**52.71**
-per class	0.69	2.41	2.27	1.79	38.41	49.57	57.15	48.38	-per class	0.49	1.52	2.97	**1.66**	33.65	44.56	52.55	**43.59**

Measuring entanglement. We measure the entanglement between $\mathcal{R}$ and $\mathcal{F}$ before and after unlearning. At a coarse level, we implement variance-based entanglement from Goldblum et al. (2020); Zhao et al. (2024): $\text{E}_{\text{Var}}^{\text{All}}(\mathcal{R}, \mathcal{F}, f) = (\frac{1}{|\mathcal{R}|}\sum_{i\in\mathcal{R}}(\boldsymbol{\phi}_i - \boldsymbol{\mu}_{\mathcal{R}})^2 + \frac{1}{|\mathcal{F}|}\sum_{j\in\mathcal{F}}(\boldsymbol{\phi}_j - \boldsymbol{\mu}_{\mathcal{F}})^2)/((\boldsymbol{\mu}_{\mathcal{R}} - \boldsymbol{\mu})^2 +$

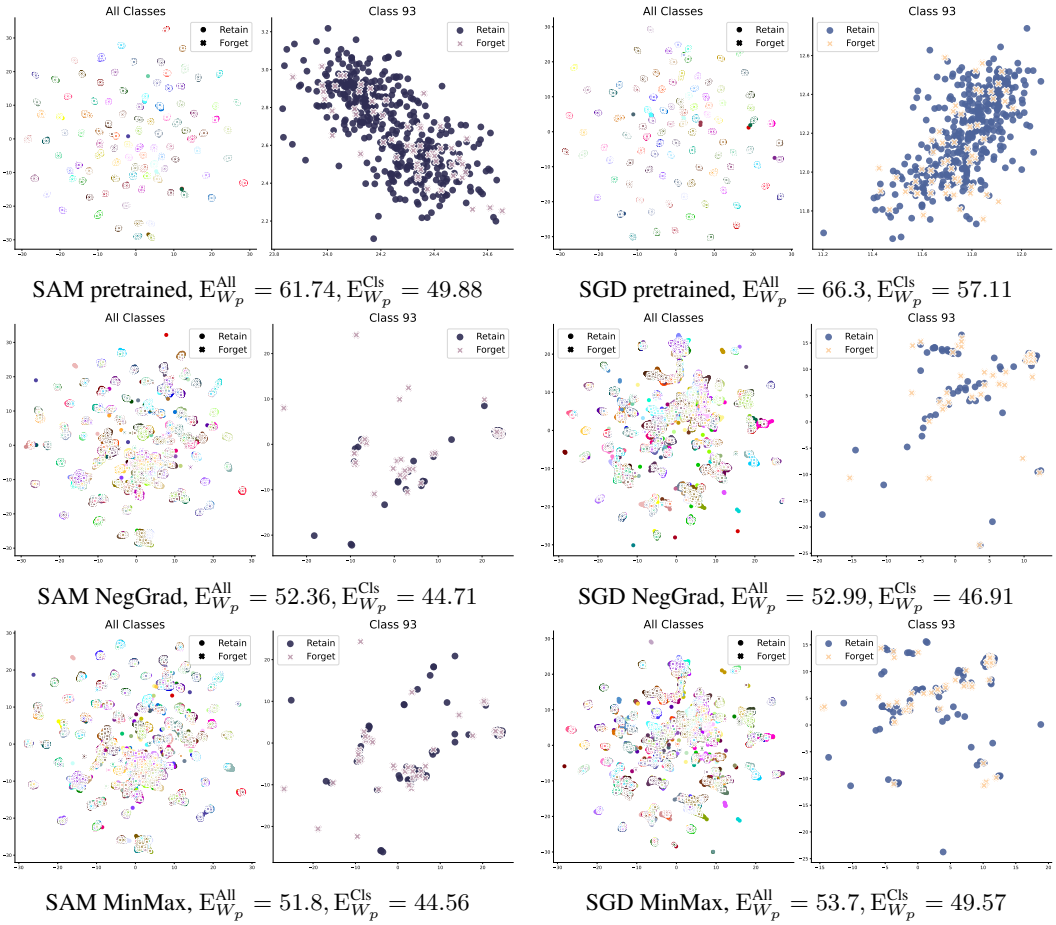

SAM pretrained, $\mathrm{E}^{\mathrm{All}}_{W_p} = 61.74, \mathrm{E}^{\mathrm{Cls}}_{W_p} = 49.88$ | SGD pretrained, $\mathrm{E}^{\mathrm{All}}_{W_p} = 66.3, \mathrm{E}^{\mathrm{Cls}}_{W_p} = 57.11$

SAM NegGrad, $\mathrm{E}^{\mathrm{All}}_{W_p} = 52.36, \mathrm{E}^{\mathrm{Cls}}_{W_p} = 44.71$ | SGD NegGrad, $\mathrm{E}^{\mathrm{All}}_{W_p} = 52.99, \mathrm{E}^{\mathrm{Cls}}_{W_p} = 46.91$

SAM MinMax, $\mathrm{E}^{\mathrm{All}}_{W_p} = 51.8, \mathrm{E}^{\mathrm{Cls}}_{W_p} = 44.56$ | SGD MinMax, $\mathrm{E}^{\mathrm{All}}_{W_p} = 53.7, \mathrm{E}^{\mathrm{Cls}}_{W_p} = 49.57$

Figure 1: UMAP (McInnes et al., 2018) feature analysis on Mid Mem $\mathcal{F}_{\text{mid}}$. At all-class level, we observe that SAM better maintains class clusters after unlearning while SGD is forming a more evident clump of features; at classwise level, we observe that while both push away forget features, SGD also scatters retain features further, suggesting overfitting. This also explains the larger clump of SGD at all-class level. We observe that SAM further pushes away forget features on $\mathcal{F}_{\text{high}}$ and SGD scatters more retain features on $\mathcal{F}_{\text{low}}$, see App. H.2 for full visualizations.

$(\boldsymbol{\mu}_{\mathcal{F}} - \boldsymbol{\mu})^2$), where $\boldsymbol{\phi}_i, \boldsymbol{\phi}_j$ denote sample embedding, $\boldsymbol{\mu}_{\mathcal{R}}, \boldsymbol{\mu}_{\mathcal{F}}$ denote mean embedding of $\mathcal{R}, \mathcal{F}$, and $\boldsymbol{\mu}$ denotes mean embedding over $\mathcal{R} \cup \mathcal{F}$. We also compute the class-wise entanglement and report weighted averaged $\mathrm{E}^{\mathrm{Cls}}_{\mathrm{Var}}$. However, $\mathrm{E}_{\mathrm{Var}}$ assumes good/convex shapes of clusters and relies heavily on cluster means. Inspired by Optimal Transport literature, we propose a refined geometry-aware entanglement based on Wasserstein distance to measure the separation of retain and forget features, $\mathrm{E}^{\mathrm{All}}_{W_p}$ and $\mathrm{E}^{\mathrm{Cls}}_{W_p}$, which computes the cost of transferring one shaped distribution to another point-wisely. From Tab. 4, we observe that both SGD and SAM unlearning have decreased entanglement with $\mathrm{E}^{\mathrm{Cls}} < \mathrm{E}^{\mathrm{All}}$. While $\mathrm{E}_{\mathrm{Var}}$ cannot further differentiate, we observe that SAM achieves better E_{W_p} than SGD at all levels. Fig. 1 visualizes the feature space of $\mathcal{A},\mathcal{U} =$ ASAM 1.0 and $\mathcal{A},\mathcal{U} =$ SGD on $\mathcal{F}_{\text{mid}}$. For all classes, we observe forget samples are assigned to wrong class clusters after unlearning, where SAM better maintains class clusters. For class-wise, we visualize the largest class in $\mathcal{F}_{\text{mid}}$ and observe that SGD unlearning scatters more retain samples than its SAM counterpart, suggesting overfitting. See App. H.2 for complete visualizations.

Reducing retain signal. We verify Lemma 3.4 by reducing α in NegGrad. Fig. 2 shows ToW changes as α decreases for various $\mathcal{A},\mathcal{U}$ pairs at different memorization levels on CIFAR-100. We observe that $\mathcal{A},\mathcal{U} =$ SGD fails the fastest and hardest, while $\mathcal{A},\mathcal{U} =$ ASAM 1.0 exhibits the best resilience. Also note that for CIFAR-100, $|\mathcal{R}|/(|\mathcal{F}| + |\mathcal{R}|) \approx 0.93$, but unlearning starts to fail at a higher α. This supports our claim that α depends more than retain-forget ratio.

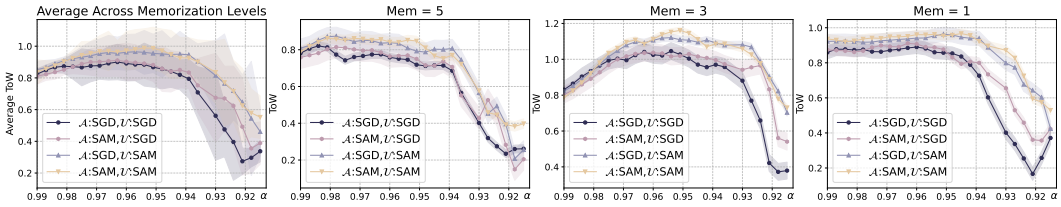

Figure 2: As α decreases, NegGrad puts less weight on retain signals and learns more from $\mathcal{F}$, leading to harmful overfitting. SAM exhibits more tolerance to insufficient retain signals, while $\mathcal{A},\mathcal{U}$ = SGD collapses the fastest. Note that ToW starts failing before $\alpha = |\mathcal{R}|/(|\mathcal{F}| + |\mathcal{R}|)$, implying more factors affecting α threshold as we point out.

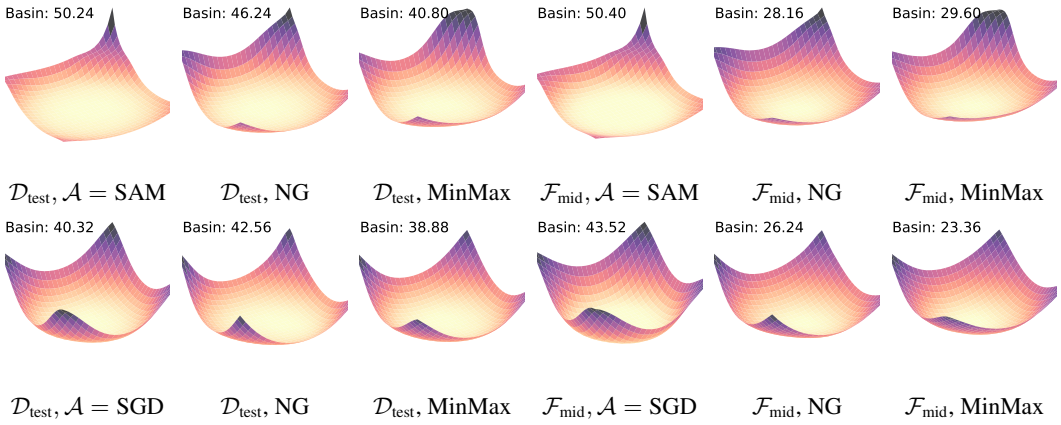

Figure 3: Loss landscapes on $\mathcal{D}_{\text{test}}$ and $\mathcal{F}_{\text{mid}}$, where first row shows a SAM pretrained model and SAM unlearned models, and second row shows SGD counterparts. While unlearning increases sharpness as suggested by reduced basin ratios, we observe SAM unlearned models still maintain flatter landscapes than SGD models do.

Loss landscape. We visualize loss landscapes of SGD and ASAM 1.0 by perturbing original model along two directions with filter normalization (Li et al., 2018), and quantify more sharpness by smaller basin ratio. Fig. 3 shows loss landscapes on $\mathcal{D}_{\text{test}}$ and $\mathcal{F}_{\text{mid}}$, where SAM unlearning generally keeps flatter landscapes. Same observations apply to different $\mathcal{F}$except that we observe SGD+NegGrad on $\mathcal{F}_{\text{high}}$ to achieve flatter landscape, which might indicate that unlearning can be an implicit regularizer, we will leave it to future work. See full visualizations and more details in App. H.1.

5 Conclusion

In this paper, we provide a refined characterization of SAM under NegGrad unlearning, and theoretical insights on bounding and choosing the weight factor to balance retain and forget signals. Extensive studies verify our analysis and reveals more underlying properties of SAM that are desired for unlearning. Based on our rethinking of overfitting, we also propose a new algorithm which further pushes the boundary of sample-specific unlearning. Our theoretical and empirical findings shed light on future design of unlearning algorithms.

REFERENCES

Idan Attias, Gintare Karolina Dziugaite, Mahdi Haghifam, Roi Livni, and Daniel M Roy. Information complexity of stochastic convex optimization: Applications to generalization and memorization. *arXiv preprint arXiv:2402.09327*, 2024.

Peter L Bartlett, Philip M Long, and Olivier Bousquet. The dynamics of sharpness-aware minimization: Bouncing across ravines and drifting towards wide minima. *arXiv preprint arXiv:2210.01513*, 2022.

Marlon Becker, Frederick Altrock, and Benjamin Risse. Momentum-sam: Sharpness aware minimization without computational overhead. *arXiv preprint arXiv:2401.12033*, 2024.

Stella Biderman, Usvsn Prashanth, Lintang Sutawika, Hailey Schoelkopf, Quentin Anthony, Shivanshu Purohit, and Edward Raff. Emergent and predictable memorization in large language models. *Advances in Neural Information Processing Systems*, 36:28072–28090, 2023.

Nicholas Carlini, Ulfar Erlingsson, and Nicolas Papernot. Distribution density, tails, and outliers in machine learning: Metrics and applications. *arXiv preprint arXiv:1910.13427*, 2019.

Zixiang Chen, Junkai Zhang, Yiwen Kou, Xiangning Chen, Cho-Jui Hsieh, and Quanquan Gu. Why does sharpness-aware minimization generalize better than sgd? *Advances in neural information processing systems*, 36:72325–72376, 2023.

Eli Chien, Haoyu Wang, Ziang Chen, and Pan Li. Langevin unlearning: A new perspective of noisy gradient descent for machine unlearning. *arXiv preprint arXiv:2401.10371*, 2024.

Luc Devroye, Abbas Mehrabian, and Tommy Reddad. The total variation distance between high-dimensional gaussians with the same mean. *arXiv preprint arXiv:1810.08693*, 2018.

Alexey Dosovitskiy, Lucas Beyer, Alexander Kolesnikov, Dirk Weissenborn, Xiaohua Zhai, Thomas Unterthiner, Mostafa Dehghani, Matthias Minderer, Georg Heigold, Sylvain Gelly, et al. An image is worth 16x16 words: Transformers for image recognition at scale. *arXiv preprint arXiv:2010.11929*, 2020.

Chongyu Fan, Jiancheng Liu, Yihua Zhang, Eric Wong, Dennis Wei, and Sijia Liu. Salun: Empowering machine unlearning via gradient-based weight saliency in both image classification and generation. *arXiv preprint arXiv:2310.12508*, 2023.

Chongyu Fan, Jiancheng Liu, Alfred Hero, and Sijia Liu. Challenging forgets: Unveiling the worst-case forget sets in machine unlearning. In *European Conference on Computer Vision*, pp. 278–297. Springer, 2024.

Chongyu Fan, Jinghan Jia, Yihua Zhang, Anil Ramakrishna, Mingyi Hong, and Sijia Liu. Towards llm unlearning resilient to relearning attacks: A sharpness-aware minimization perspective and beyond. *arXiv preprint arXiv:2502.05374*, 2025.

Vitaly Feldman. Does learning require memorization? a short tale about a long tail. In *Proceedings of the 52nd Annual ACM SIGACT Symposium on Theory of Computing*, pp. 954–959, 2020.

Vitaly Feldman and Chiyuan Zhang. What neural networks memorize and why: Discovering the long tail via influence estimation. *Advances in Neural Information Processing Systems*, 33:2881–2891, 2020.

Pierre Foret, Ariel Kleiner, Hossein Mobahi, and Behnam Neyshabur. Sharpness-aware minimization for efficiently improving generalization. *arXiv preprint arXiv:2010.01412*, 2020.

Kristian Georgiev, Roy Rinberg, Sung Min Park, Shivam Garg, Andrew Ilyas, Aleksander Madry, and Seth Neel. Attribute-to-delete: Machine unlearning via datamodel matching. *arXiv preprint arXiv:2410.23232*, 2024.

Aditya Golatkar, Alessandro Achille, and Stefano Soatto. Eternal sunshine of the spotless net: Selective forgetting in deep networks. In *Proceedings of the IEEE/CVF conference on computer vision and pattern recognition*, pp. 9304–9312, 2020.

Micah Goldblum, Steven Reich, Liam Fowl, Renkun Ni, Valeriia Cherepanova, and Tom Goldstein. Unraveling meta-learning: Understanding feature representations for few-shot tasks. In *International Conference on Machine Learning*, pp. 3607–3616. PMLR, 2020.

Laura Graves, Vineel Nagisetty, and Vijay Ganesh. Amnesiac machine learning. In *Proceedings of the AAAI Conference on Artificial Intelligence*, volume 35, pp. 11516–11524, 2021.

Kaiming He, Xiangyu Zhang, Shaoqing Ren, and Jian Sun. Deep residual learning for image recognition. In *Proceedings of the IEEE conference on computer vision and pattern recognition*, pp. 770–778, 2016.

Dan Hendrycks and Thomas Dietterich. Benchmarking neural network robustness to common corruptions and perturbations. *arXiv preprint arXiv:1903.12261*, 2019.

Zachary Izzo, Mary Anne Smart, Kamalika Chaudhuri, and James Zou. Approximate data deletion from machine learning models. In *International Conference on Artificial Intelligence and Statistics*, pp. 2008–2016. PMLR, 2021.

Jinghan Jia, Jiancheng Liu, Parikshit Ram, Yuguang Yao, Gaowen Liu, Yang Liu, Pranay Sharma, and Sijia Liu. Model sparsity can simplify machine unlearning. *Advances in Neural Information Processing Systems*, 36:51584–51605, 2023.

Pham Khanh, Hoang-Chau Luong, Boris Mordukhovich, and Dat Tran. Fundamental convergence analysis of sharpness-aware minimization. *Advances in Neural Information Processing Systems*, 37:13149–13182, 2024.

Young In Kim, Pratiksha Agrawal, Johannes O Royset, and Rajiv Khanna. On memorization and privacy risks of sharpness aware minimization. *arXiv preprint arXiv:2310.00488*, 2023.

Myeongseob Ko, Henry Li, Zhun Wang, Jonathan Patsenker, Jiachen Tianhao Wang, Qinbin Li, Ming Jin, Dawn Song, and Ruoxi Jia. Boosting alignment for post-unlearning text-to-image generative models. *Advances in Neural Information Processing Systems*, 37:85131–85154, 2024.

Yiwen Kou, Zixiang Chen, Yuanzhou Chen, and Quanquan Gu. Benign overfitting in two-layer relu convolutional neural networks. In *International conference on machine learning*, pp. 17615–17659. PMLR, 2023.

Alex Krizhevsky et al. Learning multiple layers of features from tiny images. *https://www.cs.toronto.edu/ kriz/learning-features-2009-TR.pdf*, 2009.

Meghdad Kurmanji, Peter Triantafillou, Jamie Hayes, and Eleni Triantafillou. Towards unbounded machine unlearning. *Advances in neural information processing systems*, 36:1957–1987, 2023.

Jungmin Kwon, Jeongseop Kim, Hyunseo Park, and In Kwon Choi. Asam: Adaptive sharpness-aware minimization for scale-invariant learning of deep neural networks. In *International Conference on Machine Learning*, pp. 5905–5914. PMLR, 2021.

Hao Li, Zheng Xu, Gavin Taylor, Christoph Studer, and Tom Goldstein. Visualizing the loss landscape of neural nets. *Advances in neural information processing systems*, 31, 2018.

Hao Li, Di Huang, Ziyu Wang, and Amir M Rahmani. Skewed memorization in large language models: Quantification and decomposition. *arXiv preprint arXiv:2502.01187*, 2025.

Yong Liu, Siqi Mai, Xiangning Chen, Cho-Jui Hsieh, and Yang You. Towards efficient and scalable sharpness-aware minimization. In *Proceedings of the IEEE/CVF Conference on Computer Vision and Pattern Recognition*, pp. 12360–12370, 2022.

Ilya Loshchilov and Frank Hutter. Decoupled weight decay regularization. *arXiv preprint arXiv:1711.05101*, 2017.

Ioannis Mavrothalassitis, Pol Puigdemont, Noam Itzhak Levi, and Volkan Cevher. Ascent fails to forget. *arXiv preprint arXiv:2509.26427*, 2025.

Leland McInnes, John Healy, and James Melville. Umap: Uniform manifold approximation and projection for dimension reduction. *arXiv preprint arXiv:1802.03426*, 2018.

Peng Mi, Li Shen, Tianhe Ren, Yiyi Zhou, Xiaoshuai Sun, Rongrong Ji, and Dacheng Tao. Make sharpness-aware minimization stronger: A sparsified perturbation approach. *Advances in Neural Information Processing Systems*, 35:30950–30962, 2022.

USVSN Sai Prashanth, Alvin Deng, Kyle O'Brien, Jyothir SV, Mohammad Aflah Khan, Jaydeep Borkar, Christopher A Choquette-Choo, Jacob Ray Fuehne, Stella Biderman, Tracy Ke, et al. Recite, reconstruct, recollect: Memorization in lms as a multifaceted phenomenon. *arXiv preprint arXiv:2406.17746*, 2024.

Olga Russakovsky, Jia Deng, Hao Su, Jonathan Krause, Sanjeev Satheesh, Sean Ma, Zhiheng Huang, Andrej Karpathy, Aditya Khosla, Michael Bernstein, et al. Imagenet large scale visual recognition challenge. *International journal of computer vision*, 115:211–252, 2015.

Yan Scholten, Stephan Günnemann, and Leo Schwinn. A probabilistic perspective on unlearning and alignment for large language models. In *The Thirteenth International Conference on Learning Representations*, 2025. URL https://openreview.net/forum?id=51WraMid8K.

Ayush Sekhari, Jayadev Acharya, Gautam Kamath, and Ananda Theertha Suresh. Remember what you want to forget: Algorithms for machine unlearning. *Advances in Neural Information Processing Systems*, 34:18075–18086, 2021.

Eleni Triantafillou, Peter Kairouz, Fabian Pedregosa, Jamie Hayes, Meghdad Kurmanji, Kairan Zhao, Vincent Dumoulin, Julio Jacques Junior, Ioannis Mitliagkas, Jun Wan, et al. Are we making progress in unlearning? findings from the first neurips unlearning competition. *arXiv preprint arXiv:2406.09073*, 2024.

Roman Vershynin. *High-dimensional probability: An introduction with applications in data science*, volume 47. Cambridge university press, 2018.

Sheng-Yu Wang, Aaron Hertzmann, Alexei Efros, Jun-Yan Zhu, and Richard Zhang. Data attribution for text-to-image models by unlearning synthesized images. *Advances in Neural Information Processing Systems*, 37:4235–4266, 2024.

Alexander Warnecke, Lukas Pirch, Christian Wressnegger, and Konrad Rieck. Machine unlearning of features and labels. *arXiv preprint arXiv:2108.11577*, 2021.

Lei Wu, Zhanxing Zhu, et al. Towards understanding generalization of deep learning: Perspective of loss landscapes. *arXiv preprint arXiv:1706.10239*, 2017.

Yimeng Zhang, Xin Chen, Jinghan Jia, Yihua Zhang, Chongyu Fan, Jiancheng Liu, Mingyi Hong, Ke Ding, and Sijia Liu. Defensive unlearning with adversarial training for robust concept erasure in diffusion models. *Advances in Neural Information Processing Systems*, 37:36748–36776, 2024.

Zhe Zhang and Guanghui Lan. Solving convex smooth function constrained optimization is almost as easy as unconstrained optimization. *arXiv preprint arXiv:2210.05807*, 2022.

Kairan Zhao, Meghdad Kurmanji, George-Octavian Bărbulescu, Eleni Triantafillou, and Peter Triantafillou. What makes unlearning hard and what to do about it. *Advances in Neural Information Processing Systems*, 37:12293–12333, 2024.

A Related Works

A.1 Machine Unlearning

A wide variety of unlearning algorithms have been proposed to erase the influence of specific data in the pre-trained model. Basic approaches involve finetuning on retain set to unlearn the forget samples with catastrophic forgetting, randomly labeling forget set to force the model to ignore the noisy forget samples, and explicitly "learning to unlearn" from the forget set via gradient ascent (Golatkar et al., 2020; Graves et al., 2021; Warnecke et al., 2021). Recent work pushes the boundaries of each genre with more advanced tools. L1-Sparse (Jia et al., 2023) finetunes on retain set with L1 penalty to improve unlearning with sparsification, NegGrad and SCRUB (Kurmanji et al., 2023) combines gradient descent on retain set and gradient ascent on forget set to jointly update the model, Influence Unlearning and Saliency Unlearning (Izzo et al., 2021; Fan et al., 2023) aim to find model parameters which are important to the forget set for more effective unlearning while preserving model performance. Theoretical work in unlearning draws insights from differential privacy and characterizes distributional closeness in (ϵ, δ)-language. Sekhari et al. (2021) studies unlearning with second-order update which computes Hessian inverse. Langevin Unlearning (Chien et al., 2024) studies approximate unlearning with privacy and efficiency guarantees based on projected noisy gradient descent. Unlearning also extends to generative vision and language tasks, addressing privacy and safety concerns, erasing concepts, and aligning with human preference (Ko et al., 2024; Wang et al., 2024; Zhang et al., 2024; Scholten et al., 2025).

A.2 Sharpness Aware Minimization

Sharpness-aware minimization (SAM) perturbs the model within a ball neighborhood to maximize the loss. Since perturbations in sharp regions result in higher penalties, SAM learns to avoid sharp landscapes and improve generalization with flatness. Recent work improves SAM's flexibility and efficiency. Adaptive SAM (Kwon et al., 2021) introduces scale-invariant adaptive sharpness to address parameter re-scaling sensitivity. GA-SAM (Zhang & Lan, 2022) adapts the perturbation based on gradient strength to improve generalization performance. Sparse SAM (Mi et al., 2022) shows that adding sparsity in perturbations can preserve or even improve performance while accelerating training. LookSAM (Liu et al., 2022) efficiently scales up SAM by only periodically computing the inner gradient ascent. Theoretical studies of SAM focus both on the convergence analysis (Khanh et al., 2024) and its dynamics (Bartlett et al., 2022). Chen et al. (2023) reveal the fundamental mechanism of SAM that prevents memorizing noisy signals by deactivating neurons based on a practical signal-to-noise analytical framework. This inspires us to investigate the intriguing properties of SAM in machine unlearning, where signals from the forget set can be naturally modeled as the noise from the perspective of maintaining model performance with remaining samples.

A.3 Data Memorization

Recent work aims to identify key factors that affect the difficulty of an unlearning task. Fan et al. (2024) define and seek the "worst-case" forget set using a gradient-based adversarial approach. Carlini et al. (2019) investigates and quantifies the atypical-ness of data samples under a differential privacy setting. Zhao et al. (2024) discovers that the more memorized the forget examples are, the harder unlearning becomes. We agree with the empirical studies in Zhao et al. (2024) and study the unlearning effectiveness under different levels of data memorization. Memorization literature provides fundamental understanding and interpretation of learning dynamics and model behaviors, characterizing generalization bounds and the interplay with data (Feldman & Zhang, 2020; Attias et al., 2024). Recent studies also investigate the effects of memorization in large-scale scenarios such as language models (Biderman et al., 2023; Prashanth et al., 2024; Li et al., 2025). Specifically, the memorization and influence scores in Feldman (2020); Feldman & Zhang (2020) provide insights into evaluating unlearning algorithms and designing new approaches. In our study, we have observed varied effectiveness of each unlearning method with respect to forget sets of different memorization levels, and aim at designing unlearning methods which perform well on forgets sets of all difficulties.

B STATEMENTS

B.1 REPRODUCIBILITY STATEMENT

Experiment environment. Our code is built upon several open-source code bases [1] and will be released. We perform all experiments on single NVIDIA A100/H100. We fix random seed for all data processing, saved precomputation (e.g., indices for data subsetting, weight masks), model splitting, pretraining and retraining for reproducible observations. For unlearning parameters and settings, we run experiments with multiple seeds to evaluate statistical significance, see App. F.1.

Theoretical Assumptions. Our theoretical analysis follows standard, existing assumptions of model size, data size, effective information in the data (signal) and Gaussian noise in data, which were previously stated in Kou et al. (2023); Chen et al. (2023). In addition to mentioned common assumptions, our Assumption D.1 also assumes conventional unlearning schemes: cross-entropy loss, ReLU activation, clean labels and reasonable size of forget set ($< 1/2$ trainset size).

B.2 LLM USAGE STATEMENT

We use GPT to fix grammar and polish short phrases to sharpen our expression. We also use GPT as a smart search engine to gather recent work of interest and summarize existing bug fixes. Zero LLM usage for any core component of our work, including data processing, implementation and experiment, theory, etc., and LLM does not guide the development of any module. No "vibe coding" and mathematical derivation from LLM.

B.3 LIMITATIONS AND FUTURE WORK

There are a few limitations based on the signal-to-noise framework, which on the other hand inspire us for future studies. First, there are more interference which can be modeled as noise in machine unlearning, such as the overlap between retain set and forget set. Using hard-cutoff or random sampling to build $\mathcal{F}$ might split two similar samples into two opposite subsets, causing interference and impacting unlearning effectiveness. We hypothesize that less overlap between $\mathcal{R}$ and $\mathcal{F}$ results in more effective unlearning, and vice versa. With more identified and modeled noise sources, another limitation comes from the uncharacterized behaviors when retain signals are weak for some upper bound. Will SAM fail into harmful overfitting under this circumstance? Theoretical and empirical studies under this situation might leverage the interplay between all signals, including different noisy signals. Another limitation comes from the design of ascent-based unlearning like NegGrad as discussed by a concurrent work Mavrothalassitis et al. (2025): while the objective encourages misclassification, the targeted retrained model should treat forget samples as never seen (generalizing or guessing). This misaligned objective might cause potential imprecision and leakage. While we show that SAM's benefits trivially apply to randomness-based unlearning (e.g. RL in Eqn. 3), and ascent-based unlearning is widely adopted in frontiers (LLM, diffusions), deeper studies are expected for more robust unlearning. Last, we observe an intriguing "regularizing" effect of unlearning using SGD via loss landscape visualization, which demands deeper investigation in future work.

[1] https://github.com/kairanzhao/RUM, https://github.com/davda54/sam, https://github.com/OPTML-Group/Unlearn-Saliency, https://pluskid.github.io/influence-memorization/

C TABLE OF NOTATIONS

Table 5:

Symbol	Meaning / Notes	Symbol	Meaning / Notes
$\mathbf{x}_i \in \mathbb{R}^{P\times d}$	Input image of sample i, vectorized into P patches of dimension d (one patch holds the signal $y_i\boldsymbol{\varphi}$ and $P-1$ patches contain noise)	$y_i \in \{\pm 1\}$	Binary class label for sample i
$\boldsymbol{\varphi} \in \mathbb{R}^d$	Universal signal vector shared across samples	$\boldsymbol{\xi}_i \in \mathbb{R}^d$	Noise vector for sample i, often drawn from $\mathcal{N}(\mathbf{0}, \sigma_p^2\mathbf{I})$
P	Number of patches per input image	d	Dimensionality of each patch and each convolutional filter
m	Number of convolutional filters per class	$\mathbf{w}_{j,r} \in \mathbb{R}^d$	Weight vector for the r-th filter of class $j \in \{\pm 1\}$
$\mathbf{W}_j$	Collection of filters $\{\mathbf{w}_{j,r}\}_{r=1}^m$ for class j	$\mathbf{W}$	Complete set of model parameters
$f(\mathbf{W}, \mathbf{x})$	Two-class CNN output: $f_{+1}(\mathbf{W}_{+1}, \mathbf{x}) - f_{-1}(\mathbf{W}_{-1}, \mathbf{x})$	$f_j(\mathbf{W}_j, \mathbf{x})$	Class-j output: $\frac{1}{m}\sum_{r=1}^m \sum_{p=1}^P \sigma(\langle \mathbf{w}_{j,r}, \mathbf{x}_p\rangle)$
$\sigma(\cdot)$	ReLU activation function	$\sigma'(\cdot)$	Derivative of ReLU used in gradients
$\mathcal{L}(\mathbf{W}, \mathcal{S})$	Cross-entropy loss over training set $\mathcal{S}$	$\ell_i'^{(t,b)}$	Gradient of the loss for sample i at epoch t, batch b
$\mathbf{w}_{j,r}^{(t,b)}$	r-th filter of class $j \in \{\pm 1\}$ after t epochs and b batches	$\kappa_{j,r}^{(t,b)}$	Learned signal coefficient for filter (j, r) at step (t, b)
$\zeta_{j,r,i}^{(t,b)}$	Learned noise coefficient from sample i on filter (j, r) at step (t, b)	$\|\boldsymbol{\varphi}\|_2, \|\boldsymbol{\xi}_i\|_2$	Euclidean norms of the signal and noise vectors
$\mathcal{F} \subseteq \mathcal{S}$	Forget set whose influence is to be removed	$\mathcal{R} = \mathcal{S} \setminus \mathcal{F}$	Retain set used for continued training
$f_{\mathcal{A}}^{T_1}$	Model after T_1 epochs of training by algorithm $\mathcal{A}$	$f_{\mathcal{U}}^{T_2}$	Model after T_2 epochs of unlearning by algorithm $\mathcal{U}$
T_1, T_2	Numbers of epochs for pretraining and unlearning	$\mathcal{I}_{t,b}^{\mathcal{R}}$, $\mathcal{I}_{t,b}^{\mathcal{F}}$	Mini-batch indices from $\mathcal{R}$ and $\mathcal{F}$ at step (t, b)
B	Batch size	η	Learning rate
$\mathrm{sgn}(\cdot)$	Sign function returning ± 1	α	Weight in NegGrad balancing retain and forget contributions
$\widehat{\boldsymbol{\epsilon}}_{j,r}^{(t,b)}$	SAM perturbation applied to $\mathbf{w}_{j,r}^{(t,b)}$	τ, ρ	Perturbation radius in theory and in practice used in SAM/ASAM
δ	Perturbation term: $\delta = \widehat{\boldsymbol{\epsilon}}_{j,r}^{(t,b)}$ for SAM and 0 for SGD	$\nabla_{\boldsymbol{\varphi}_i}$, $\nabla_{\boldsymbol{\xi}_i}$	Gradient contributions for the signal and noise in NegGrad updates
$\Delta_{\text{epoch}}^{\text{SAM}}\kappa_{j,r}$	Per-epoch change of $\kappa_{j,r}$ under SAM	$\Delta_{\text{epoch}}^{\text{SGD}}\kappa_{j,r}$	Per-epoch change of $\kappa_{j,r}$ under SGD
$\mathrm{Acc}(\theta, \mathcal{D})$	Classification accuracy model on dataset; $\theta, \mathcal{D}$ are abbreviated terms in $\mathrm{Acc}()$	$\mathrm{ToW}(f_{\mathcal{U}})$	"Tug-of-war" metric combining retain, forget and test accuracies
$\mathcal{D}$	data distribution	$\mathcal{F}_{\text{high}}$	Forget sets of high memorization difficulty; same for mid, low
$\mathrm{mem}(\mathcal{A}, \mathcal{S}, i)$	Memorization score: $\Pr[f(\mathcal{S}) = y_i] - \Pr[f(\mathcal{S} \setminus i) = y_i]$	$\mathcal{S} \setminus i$	Training set $\mathcal{S}$ with sample i removed
$\boldsymbol{\phi}_i$	Feature embedding of sample i used in entanglement analysis	$\boldsymbol{\mu}_{\mathcal{R}}$, $\boldsymbol{\mu}_{\mathcal{F}}$, $\boldsymbol{\mu}$	Mean embeddings of retain set, forget set and all data

Continued on next page

Table 5: (Continued)

Symbol	Meaning / Notes	Symbol	Meaning / Notes
$\mathrm{E}_{\mathrm{Var}}^{\mathrm{All}}(\mathcal{R},\mathcal{F},f)$	Variance-based entanglement measure between $\mathcal{R}$ and $\mathcal{F}$, given model f	$\mathrm{E}_{\mathrm{Var}}^{\mathrm{Cls}}$	Class-wise version of the variance-based entanglement
$\mathrm{E}_{W_p}^{\mathrm{All}}$, $\mathrm{E}_{W_p}^{\mathrm{Cls}}$	Geometry-aware entanglement measures based on Wasserstein distance (all/class-wise)	$\mathcal{A}$, $\mathcal{U}$	Training algorithm (e.g. SGD, SAM) and unlearning algorithm (e.g. NegGrad, RL, with default SGD optimization, can be used with SAM)
$\kappa_{j,r}^{(0,0)}$	Initial signal coefficient for filter (j,r)	$\zeta_{j,r,i}^{(0,0)}$	Initial noise coefficient for sample i on filter (j,r)
$\lvert\mathcal{F}\rvert$, $\lvert\mathcal{R}\rvert$	Cardinalities of the forget and retain sets, which is size in our work	n	Total number of samples ($\lvert\mathcal{S}\rvert$)
$\mathcal{D}_{\text{test}}$	Test dataset used for evaluation	α^{SGD}, α^{SAM}	α weight coeff for SGD and SAM, respectively

D Detailed Formulations and Proofs

We prove our theorems and lemmas based on previous theoretical results in Kou et al. (2023); Chen et al. (2023). Specifically, we prove that with additional yet necessary conditions for effective unlearning, the final test errors can be preserved, while we identify and characterize the changed internal dynamics. We begin by expanding and restating κ, ζ update rule for NegGrad in Eq. 7:

$$\begin{aligned}
\kappa_{j,r}^{(t,b+1)} - \kappa_{j,r}^{(t,b)} &= -\frac{\eta\|\boldsymbol{\varphi}\|_2^2}{Bm}\Bigg[\alpha\sum_{i\in\mathcal{I}_{t,b}^{\mathcal{R}}}\ell_i'^{(t,b)}\sigma'(\langle\mathbf{w}_{j,r}^{(t,b)}+\Delta, y_i\boldsymbol{\varphi}\rangle) \\
&\qquad -(1-\alpha)\sum_{i\in\mathcal{I}_{t,b}^{\mathcal{F}}}\ell_i'^{(t,b)}\sigma'(\langle\mathbf{w}_{j,r}^{(t,b)}+\Delta, y_i\boldsymbol{\varphi}\rangle)\Bigg], \\
\overline{\zeta}_{j,r}^{(t,b+1)} - \overline{\zeta}_{j,r}^{(t,b)} &= -\frac{\eta(P-1)^2}{Bm}\Bigg[\alpha\sum_{i\in\mathcal{I}_{t,b}^{\mathcal{R}}}\|\boldsymbol{\xi}_i\|_2^2\ell_i'^{(t,b)}\sigma'(\langle\mathbf{w}_{j,r}^{(t,b)}+\Delta, \boldsymbol{\xi}_i\rangle)\cdot\mathbb{1}(y_i=j) \\
&\qquad -(1-\alpha)\sum_{i\in\mathcal{I}_{t,b}^{\mathcal{F}}}\|\boldsymbol{\xi}_i\|_2^2\ell_i'^{(t,b)}\sigma'(\langle\mathbf{w}_{j,r}^{(t,b)}+\Delta, \boldsymbol{\xi}_i\rangle)\cdot\mathbb{1}(y_i=j)\Bigg], \\
\underline{\zeta}_{j,r}^{(t,b+1)} - \underline{\zeta}_{j,r}^{(t,b)} &= +\frac{\eta(P-1)^2}{Bm}\Bigg[\alpha\sum_{i\in\mathcal{I}_{t,b}^{\mathcal{R}}}\|\boldsymbol{\xi}_i\|_2^2\ell_i'^{(t,b)}\sigma'(\langle\mathbf{w}_{j,r}^{(t,b)}+\Delta, \boldsymbol{\xi}_i\rangle)\cdot\mathbb{1}(y_i\neq j) \\
&\qquad -(1-\alpha)\sum_{i\in\mathcal{I}_{t,b}^{\mathcal{F}}}\|\boldsymbol{\xi}_i\|_2^2\ell_i'^{(t,b)}\sigma'(\langle\mathbf{w}_{j,r}^{(t,b)}+\Delta, \boldsymbol{\xi}_i\rangle)\cdot\mathbb{1}(y_i\neq j)\Bigg],
\end{aligned} \tag{11}$$

where $\Delta = \widehat{\boldsymbol{\epsilon}}_{j,r}^{(t,b)}$ for SAM and 0 for SGD, $\zeta_{j,r}^{(t,b)}$ is split into $\overline{\zeta}_{j,r}^{(t,b)} := \zeta_{j,r}^{(t,b)}\mathbb{1}(\zeta_{j,r}^{(t,b)} \geq 0)$ and $\underline{\zeta}_{j,r}^{(t,b)} := \zeta_{j,r}^{(t,b)}\mathbb{1}(\zeta_{j,r}^{(t,b)} \leq 0)$ based on label agreement. We summarize several reasonable assumptions from previous work in addition to our conditions which ensure unlearning to progress:

Assumption D.1 *Suppose there exists a sufficiently large constant C, such that the following hold:*

1. *Sufficiently large dimension d:* $d \geq C\max\{n\sigma_p^{-2}\|\boldsymbol{\varphi}\|_2^2\log(T^*), n^2\log(nm/\delta)(\log(T^*))^2\}$, *for some* $T^* = \Omega(\eta^{-1}Bmd^{-1}P^{-2}\sigma_p^{-2})$.

2. *The size of $\mathcal{S}$ and the CNN width satisfy* $n \geq C\log(m/\delta), m \geq C\log(n/\delta)$.
3. *The signal strength satisfies* $\|\boldsymbol{\varphi}\|_2^2 \geq C\sigma_p^2\log(n/\delta)$.
4. *For the Gaussian noise initialization,* $\sigma_0 \leq (C\max\{\sigma_p d/\sqrt{n}, \sqrt{\log(m/\delta)}\cdot\|\boldsymbol{\varphi}\|_2\})^{-1}$.
5. *The learning rate* η *satisfies* $\eta \leq (C\max\{\sigma_p^2 d^{3/2}/(n^2 m\sqrt{\log(n/\delta)}), \sigma_p^2 d/n\})^{-1}$.
6. *Assume cross-entropy loss:* $\ell(z) = \log(1+\exp(-z)) \Longrightarrow \ell' = -1/(1+\exp(z))$.
7. *Assume ReLU activation.*
8. *Assume all clean labels and $\mathcal{F}$ signals do not dominate:* $\alpha \geq |\mathcal{R}|/(|\mathcal{F}|+|\mathcal{R}|) := \beta > 0.5$.

We then obtain several proven quantities from previous work, which are achieved during pretraining and can be leveraged at the start of unlearning:

- $\sum_{i=1}^n \overline{\zeta}_{j,r,i}^{(t)}/\kappa_{j',r'}^{(t)} = \Theta(\mathrm{SNR}^{-2})$, for the signal-to-noise ratio $\mathrm{SNR} = \frac{\|\boldsymbol{\varphi}\|_2}{(P-1)\sigma_p\sqrt{d}}$.
- $\sum_{i=1}^n \overline{\zeta}_{j,r,i}^{(t)} = \Omega(n) = O(n\log(T^*)) = \widetilde{\Theta}(n)$, for some $T^* = \Omega(\eta^{-1}Bmd^{-1}P^{-2}\sigma_p^{-2})$.
- $\max_{j,r,i}|\underline{\zeta}_{j,r,i}^{(t)}| = \max\{O(\sqrt{\log(mn/\delta)}\cdot\sigma_0\sigma_p\sqrt{d}), O(\sqrt{\log(n/\delta)}\log(T^*)\cdot n/\sqrt{d})\}$.
- $\kappa_{j,r}^{(T^*)} = \Theta(\widehat{\kappa})$, where $\widehat{\kappa} = n\cdot\mathrm{SNR}^2$.

D.1 Proof to Theorem 3.2

Under NegGrad, we want to predict retain samples in $\mathcal{R}$ correctly while we count correct predictions in $\mathcal{F}$ as errors, yielding same bounds for $\mathbb{P}_{(\mathbf{x},y)\sim\mathcal{R}}(yf(\mathbf{W}^{(t)},\mathbf{x}) \leq 0)$ and $\mathbb{P}_{(\mathbf{x},y)\sim\mathcal{F}}(yf(\mathbf{W}^{(t)},\mathbf{x}) > 0)$ based on inverse objectives. However, when considering the test error on the model that is jointly updated by gradient descent on $\mathcal{R}$ and gradient ascent on $\mathcal{F}$, we still measure the error rate by wrong predictions. In other words, fitting forget samples will reduce the generalization performance. We can decompose the test error as follows:

$$\begin{aligned}
&\mathbb{P}_{(\mathbf{x},y)\sim\mathcal{D}}\left(y \neq \mathrm{sign}\left(f\left(\mathbf{W}^{(t)},\mathbf{x}\right)\right)\right) = \mathbb{P}_{(\mathbf{x},y)\sim\mathcal{D}}\left(yf\left(\mathbf{W}^{(t)},\mathbf{x}\right) \leq 0\right)\\
=&\mathbb{P}_{(\mathbf{x},y)\sim\mathcal{D}}\left(yf\left(\mathbf{W}^{(t)},\mathbf{x}\right) \leq 0, (\mathbf{x},y)\in\mathcal{R}\right) + \mathbb{P}_{(\mathbf{x},y)\sim\mathcal{D}}\left(yf\left(\mathbf{W}^{(t)},\mathbf{x}\right) \leq 0, (\mathbf{x},y)\in\mathcal{F}\right)\\
=&\beta\cdot\mathbb{P}_{(\mathbf{x},y)\sim\mathcal{R}}\left(yf\left(\mathbf{W}^{(t)},\mathbf{x}\right) \leq 0\right) + (1-\beta)\cdot\mathbb{P}_{(\mathbf{x},y)\sim\mathcal{F}}\left(yf\left(\mathbf{W}^{(t)},\mathbf{x}\right) \leq 0\right)\\
=&\beta\cdot\mathbb{P}_{(\mathbf{x},y)\sim\mathcal{R}}\left(yf\left(\mathbf{W}^{(t)},\mathbf{x}\right) \leq 0\right) + (1-\beta)\cdot\left(1-\mathbb{P}_{(\mathbf{x},y)\sim\mathcal{F}}\left(yf\left(\mathbf{W}^{(t)},\mathbf{x}\right) > 0\right)\right).
\end{aligned} \tag{12}$$

Note that in practice, $\mathcal{R}$ and $\mathcal{F}$ come from training set $\mathcal{S}$. During inference and evaluation, we convert the data augmentations of $\mathcal{R},\mathcal{F}$ to test transforms, thus measuring proxy-test errors on $\mathcal{R}$-like and $\mathcal{F}$-like samples. To bound the test error, first decompose $yf(\mathbf{W}^{(t)},\mathbf{x})$ into signal and noise learning of both positive and negative classes, considering $\Delta = 0$ for SGD:

$$\begin{aligned}
yf\left(\mathbf{W}^{(t)},\mathbf{x}\right) &= \frac{1}{m}\sum_{j,r} yj\left[\sigma\left(\left\langle\mathbf{w}_{j,r}^{(t)}, y\boldsymbol{\varphi}\right\rangle\right) + \sigma\left(\left\langle\mathbf{w}_{j,r}^{(t)},\boldsymbol{\xi}\right\rangle\right)\right]\\
&= \frac{1}{m}\sum_{r}\left[\sigma\left(\left\langle\mathbf{w}_{y,r}^{(t)}, y\boldsymbol{\varphi}\right\rangle\right) + (P-1)\sigma\left(\left\langle\mathbf{w}_{y,r}^{(t)},\boldsymbol{\xi}\right\rangle\right)\right]\\
&\quad - \frac{1}{m}\sum_{r}\left[\sigma\left(\left\langle\mathbf{w}_{-y,r}^{(t)}, y\boldsymbol{\varphi}\right\rangle\right) + (P-1)\sigma\left(\left\langle\mathbf{w}_{-y,r}^{(t)},\boldsymbol{\xi}\right\rangle\right)\right].
\end{aligned} \tag{13}$$

Remark D.2 *The following proof process for bounding $\mathbb{P}_{(\mathbf{x},y)\sim\mathcal{R}}(yf(\mathbf{W}^{(t)},\mathbf{x})$ comes from Kou et al. (2023). We include it here for readability, since we will leverage the results when combining $\mathcal{R}$ and $\mathcal{F}$ in the end, as well as make adaptations for proving Theorem 3.3. Our results benefit from previous work as we consider the unlearning process as an extension of the second stage in Chen et al. (2023).*

We begin by two lemmas that bound the signal, noise norm, and the related inner products:

Lemma D.3 *(Lemma B.4 in Kou et al. (2023)). Suppose that $\delta > 0$ and $d = \Omega(\log(6n/\delta))$. Then with probability at least $1 - \delta$,*

$$\sigma_p^2 d/2 \le \|\boldsymbol{\xi}_i\|_2^2 \le 3\sigma_p^2 d/2,$$
$$|\langle \boldsymbol{\xi}_i, \boldsymbol{\xi}_{i'} \rangle| \le 2\sigma_p^2 \cdot \sqrt{d \log(6n^2/\delta)},$$
$$|\langle \boldsymbol{\xi}_i, \boldsymbol{\varphi} \rangle| \le \|\boldsymbol{\varphi}\|_2 \sigma_p \cdot \sqrt{2\log(6n/\delta)},$$

for all $i, i' \in [n]$.

Lemma D.4 *(Lemma B.5 in Kou et al. (2023)). Suppose that $d = \Omega(\log(mn/\delta)), m = \Omega(\log(1/\delta))$. Then with probability at least $1 - \delta$,*

$$\sigma_0^2 d/2 \le \left\| \mathbf{w}_{j,r}^{(0,0)} \right\|_2^2 \le 3\sigma_0^2 d/2,$$
$$\left| \left\langle \mathbf{w}_{j,r}^{(0,0)}, \boldsymbol{\varphi} \right\rangle \right| \le \sqrt{2\log(12m/\delta)} \cdot \sigma_0 \|\boldsymbol{\varphi}\|_2,$$
$$\left| \left\langle \mathbf{w}_{j,r}^{(0,0)}, \boldsymbol{\xi}_i \right\rangle \right| \le 2\sqrt{\log(12mn/\delta)} \cdot \sigma_0 \sigma_p \sqrt{d},$$

for all $r \in [m], j \in \{\pm 1\}$ and $i \in [n]$. Moreover,

$$\sigma_0 \|\boldsymbol{\varphi}\|_2/2 \le \max_{r \in [m]} j \cdot \left\langle \mathbf{w}_{j,r}^{(0,0)}, \boldsymbol{\varphi} \right\rangle \le \sqrt{2\log(12m/\delta)} \cdot \sigma_0 \|\boldsymbol{\varphi}\|_2,$$
$$\sigma_0 \sigma_p \sqrt{d}/4 \le \max_{r \in [m]} j \cdot \left\langle \mathbf{w}_{j,r}^{(0,0)}, \boldsymbol{\xi}_i \right\rangle \le 2\sqrt{\log(12mn/\delta)} \cdot \sigma_0 \sigma_p \sqrt{d},$$

for all $j \in \{\pm 1\}$ and $i \in [n]$.

Plug in the weight update decomposition in Eq. 2, we can first bound the inner product for $j = y$:

$$\begin{aligned}
&\left\langle \mathbf{w}_{y,r}^{(t)}, y\boldsymbol{\varphi} \right\rangle = \left\langle \mathbf{w}_{y,r}^{(0)}, y\boldsymbol{\varphi} \right\rangle + \kappa_{y,r}^{(t)} \\
&+ \frac{1}{P-1} \sum_{i=1}^{n} \overline{\zeta}_{y,r,i}^{(t)} \|\boldsymbol{\xi}_i\|_2^{-2} \langle \boldsymbol{\xi}_i, y\boldsymbol{\varphi} \rangle + \frac{1}{P-1} \sum_{i=1}^{n} \underline{\zeta}_{y,r,i}^{(t)} \|\boldsymbol{\xi}_i\|_2^{-2} \langle \boldsymbol{\xi}_i, y\boldsymbol{\varphi} \rangle \\
\ge& -\sqrt{2\log(12m/\delta)} \cdot \sigma_0 \|\boldsymbol{\varphi}\|_2 + \kappa_{y,r}^{(t)} \\
&- \frac{\sqrt{2\log(6n/\delta)}}{P-1} \cdot \sigma_p \|\boldsymbol{\varphi}\|_2 \cdot \left(\sigma_p^2 d/2\right)^{-1} \left[\sum_{i=1}^{n} \overline{\zeta}_{y,r,i}^{(t)} + \sum_{i=1}^{n} |\, \underline{\zeta}_{y,r,i}^{(t)} \,| \right] \\
=& -\Theta\left(\sqrt{\log(m/\delta)} \sigma_0 \|\boldsymbol{\varphi}\|_2\right) + \kappa_{y,r}^{(t)} - \Theta\left(\sqrt{\log(n/\delta)} \left(P\sigma_p d\right)^{-1} \|\boldsymbol{\varphi}\|_2\right) \cdot \Theta\left(\mathrm{SNR}^{-2}\right) \cdot \kappa_{y,r}^{(t)} \\
=& -\Theta\left(\sqrt{\log(m/\delta)} \left(\sigma_p d\right)^{-1} \sqrt{n} \|\boldsymbol{\varphi}\|_2\right) + \left[1 - \Theta\left(\sqrt{\log(n/\delta)} \cdot P\sigma_p / \|\boldsymbol{\varphi}\|_2\right)\right] \kappa_{y,r}^{(t)} \\
=& \Theta\left(\kappa_{y,r}^{(t)}\right),
\end{aligned} \tag{14}$$

where the inequality is by Lemma D.3 and Lemma D.4; the second equality is obtained by plugging in the coefficient orders we summarized at the beginning of the section; the third equality is by $\sigma_0 \le C^{-1}(\sigma_p d)^{-1}\sqrt{n}$ in Assumption D.1 and $\mathrm{SNR} = \|\boldsymbol{\varphi}\|_2/((P-1)\sigma_p\sqrt{d})$. The fourth equality is by $\kappa_{j,r}^{(t)} = \Theta(\widehat{\kappa})$, where $\widehat{\kappa} = n \cdot \mathrm{SNR}^2$. Also $\sqrt{\log(n/\delta)} \cdot \sigma_p/\|\boldsymbol{\varphi}\|_2 \le 1/\sqrt{C}$ and $\sqrt{\log(m/\delta)}(\sigma_p d)^{-1}\sqrt{n}\|\boldsymbol{\varphi}\|_2/\widehat{\kappa} = \sqrt{\log(m/\delta)}\sigma_p/(\sqrt{n}\|\boldsymbol{\varphi}\|_2) \le \sqrt{\log(m/\delta)/n} \cdot 1/(\sqrt{C\log(n/\delta)}) \le 1/(C\sqrt{\log(n/\delta)})$ holds by $\|\varphi\|_2^2 \ge C \cdot \sigma_p^2 \log(n/\delta)$ and $n \ge C\log(m/\delta)$ in Assumption D.1, so for sufficiently large constant C the equality holds. Similarly, we can show that $\langle \mathbf{w}_{-y,r}^{(t)}, y\boldsymbol{\varphi} \rangle = -\Theta(\kappa_{y,r}^{(t)}) < 0$ for $j \ne y$.

Next denote $g(\boldsymbol{\xi})$ as $\sum_r \sigma(\langle \mathbf{w}_{-y,r}^{(t)}, \boldsymbol{\xi} \rangle)$. Since $\boldsymbol{\xi} \sim \mathcal{N}(\mathbf{0}, \sigma_p^2 \mathbf{I})$, we can leverage the Gaussian concentration bound for $x \ge 0$:

$$\mathbb{P}(g(\boldsymbol{\xi}) - \mathbb{E}g(\boldsymbol{\xi}) \ge x) \le \exp\left(-\frac{cx^2}{\sigma_p^2 \|g\|_{\mathrm{Lip}}^2}\right), \tag{15}$$

where c is a constant. To calculate the Lipschitz norm, we have

$$\begin{aligned}|g(\boldsymbol{\xi}) - g(\boldsymbol{\xi}')| &= \left|\sum_{r=1}^{m}\sigma\left(\left\langle \mathbf{w}_{-y,r}^{(t)}, \boldsymbol{\xi}\right\rangle\right) - \sum_{r=1}^{m}\sigma\left(\left\langle \mathbf{w}_{-y,r}^{(t)}, \boldsymbol{\xi}'\right\rangle\right)\right| \\ &\le \sum_{r=1}^{m}\left|\sigma\left(\left\langle \mathbf{w}_{-y,r}^{(t)}, \boldsymbol{\xi}\right\rangle\right) - \sigma\left(\left\langle \mathbf{w}_{-y,r}^{(t)}, \boldsymbol{\xi}'\right\rangle\right)\right| \\ &\le \sum_{r=1}^{m}\left|\left\langle \mathbf{w}_{-y,r}^{(t)}, \boldsymbol{\xi} - \boldsymbol{\xi}'\right\rangle\right| \le \sum_{r=1}^{m}\left\|\mathbf{w}_{-y,r}^{(t)}\right\|_2 \cdot \|\boldsymbol{\xi} - \boldsymbol{\xi}'\|_2 .\end{aligned} \tag{16}$$

The first inequality is by triangle inequality; the second inequality is by the property of ReLU; the last inequality is by Cauchy-Schwartz inequality. Therefore, we have $\|g\|_{\mathrm{Lip}} \le \sum_{r=1}^{m}\|\mathbf{w}_{-y,r}^{(t)}\|_2$, and since $\langle \mathbf{w}_{-y,r}^{(t)}, \boldsymbol{\xi}\rangle \sim \mathcal{N}(0, \|\mathbf{w}_{-y,r}^{(t)}\|_2^2\sigma_p^2)$, we can get

$$\mathbb{E}g(\boldsymbol{\xi}) = \sum_{r=1}^{m}\mathbb{E}\sigma\left(\left\langle \mathbf{w}_{-y,r}^{(t)}, \boldsymbol{\xi}\right\rangle\right) = \sum_{r=1}^{m}\frac{\left\|\mathbf{w}_{-y,r}^{(t)}\right\|_2\sigma_p}{\sqrt{2\pi}} = \frac{\sigma_p}{\sqrt{2\pi}}\sum_{r=1}^{m}\left\|\mathbf{w}_{-y,r}^{(t)}\right\|_2 . \tag{17}$$

Then, we seek to upper bound the 2-norm of $\mathbf{w}_{j,r}^{(t)}$. First we have

$$\begin{aligned}&\left\|\sum_{i=1}^{n}\zeta_{j,r,i}^{(t)}\cdot\|\boldsymbol{\xi}_i\|_2^{-2}\cdot\boldsymbol{\xi}_i\right\|_2^2 \\ =&\underbrace{\sum_{i=1}^{n}{\zeta_{j,r,i}^{(t)}}^2\cdot\|\boldsymbol{\xi}_i\|_2^{-2}}_{\text{diagonal}} + \underbrace{2\sum_{1\le i_1<i_2\le n}\zeta_{j,r,i_1}^{(t)}\zeta_{j,r,i_2}^{(t)}\cdot\|\boldsymbol{\xi}_{i_1}\|_2^{-2}\|\boldsymbol{\xi}_{i_2}\|_2^{-2}\cdot\langle\boldsymbol{\xi}_{i_1},\boldsymbol{\xi}_{i_2}\rangle}_{\text{off-diagonal}} \\ \le&4\sigma_p^{-2}d^{-1}\sum_{i=1}^{n}{\zeta_{j,r,i}^{(t)}}^2 + 2\sum_{1\le i_1<i_2\le n}\left|\zeta_{j,r,i_1}^{(t)}\zeta_{j,r,i_2}^{(t)}\right|\cdot\left(16\sigma_p^{-4}d^{-2}\right)\cdot\left(2\sigma_p^2\sqrt{d\log\left(6n^2/\delta\right)}\right) \\ =&4\sigma_p^{-2}d^{-1}\sum_{i=1}^{n}{\zeta_{j,r,i}^{(t)}}^2 + 32\sigma_p^{-2}d^{-3/2}\sqrt{\log\left(6n^2/\delta\right)}\left[\left(\sum_{i=1}^{n}\left|\zeta_{j,r,i}^{(t)}\right|\right)^2 - \sum_{i=1}^{n}{\zeta_{j,r,i}^{(t)}}^2\right] \\ =&\Theta\left(\sigma_p^{-2}d^{-1}\right)\sum_{i=1}^{n}{\zeta_{j,r,i}^{(t)}}^2 + \widetilde{\Theta}\left(\sigma_p^{-2}d^{-3/2}\right)\left(\sum_{i=1}^{n}\left|\zeta_{j,r,i}^{(t)}\right|\right)^2 \\ \le&\left[\Theta\left(\sigma_p^{-2}d^{-1}n^{-1}\right) + \widetilde{\Theta}\left(\sigma_p^{-2}d^{-3/2}\right)\right]\left(\sum_{i=1}^{n}\left|\overline{\zeta}_{j,r,i}^{(t)}\right| + \sum_{i=1}^{n}\left|\underline{\zeta}_{j,r,i}^{(t)}\right|\right)^2 \\ \le&\Theta\left(\sigma_p^{-2}d^{-1}n^{-1}\right)\left(\sum_{i=1}^{n}\overline{\zeta}_{j,r,i}^{(t)}\right)^2 .\end{aligned} \tag{18}$$

The first inequality is by Lemma D.3; for the second inequality we used the definition of $\overline{\zeta}, \underline{\zeta}$; for the second to last equation we plugged in coefficient orders. We can thus upper bound the 2-norm of $\mathbf{w}_{j,r}^{(t)}$ as:

$$\begin{aligned}\left\|\mathbf{w}_{j,r}^{(t)}\right\|_2 &\le \left\|\mathbf{w}_{j,r}^{(0)}\right\|_2 + \kappa_{j,r}^{(t)}\cdot\|\boldsymbol{\varphi}\|_2^{-1} + \frac{1}{P-1}\left\|\sum_{i=1}^{n}\zeta_{j,r,i}^{(t)}\cdot\|\boldsymbol{\xi}_i\|_2^{-2}\cdot\boldsymbol{\xi}_i\right\|_2 \\ &\le \left\|\mathbf{w}_{j,r}^{(0)}\right\|_2 + \kappa_{j,r}^{(t)}\cdot\|\boldsymbol{\varphi}\|_2^{-1} + \Theta\left(P^{-1}\sigma_p^{-1}d^{-1/2}n^{-1/2}\right)\cdot\sum_{i=1}^{n}\overline{\zeta}_{j,r,i}^{(t)} \\ &= \Theta\left(P^{-1}\sigma_p^{-1}d^{-1/2}n^{-1/2}\right)\cdot\sum_{i=1}^{n}\overline{\zeta}_{j,r,i}^{(t)},\end{aligned} \tag{19}$$

where the first inequality is due to the triangle inequality, and the equality is due to the following:

$$\begin{aligned}&\frac{\kappa_{j,r}^{(t)} \cdot \|\boldsymbol{\varphi}\|_2^{-1}}{\Theta\left(P^{-1}\sigma_p^{-1}d^{-1/2}n^{-1/2}\right) \cdot \sum_{i=1}^n \overline{\zeta}_{j,r,i}^{(t)}} = \Theta\left(P^{-1}\sigma_p d^{1/2}n^{1/2}\|\boldsymbol{\varphi}\|_2^{-1}\mathrm{SNR}^2\right)\\ =&\Theta\left(P^{-1}\sigma_p^{-1}d^{-1/2}n^{1/2}\|\boldsymbol{\varphi}\|_2\right) = O(1),\end{aligned} \tag{20}$$

based on the coefficient order $\sum_{i=1}^n \overline{\zeta}_{j,r,i}^{(t)}/\kappa_{j,r}^{(t)} = \Theta(\mathrm{SNR}^{-2})$, the definition of SNR, and the condition for d in Assumption D.1. Similarly,

$$\begin{aligned}&\frac{\left\|\mathbf{w}_{j,r}^{(0)}\right\|_2}{\Theta\left(P^{-1}\sigma_p^{-1}d^{-1/2}n^{-1/2}\right) \cdot \sum_{i=1}^n \overline{\zeta}_{j,r,i}^{(t)}} = \frac{\Theta\left(\sigma_0\sqrt{d}\right)}{\Theta\left(P^{-1}\sigma_p^{-1}d^{-1/2}n^{-1/2}\right) \cdot \sum_{i=1}^n \overline{\zeta}_{j,r,i}^{(t)}}\\ =&O\left(P\sigma_0\sigma_p d n^{-1/2}\right) = O(1),\end{aligned} \tag{21}$$

based on Lemma D.4, the coefficient order $\sum_{i=1}^n \overline{\zeta}_{j,r,i}^{(t)} = \Omega(n)$, and the condition for σ_0 in Assumption D.1. Then we can give an analysis of the following key component:

$$\begin{aligned}\frac{\sum_r \sigma\left(\left\langle \mathbf{w}_{y,r}^{(t)}, y\boldsymbol{\varphi}\right\rangle\right)}{(P-1)\sigma_p \sum_{r=1}^m \left\|\mathbf{w}_{-y,r}^{(t)}\right\|_2} \geq& \frac{\Theta\left(\sum_r \kappa_{y,r}^{(t)}\right)}{\Theta\left(d^{-1/2}n^{-1/2}\right) \cdot \sum_{r,i} \overline{\zeta}_{-y,r,i}^{(t)}}\\ =&\Theta\left(d^{1/2}n^{1/2}\mathrm{SNR}^2\right) = \Theta\left(n^{1/2}\|\boldsymbol{\varphi}\|_2^2/(P^2\sigma_p^2 d^{1/2})\right).\end{aligned} \tag{22}$$

Then for $\|\boldsymbol{\varphi}\|_2 \geq C_1^{1/4} n^{-1/4} P\sigma_p d^{1/4}$ for some large constant C_1, we have

$$\sum_r \sigma\left(\left\langle \mathbf{w}_{y,r}^{(t)}, y\boldsymbol{\varphi}\right\rangle\right) - \frac{(P-1)\sigma_p}{\sqrt{2\pi}} \sum_{r=1}^m \left\|\mathbf{w}_{-y,r}^{(t)}\right\|_2 > 0. \tag{23}$$

Upper bound. Now plug in previous results to obtain

$$\begin{aligned}&\mathbb{P}_{(\mathbf{x},y)\sim\mathcal{R}}\left(yf\left(\mathbf{W}^{(t)},\mathbf{x}\right) \leq 0\right) \leq \mathbb{P}_{(\mathbf{x},y)\sim\mathcal{R}}\left((P-1)\sum_r \sigma\left(\left\langle \mathbf{w}_{-y,r}^{(t)}, \boldsymbol{\xi}\right\rangle\right) \geq \sum_r \sigma\left(\left\langle \mathbf{w}_{y,r}^{(t)}, y\boldsymbol{\varphi}\right\rangle\right)\right)\\ =&\mathbb{P}_{(\mathbf{x},y)\sim\mathcal{R}}\left(g(\boldsymbol{\xi}) - \mathbb{E}g(\boldsymbol{\xi}) \geq 1/(P-1)\sum_r \sigma\left(\left\langle \mathbf{w}_{y,r}^{(t)}, y\boldsymbol{\varphi}\right\rangle\right) - \frac{\sigma_p}{\sqrt{2\pi}}\sum_{r=1}^m \left\|\mathbf{w}_{-y,r}^{(t)}\right\|_2\right)\\ \leq&\exp\left[-\frac{c\left(1/(P-1)\sum_r \sigma\left(\left\langle \mathbf{w}_{y,r}^{(t)}, y\boldsymbol{\varphi}\right\rangle\right) - \left(\sigma_p/\sqrt{2\pi}\right)\sum_{r=1}^m \left\|\mathbf{w}_{-y,r}^{(t)}\right\|_2\right)^2}{\sigma_p^2\left(\sum_{r=1}^m \left\|\mathbf{w}_{-y,r}^{(t)}\right\|_2\right)^2}\right]\\ =&\exp\left[-c\left(\frac{\sum_r \sigma\left(\left\langle \mathbf{w}_{y,r}^{(t)}, y\boldsymbol{\varphi}\right\rangle\right)}{(P-1)\sigma_p\sum_{r=1}^m \left\|\mathbf{w}_{-y,r}^{(t)}\right\|_2} - 1/\sqrt{2\pi}\right)^2\right]\\ \leq&\exp(c/2\pi)\exp\left(-0.5c\left(\frac{\sum_r \sigma\left(\left\langle \mathbf{w}_{y,r}^{(t)}, y\boldsymbol{\varphi}\right\rangle\right)}{(P-1)\sigma_p\sum_{r=1}^m \left\|\mathbf{w}_{-y,r}^{(t)}\right\|_2}\right)^2\right).\end{aligned} \tag{24}$$

The second inequality is by Eq. 23 and plugging $\|g\|_{\text{Lip}} \leq \sum_{r=1}^{m} \|\mathbf{w}_{-y,r}^{(t)}\|_2$ into Eq. 15; the third inequality is due to $(s-t)^2 \geq s^2/2 - t^2, \forall s,t \geq 0$. And from Eq. 22 and Eq. 24 we have

$$\begin{aligned}
\mathbb{P}_{(\mathbf{x},y)\sim\mathcal{R}}\left(yf\left(\mathbf{W}^{(t)},\mathbf{x}\right)\leq 0\right) &\leq \exp(c/2\pi)\exp\left(-0.5c\left(\frac{\sum_r \sigma\left(\left\langle \mathbf{w}_{y,r}^{(t)}, y\boldsymbol{\varphi}\right\rangle\right)}{(P-1)\sigma_p\sum_{r=1}^{m}\left\|\mathbf{w}_{-y,r}^{(t)}\right\|_2}\right)^2\right) \\
&= \exp\left(\frac{c}{2\pi} - \frac{n\|\boldsymbol{\varphi}\|_2^4}{C(P-1)^4\sigma_p^4 d}\right) \\
&\leq \exp\left(-\frac{n\|\boldsymbol{\varphi}\|_2^4}{2C_1(P-1)^4\sigma_p^4 d}\right) \\
&= \exp\left(-\frac{n\|\boldsymbol{\varphi}\|_2^4}{C_2(P-1)^4\sigma_p^4 d}\right) = \epsilon,
\end{aligned} \tag{25}$$

where $C = O(1)$; the last inequality holds if we choose $C_1 \geq cC/\pi$; the last equality holds if we choose C_2 as $2C$.

For the forget set $\mathcal{F}$, we thus have

$$\mathbb{P}_{(\mathbf{x},y)\sim\mathcal{F}}\left(yf\left(\mathbf{W}^{(t)},\mathbf{x}\right)>0\right)\leq\epsilon. \tag{26}$$

Lower bound. Without loss of generality, let $\sum_r \kappa_{1,r}^{(t)} = \max\left\{\sum_r \kappa_{1,r}^{(t)}, \sum_r \kappa_{-1,r}^{(t)}\right\}$. Denote $\mathbf{v} = \lambda\cdot\sum_i \mathbb{1}\left(y_i=1\right)\boldsymbol{\xi}_i$, where $\lambda = C_7\text{SNR}^2 = C_7\|\boldsymbol{\varphi}\|_2^2/\left((P-1)^2\sigma_p^2 d\right)$ and C_7 is a sufficiently large constant. Since ReLU is convex, we have

$$\begin{aligned}
\sigma\left(\left\langle \mathbf{w}_{1,r}^{(t)}, \boldsymbol{\xi}+\mathbf{v}\right\rangle\right) - \sigma\left(\left\langle \mathbf{w}_{1,r}^{(t)}, \boldsymbol{\xi}\right\rangle\right) &\geq \sigma'\left(\left\langle \mathbf{w}_{1,r}^{(t)}, \boldsymbol{\xi}\right\rangle\right)\left\langle \mathbf{w}_{1,r}^{(t)}, \mathbf{v}\right\rangle, \\
\sigma\left(\left\langle \mathbf{w}_{1,r}^{(t)}, -\boldsymbol{\xi}+\mathbf{v}\right\rangle\right) - \sigma\left(\left\langle \mathbf{w}_{1,r}^{(t)}, -\boldsymbol{\xi}\right\rangle\right) &\geq \sigma'\left(\left\langle \mathbf{w}_{1,r}^{(t)}, -\boldsymbol{\xi}\right\rangle\right)\left\langle \mathbf{w}_{1,r}^{(t)}, \mathbf{v}\right\rangle.
\end{aligned} \tag{27}$$

Summing the above two, we have that almost surely for all $\boldsymbol{\xi}$

$$\begin{aligned}
&\sigma\left(\left\langle \mathbf{w}_{1,r}^{(t)}, \boldsymbol{\xi}+\mathbf{v}\right\rangle\right) - \sigma\left(\left\langle \mathbf{w}_{1,r}^{(t)}, \boldsymbol{\xi}\right\rangle\right) + \sigma\left(\left\langle \mathbf{w}_{1,r}^{(t)}, -\boldsymbol{\xi}+\mathbf{v}\right\rangle\right) - \sigma\left(\left\langle \mathbf{w}_{1,r}^{(t)}, -\boldsymbol{\xi}\right\rangle\right) \\
&\geq \left\langle \mathbf{w}_{1,r}^{(t)}, \mathbf{v}\right\rangle \\
&\geq \lambda\left[\sum_{y_i=1}\bar{\zeta}_{1,r,i}^{(t)} - 2n\sqrt{\log(12mn/\delta)}\cdot\sigma_0\sigma_p\sqrt{d} - 5n^2\alpha\sqrt{\log\left(6n^2/\delta\right)/d}\right],
\end{aligned} \tag{28}$$

where the last inequality is by Lemma C.3 in Kou et al. (2023) and Lemma D.4. Additionally, since ReLU is a Liptchitz, we also have that

$$\begin{aligned}
&\sigma\left(\left\langle \mathbf{w}_{-1,r}^{(t)}, \boldsymbol{\xi}+\mathbf{v}\right\rangle\right) - \sigma\left(\left\langle \mathbf{w}_{-1,r}^{(t)}, \boldsymbol{\xi}\right\rangle\right) + \sigma\left(\left\langle \mathbf{w}_{-1,r}^{(t)}, -\boldsymbol{\xi}+\mathbf{v}\right\rangle\right) - \sigma\left(\left\langle \mathbf{w}_{-1,r}^{(t)}, -\boldsymbol{\xi}\right\rangle\right) \\
&\leq 2\left|\left\langle \mathbf{w}_{-1,r}^{(t)}, \mathbf{v}\right\rangle\right| \\
&\leq 2\lambda\left[\sum_{y_i=1}\zeta_{-1,r,i}^{(t)} + 2n\sqrt{\log(12mn/\delta)}\cdot\sigma_0\sigma_p\sqrt{d} + 5n^2\alpha\sqrt{\log\left(6n^2/\delta\right)/d}\right].
\end{aligned} \tag{29}$$

Therefore, by plugging Eq. 28 and Eq. 29, we have that

$$\begin{aligned}
&g(\boldsymbol{\xi}+\mathbf{v})-g(\boldsymbol{\xi})+g(-\boldsymbol{\xi}+\mathbf{v})-g(-\boldsymbol{\xi}) \\
&\geq \lambda\left[\sum_r\sum_{y_i=1}\overline{\zeta}_{1,r,i}^{(t)}-6nm\sqrt{\log(12mn/\delta)}\cdot\sigma_0\sigma_p\sqrt{d}-15mn^2\alpha\sqrt{\log\left(6n^2/\delta\right)/d}\right] \\
&\geq (\lambda/2)\cdot\sum_r\sum_{y_i=1}\overline{\zeta}_{1,r,i}^{(t)} \\
&\geq \lambda/2\cdot\Theta\left(\mathrm{SNR}^{-2}\right)\sum_r\kappa_{1,r}^{(t)} \\
&\geq 4C_6\sum_r\kappa_{1,r}^{(t)},
\end{aligned} \tag{30}$$

where the second inequality is by Lemma D.1 in Kou et al. (2023) and Assumption D.1; the third inequality is by $\sum_{i=1}^n\overline{\zeta}_{j,r,i}^{(t)}/\kappa_{j',r'}^{(t)}=\Theta(\mathrm{SNR}^{-2})$. Finally, it is worth noting that the norm

$$\|\mathbf{v}\|_2=\left\|\lambda\cdot\sum_i\mathbb{1}\left(y_i=1\right)\boldsymbol{\xi}_i\right\|_2=\Theta\left(\sqrt{\frac{n\|\boldsymbol{\varphi}\|_2^4}{P^4\sigma_p^4d}}\right)\leq 0.06\sigma_p. \tag{31}$$

where the last inequality is by condition $\|\boldsymbol{\varphi}\|_2\leq C_3d^{1/4}n^{-1/4}P\sigma_p$ with sufficiently large C_3. Then we present a Lemma which bounds the Total Variation (TV) distance between two Gaussian with the same covariance matrix.

Lemma D.5 *(Proposition 2.1 by Devroye et al. (2018)). The TV distance between $\mathcal{N}\left(0,\sigma_p^2\mathbf{I}_d\right)$ and $\mathcal{N}\left(\mathbf{v},\sigma_p^2\mathbf{I}_d\right)$ is smaller than $\|\mathbf{v}\|_2/2\sigma_p$.*

Finally, we can prove the lower bound for $\mathcal{R}$:

$$\begin{aligned}
&\mathbb{P}_{(\mathbf{x},y)\sim\mathcal{R}}\left(yf\left(\mathbf{W}^{(t)},\mathbf{x}\right)\leq 0\right) \\
=&\mathbb{P}_{(\mathbf{x},y)\sim\mathcal{R}}\left(\sum_r\sigma\left(\left\langle\mathbf{w}_{-y,r}^{(t)},\boldsymbol{\xi}\right\rangle\right)-\sum_r\sigma\left(\left\langle\mathbf{w}_{y,r}^{(t)},\boldsymbol{\xi}\right\rangle\right)\geq\sum_r\sigma\left(\left\langle\mathbf{w}_{y,r}^{(t)},y\boldsymbol{\varphi}\right\rangle\right)-\sum_r\sigma\left(\left\langle\mathbf{w}_{-y,r}^{(t)},y\boldsymbol{\varphi}\right\rangle\right)\right) \\
\geq&0.5\mathbb{P}_{(\mathbf{x},y)\sim\mathcal{R}}\left(\left|\sum_r\sigma\left(\left\langle\mathbf{w}_{-y,r}^{(t)},\boldsymbol{\xi}\right\rangle\right)-\sum_r\sigma\left(\left\langle\mathbf{w}_{y,r}^{(t)},\boldsymbol{\xi}\right\rangle\right)\right|\geq C_6\max\left\{\sum_r\kappa_{1,r}^{(t)},\sum_r\kappa_{-1,r}^{(t)}\right\}\right),
\end{aligned} \tag{32}$$

where C_6 is a constant, the inequality holds since if $|\sum_r\sigma(\langle\mathbf{w}_{1,r}^{(t)},\boldsymbol{\xi}\rangle)-\sum_r\sigma(\langle\mathbf{w}_{-1,r}^{(t)},\boldsymbol{\xi}\rangle)|$ is too large, we can always pick a corresponding y given $\boldsymbol{\xi}$ to make a wrong prediction.

Let $g(\boldsymbol{\xi})=\sum_r\sigma(\langle\mathbf{w}_{1,r}^{(t)},\boldsymbol{\xi}\rangle)-\sum_r\sigma(\langle\mathbf{w}_{-1,r}^{(t)},\boldsymbol{\xi}\rangle)$, and denote the set $\Omega:=\{\boldsymbol{\xi}\mid|g(\boldsymbol{\xi})|\geq C_6\max\{\sum_r\kappa_{1,r}^{(t)},\sum_r\kappa_{-1,r}^{(t)}\}\}$. Thus we have

$$\mathbb{P}_{(\mathbf{x},y)\sim\mathcal{R}}\left(yf\left(\boldsymbol{W}^{(t)},\mathbf{x}\right)\leq 0\right)\geq 0.5\mathbb{P}(\Omega). \tag{33}$$

By Lemma 5.8 of Kou et al. (2023), we have that $\sum_j[g(j\boldsymbol{\xi}+\mathbf{v})-g(j\boldsymbol{\xi})]\geq 4C_6\max_j\left\{\sum_r\kappa_{j,r}^{(t)}\right\}$. Therefore, by pigeonhole principle, one of $[\boldsymbol{\xi},-\boldsymbol{\xi},\boldsymbol{\xi}+\mathbf{v},-\boldsymbol{\xi}+\mathbf{v}]$ must belong to Ω, thus $\Omega\cup-\Omega\cup\Omega-\{\mathbf{v}\}\cup-\Omega-\{\mathbf{v}\}=\mathbb{R}^d$. Therefore, at least one of $\mathbb{P}(\Omega),\mathbb{P}(-\Omega),\mathbb{P}(\Omega-\{\mathbf{v}\}),\mathbb{P}(-\Omega-\{\mathbf{v}\})$ is greater than $\frac{1}{4}$. Note that $\mathbb{P}(-\Omega)=\mathbb{P}(\Omega)$ and

$$\begin{aligned}
|\mathbb{P}(\Omega)-\mathbb{P}(\Omega-\mathbf{v})|&=\left|\mathbb{P}_{\boldsymbol{\xi}\sim\mathcal{N}\left(0,\sigma_p^2\mathbf{I}_d\right)}(\boldsymbol{\xi}\in\Omega)-\mathbb{P}_{\boldsymbol{\xi}\sim\mathcal{N}\left(\mathbf{v},\sigma_p^2\mathbf{I}_d\right)}(\boldsymbol{\xi}\in\Omega)\right| \\
&\leq\mathrm{TV}\left(\mathcal{N}\left(0,\sigma_p^2\mathbf{I}_d\right),\mathcal{N}\left(\mathbf{v},\sigma_p^2\mathbf{I}_d\right)\right) \\
&\leq\frac{\|\mathbf{v}\|_2}{2\sigma_p}\leq 0.03,
\end{aligned} \tag{34}$$

where the first inequality is by the definition of TV distance, the second inequality is by Lemma D.5. Hence, we have that $\mathbb{P}(\Omega) \geq \frac{1}{4} - 0.03 = 0.22$, and plugging this into Eq. 33, we get

$$\mathbb{P}_{(\mathbf{x},y)\sim\mathcal{R}}\left(yf\left(\mathbf{W}^{(t)},\mathbf{x}\right)\leq 0\right) \geq 0.5\mathbb{P}(\Omega) = 0.11 \geq 0.1. \tag{35}$$

Like the upper bound, the derived lower bounds also applies to $\mathbb{P}_{(\mathbf{x},y)\sim\mathcal{F}}(yf(\mathbf{W}^{(t)},\mathbf{x})>0)$. Hence, if $\|\boldsymbol{\varphi}\|_2 \geq C_1 d^{1/4} n^{-1/4} P\sigma_p$,

$$\begin{aligned}
&\mathcal{L}^{\text{test}}(\mathbf{W}^{T_2},\mathcal{D}) = \mathbb{P}_{(\mathbf{x},y)\sim\mathcal{D}}\left(y\neq \operatorname{sign}\left(f\left(\mathbf{W}^{T_2},\mathbf{x}\right)\right)\right)\\
=&\beta\cdot\underbrace{\mathbb{P}_{(\mathbf{x},y)\sim\mathcal{R}}\left(yf\left(\mathbf{W}^{T_2},\mathbf{x}\right)\leq 0\right)}_{\leq\epsilon_{\mathcal{R}}} + (1-\beta)\cdot\left(1-\underbrace{\mathbb{P}_{(\mathbf{x},y)\sim\mathcal{F}}\left(yf\left(\mathbf{W}^{T_2},\mathbf{x}\right)>0\right)}_{\leq\epsilon_{\mathcal{F}}}\right)\\
\Longrightarrow&\lim_{\beta\to 1}\mathcal{L}^{\text{test}}(\mathbf{W}^{T_2},\mathcal{D}) \leq \epsilon_{\mathcal{R}} = \epsilon.
\end{aligned} \tag{36}$$

On the other hand, when $\beta \to 0.5$, we have $\lim_{\beta\to 0.5}\mathcal{L}^{\text{test}}(\mathbf{W}^{T_2},\mathcal{D}) \leq 0.5 + 0.5\epsilon_{\mathcal{R}} - 0.5\epsilon_{\mathcal{F}} = \epsilon$. Depending on the size ratio of $\mathcal{R}$ and $\mathcal{F}$, ϵ ranges from a very small constant to a minimally PAC-learnable threshold.

For harmful overfitting where $\|\boldsymbol{\varphi}\|_2 \leq C_3 d^{1/4} n^{-1/4} P\sigma_p$,

$$\begin{aligned}
&\mathcal{L}^{\text{test}}(\mathbf{W}^{T_2},\mathcal{D}) = \mathbb{P}_{(\mathbf{x},y)\sim\mathcal{D}}\left(y\neq \operatorname{sign}\left(f\left(\mathbf{W}^{T_2},\mathbf{x}\right)\right)\right)\\
=&\beta\cdot\underbrace{\mathbb{P}_{(\mathbf{x},y)\sim\mathcal{R}}\left(yf\left(\mathbf{W}^{T_2},\mathbf{x}\right)\leq 0\right)}_{\geq 0.1} + (1-\beta)\cdot\left(1-\underbrace{\mathbb{P}_{(\mathbf{x},y)\sim\mathcal{F}}\left(yf\left(\mathbf{W}^{T_2},\mathbf{x}\right)>0\right)}_{\geq 0.1}\right)\\
\Longrightarrow&\lim_{\beta\to 1}\mathcal{L}^{\text{test}}(\mathbf{W}^{T_2},\mathcal{D}) \geq 0.1.
\end{aligned} \tag{37}$$

On the other hand, when $\beta \to 0.5$, we have $\lim_{\beta\to 0.5}\mathcal{L}^{\text{test}}(\mathbf{W}^{T_2},\mathcal{D}) \geq 0.05$.

D.2 Proof to Theorem 3.3

First we have the same decomposition for NegGrad:

$$\begin{aligned}
\mathcal{L}^{\text{test}}(\mathbf{W}^{T_2},\mathcal{D}) =&\mathbb{P}_{(\mathbf{x},y)\sim\mathcal{D}}\left(y\neq\operatorname{sign}\left(f\left(\mathbf{W}^{(t)},\mathbf{x}\right)\right)\right)\\
=&\beta\cdot\mathbb{P}_{(\mathbf{x},y)\sim\mathcal{R}}\left(yf\left(\mathbf{W}^{(t)},\mathbf{x}\right)\leq 0\right) + (1-\beta)\cdot\left(1-\mathbb{P}_{(\mathbf{x},y)\sim\mathcal{F}}\left(yf\left(\mathbf{W}^{(t)},\mathbf{x}\right)>0\right)\right);\\
yf\left(\mathbf{W}^{(t)},\mathbf{x}\right) =&\frac{1}{m}\sum_{j,r} yj\left[\sigma\left(\left\langle\mathbf{w}_{j,r}^{(t)},y\boldsymbol{\varphi}\right\rangle\right)+\sigma\left(\left\langle\mathbf{w}_{j,r}^{(t)},\boldsymbol{\xi}\right\rangle\right)\right]\\
=&\frac{1}{m}\sum_{r}\left[\sigma\left(\left\langle\mathbf{w}_{y,r}^{(t)},y\boldsymbol{\varphi}\right\rangle\right)+(P-1)\sigma\left(\left\langle\mathbf{w}_{y,r}^{(t)},\boldsymbol{\xi}\right\rangle\right)\right]\\
&-\frac{1}{m}\sum_{r}\left[\sigma\left(\left\langle\mathbf{w}_{-y,r}^{(t)},y\boldsymbol{\varphi}\right\rangle\right)+(P-1)\sigma\left(\left\langle\mathbf{w}_{-y,r}^{(t)},\boldsymbol{\xi}\right\rangle\right)\right].
\end{aligned} \tag{38}$$

However, note that for $(\mathbf{x},y)\sim\mathcal{F}$, SAM gives up its denoising property. We first show this by proving Lemma 3.1.

D.2.1 Proof to Lemma 3.1

Proof. Consider extending Lemma D.5 in Chen et al. (2023) to the NegGrad setting by rewriting $\left\langle\widehat{\boldsymbol{\epsilon}}_{j,r}^{(t,b)},\boldsymbol{\xi}_k\right\rangle$. First we have the Frobenius norm upper bounded by the same quantity:

$$\begin{aligned}
\|\nabla_{\mathbf{W}}\mathcal{L}_{\mathcal{I}_{t,b}}(\mathbf{W}^{(t,b)})\|_F &= \|\alpha\nabla_{\mathbf{W}}\mathcal{L}_{\mathcal{I}_{t,b}^{\mathcal{R}}}(\mathbf{W}^{(t,b)}) - (1-\alpha)\nabla_{\mathbf{W}}\mathcal{L}_{\mathcal{I}_{t,b}^{\mathcal{F}}}(\mathbf{W}^{(t,b)})\|_F\\
&\leq \alpha\|\nabla_{\mathbf{W}}\mathcal{L}_{\mathcal{I}_{t,b}^{\mathcal{R}}}(\mathbf{W}^{(t,b)})\|_F + (1-\alpha)\|\nabla_{\mathbf{W}}\mathcal{L}_{\mathcal{I}_{t,b}^{\mathcal{F}}}(\mathbf{W}^{(t,b)})\|_F\\
&= \|\nabla_{\mathbf{W}}\mathcal{L}_{\mathcal{I}_{t,b}}(\mathbf{W}^{(t,b)})\|_F \leq 2\sqrt{2}P\sigma_p\sqrt{d/Bm},
\end{aligned} \tag{39}$$

where the first inequality comes from triangle inequality; the second equality holds because $\mathcal{R}, \mathcal{F}$ are split from $\mathcal{S}$ and come from the same $\mathcal{D}$, thus having the same gradient norm; the second inequality comes from the original bounds in Chen et al. (2023). Next we expand $\left\langle \widehat{\boldsymbol{\epsilon}}_{j,r}^{(t,b)}, \boldsymbol{\xi}_k \right\rangle$ under NegGrad:

$$\begin{aligned}\left\langle \widehat{\boldsymbol{\epsilon}}_{j,r}^{(t,b)}, \boldsymbol{\xi}_k \right\rangle =& \frac{\tau}{mB} \left\| \nabla_{\mathbf{W}} \mathcal{L}_{\mathcal{I}_{t,b}}(\mathbf{W}^{(t,b)}) \right\|_F^{-1} \sum_{i \in \mathcal{I}_{t,b}} \sum_{p \in [P]} \ell_i'^{(t)} j \cdot y_i \sigma'(\langle \mathbf{w}_{j,r}^{(t)}, \mathbf{x}_{i,p} \rangle) \langle \mathbf{x}_{i,p}, \boldsymbol{\xi}_k \rangle \\ =& \frac{\tau}{mB} \left\| \nabla_{\mathbf{W}} \mathcal{L}_{\mathcal{I}_{t,b}}(\mathbf{W}^{(t,b)}) \right\|_F^{-1} \Bigg[\alpha \sum_{i \in \mathcal{I}_{t,b}^{\mathcal{R}}} \sum_{p \in [P]} \ell_i'^{(t)} j \cdot y_i \sigma'(\langle \mathbf{w}_{j,r}^{(t)}, \mathbf{x}_{i,p} \rangle) \langle \mathbf{x}_{i,p}, \boldsymbol{\xi}_k \rangle \\ & -(1-\alpha) \sum_{i \in \mathcal{I}_{t,b}^{\mathcal{F}}} \sum_{p \in [P]} \ell_i'^{(t)} j \cdot y_i \sigma'(\langle \mathbf{w}_{j,r}^{(t)}, \mathbf{x}_{i,p} \rangle) \langle \mathbf{x}_{i,p}, \boldsymbol{\xi}_k \rangle \Bigg] .\end{aligned} \tag{40}$$

Note that $\langle \mathbf{x}_{i,p}, \boldsymbol{\xi}_k \rangle$ can be divided into three different terms:

$$|\langle \mathbf{x}_{i,p}, \boldsymbol{\xi}_k \rangle| = \begin{cases} \|\boldsymbol{\xi}_k\|_2^2 \le 3\sigma_p^2 d/2, & \text{if } i = k, x_{k,p} = \boldsymbol{\xi}_k \\ |\langle \boldsymbol{\xi}_i, \boldsymbol{\xi}_k \rangle| \le 2\sigma_p^2 \sqrt{d \log(6n^2/\delta)}, & \text{if } i \ne k, x_{i,p} = \boldsymbol{\xi}_i \\ |\langle y_i \boldsymbol{\varphi}, \boldsymbol{\xi}_k \rangle| \le \|\boldsymbol{\varphi}\|_2 \, \sigma_p \sqrt{2 \log(6n^2/\delta)}, & \text{if } x_{i,p} = y_i \boldsymbol{\varphi} \end{cases} \tag{41}$$

The upper bounds come from Lemma D.3. Based on Assumption D.1 and Lemma D.4 of Chen et al. (2023), the $i = k$ term will dominate the upper bound and we can write

$$\begin{aligned}\left\langle \widehat{\boldsymbol{\epsilon}}_{j,r}^{(t,b)}, \boldsymbol{\xi}_k \right\rangle \le \frac{\tau}{mB \cdot 2\sqrt{2} P \sigma_p \sqrt{d/Bm}} \big[& -0.15\alpha(P-1) C_1 \sigma_p^2 d \mathbb{1}[k \in \mathcal{I}_{t,b}^{\mathcal{R}}] \\ & +0.15(1-\alpha)(P-1) C_1 \sigma_p^2 d \mathbb{1}[k \in \mathcal{I}_{t,b}^{\mathcal{F}}] \big]\end{aligned} \tag{42}$$

Thus, when $k \in \mathcal{I}_{t,b}^{\mathcal{R}}$, we can preserve the original bound with additional α:

$$\left\langle \widehat{\boldsymbol{\epsilon}}_{j,r}^{(t,b)}, \boldsymbol{\xi}_k \right\rangle < -C \frac{\alpha \tau \sigma_p \sqrt{d}}{m\sqrt{B}}. \tag{43}$$

Choosing $\tau = \frac{m\sqrt{B}}{C_3 \alpha P \sigma_p \sqrt{d}}$ will cancel with $\left\langle \mathbf{w}_{j,r}^{(t)}, \boldsymbol{\xi}_k \right\rangle$ to deactivate the neuron. When $k \in \mathcal{I}_{t,b}^{\mathcal{F}}$, the entire $\langle \mathbf{w}_{j,r}^{(t,b)} + \widehat{\boldsymbol{\epsilon}}_{j,r}^{(t,b)}, \boldsymbol{\xi}_k \rangle$ will remain activated:

$$0 \le \left\langle \widehat{\boldsymbol{\epsilon}}_{j,r}^{(t,b)}, \boldsymbol{\xi}_k \right\rangle < C \frac{(1-\alpha)\tau \sigma_p \sqrt{d}}{m\sqrt{B}} \Longrightarrow \left\langle \mathbf{w}_{j,r}^{(t,b)} + \widehat{\boldsymbol{\epsilon}}_{j,r}^{(t,b)}, \boldsymbol{\xi}_k \right\rangle \ge \left\langle \mathbf{w}_{j,r}^{(t,b)}, \boldsymbol{\xi}_k \right\rangle \ge 0. \tag{44}$$

This fundamentally differs SAM's behaviors towards unlearning $\mathcal{F}$ from behaviors towards learning $\mathcal{R}$ as how SGD differs from SAM. For gradient ascent on $\mathcal{F}$ under NegGrad, we now know SAM learns from activated noise products as much as SGD. The activation patterns are further utilized to bound products and norms of the weight, signal and noise, which characterize the final test errors.

Our task is reduced to bounding $\mathbb{P}_{(\mathbf{x},y)\sim\mathcal{R}}(yf\left(\mathbf{W}^{(t)},\mathbf{x}\right)\leq 0)$, then use previous error bounds for SGD in App. D.1 for $\mathbb{P}_{(\mathbf{x},y)\sim\mathcal{F}}(yf(\mathbf{W}^{(t)},\mathbf{x})>0)$. The inner product with $j=y$ can be bounded as

$$\begin{aligned}
\left\langle \mathbf{w}_{y,r}^{(t)}, y\boldsymbol{\varphi}\right\rangle &= \left\langle \mathbf{w}_{y,r}^{(0)}, y\boldsymbol{\varphi}\right\rangle + \kappa_{y,r}^{(t)} + \frac{1}{(P-1)}\sum_{i=1}^{n}\overline{\zeta}_{y,r,i}^{(t)}\cdot\|\boldsymbol{\xi}_i\|_2^{-2}\cdot\langle\boldsymbol{\xi}_i, y\boldsymbol{\varphi}\rangle \\
&\quad + \frac{1}{(P-1)}\sum_{i=1}^{n}\underline{\zeta}_{y,r,i}^{(t)}\cdot\|\boldsymbol{\xi}_i\|_2^{-2}\cdot\langle\boldsymbol{\xi}_i, y\boldsymbol{\varphi}\rangle \\
&\geq \left\langle \mathbf{w}_{y,r}^{(0)}, y\boldsymbol{\varphi}\right\rangle + \kappa_{y,r}^{(t)} \\
&\quad - \frac{\sqrt{2\log(6n/\delta)}}{P-1}\cdot\sigma_p\|\boldsymbol{\varphi}\|_2\cdot\left(\sigma_p^2 d/2\right)^{-1}\left[\sum_{i=1}^{n}\overline{\zeta}_{y,r,i}^{(t)} + \sum_{i=1}^{n}\left|\underline{\zeta}_{y,r,i}^{(t)}\right|\right] \\
&= \left\langle \mathbf{w}_{y,r}^{(0)}, y\boldsymbol{\varphi}\right\rangle + \kappa_{y,r}^{(t)} - \Theta\left(\sqrt{\log(n/\delta)}\cdot(P\sigma_p d)^{-1}\|\boldsymbol{\varphi}\|_2\right)\cdot\Theta\left(\mathrm{SNR}^{-2}\right)\cdot\kappa_{y,r}^{(t)} \\
&= \left\langle \mathbf{w}_{y,r}^{(0)}, y\boldsymbol{\varphi}\right\rangle + \left[1-\Theta\left(\sqrt{\log(n/\delta)}\cdot P\sigma_p/\|\boldsymbol{\varphi}\|_2\right)\right]\kappa_{y,r}^{(t)} \\
&= \left\langle \mathbf{w}_{y,r}^{(0)}, y\boldsymbol{\varphi}\right\rangle + \Theta\left(\kappa_{y,r}^{(t)}\right) = \Theta(1),
\end{aligned} \tag{45}$$

where the inequality is by Lemma D.3; the second equality is obtained by plugging in the coefficient orders we summarized; the third equality is by $\mathrm{SNR}=\|\boldsymbol{\varphi}\|_2/(P\sigma_p\sqrt{d})$; the fourth equality is by $\|\boldsymbol{\varphi}\|_2^2\geq C\cdot P^2\sigma_p^2\log(n/\delta)$ in Assumption D.1 for sufficiently large constant C; the last equality is by Lemma D.7 of Chen et al. (2023).We similarly have $\langle\mathbf{w}_{y,r}^{(t)}, y\boldsymbol{\varphi}\rangle = -\Theta(1)<0$.

Denote $g(\boldsymbol{\xi})$ as $\sum_r\sigma(\langle\mathbf{w}_{-y,r}^{(t)},\boldsymbol{\xi}\rangle)$. The results for noise learning from SGD in App. D.1 still apply:

$$\begin{aligned}
&|g(\boldsymbol{\xi})-g(\boldsymbol{\xi}')|\leq\sum_{r=1}^{m}\left\|\mathbf{w}_{-y,r}^{(t)}\right\|_2\cdot\|\boldsymbol{\xi}-\boldsymbol{\xi}'\|_2; \\
&\mathbb{E}g(\boldsymbol{\xi}) = \frac{\sigma_p}{\sqrt{2\pi}}\sum_{r=1}^{m}\left\|\mathbf{w}_{-y,r}^{(t)}\right\|_2; \\
&\left\|\sum_{i=1}^{n}\zeta_{j,r,i}^{(t)}\cdot\|\boldsymbol{\xi}_i\|_2^{-2}\cdot\boldsymbol{\xi}_i\right\|_2^2\leq\Theta\left(\sigma_p^{-2}d^{-1}n^{-1}\right)\left(\sum_{i=1}^{n}\overline{\zeta}_{j,r,i}^{(t)}\right)^2.
\end{aligned} \tag{46}$$

We can thus upper bound the 2-norm of $\mathbf{w}_{j,r}^{(t)}$ as:

$$\begin{aligned}
\left\|\mathbf{w}_{j,r}^{(t)}\right\|_2 &\leq \left\|\mathbf{w}_{j,r}^{(0)}\right\|_2 + \kappa_{j,r}^{(t)}\cdot\|\boldsymbol{\varphi}\|_2^{-1} + \frac{1}{P-1}\left\|\sum_{i=1}^{n}\zeta_{j,r,i}^{(t)}\cdot\|\boldsymbol{\xi}_i\|_2^{-2}\cdot\boldsymbol{\xi}_i\right\|_2 \\
&\leq \left\|\mathbf{w}_{j,r}^{(0)}\right\|_2 + \kappa_{j,r}^{(t)}\cdot\|\boldsymbol{\varphi}\|_2^{-1} + \Theta\left(P^{-1}\sigma_p^{-1}d^{-1/2}n^{-1/2}\right)\cdot\sum_{i=1}^{n}\overline{\zeta}_{j,r,i}^{(t)} \\
&= \Theta(\sigma_0\sqrt{d}) + \Theta\left(P^{-1}\sigma_p^{-1}d^{-1/2}n^{-1/2}\right)\cdot\sum_{i=1}^{n}\overline{\zeta}_{j,r,i}^{(t)},
\end{aligned} \tag{47}$$

based on $\mathrm{SNR}=\|\boldsymbol{\varphi}\|_2/(P\sigma_p\sqrt{d})$ and $\sum_{i=1}^{n}\overline{\zeta}_{j,r,i}^{(t)}/\kappa_{j,r}^{(t)}=\Theta\left(\mathrm{SNR}^{-2}\right)$, and the condition for d in Assumption D.1, and also $\left\|\mathbf{w}_{j,r}^{(0)}\right\|_2=\Theta\left(\sigma_0\sqrt{d}\right)$ based on Lemma D.7 of Chen et al. (2023). Then

we have

$$\begin{aligned}
\frac{\sum_r \sigma\left(\left\langle \mathbf{w}_{y,r}^{(t)}, y\boldsymbol{\varphi}\right\rangle\right)}{(P-1)\sigma_p \sum_{r=1}^m \left\|\mathbf{w}_{-y,r}^{(t)}\right\|_2} &\geq \frac{\Theta(1)}{\Theta\left(\sigma_0\sqrt{d}\right) + \Theta\left(P^{-1}\sigma_p^{-1}d^{-1/2}n^{-1/2}\right)\cdot \sum_{i=1}^n \overline{\zeta}_{j,r,i}^{(t)}} \\
&\geq \frac{\Theta(1)}{\Theta\left(\sigma_0\sqrt{d}\right) + O\left(P^{-1}\sigma_p^{-1}d^{-1/2}n^{1/2}\alpha\right)} \\
&\geq \min\left\{\Omega\left(\sigma_0^{-1}d^{-1/2}\right), \Omega\left(P\sigma_p d^{1/2}n^{-1/2}\alpha^{-1}\right)\right\} \\
&\geq 1 \\
\implies \sum_r \sigma\left(\left\langle \mathbf{w}_{y,r}^{(t)}, y\boldsymbol{\varphi}\right\rangle\right) &- \frac{(P-1)\sigma_p}{\sqrt{2\pi}} \sum_{r=1}^m \left\|\mathbf{w}_{-y,r}^{(t)}\right\|_2 > 0.
\end{aligned} \tag{48}$$

Upper bound. Now plug in previous results to obtain

$$\begin{aligned}
&\mathbb{P}_{(\mathbf{x},y)\sim\mathcal{R}}\left(yf\left(\mathbf{W}^{(t)},\mathbf{x}\right)\leq 0\right) \leq \mathbb{P}_{(\mathbf{x},y)\sim\mathcal{R}}\left((P-1)\sum_r \sigma\left(\left\langle \mathbf{w}_{-y,r}^{(t)}, \boldsymbol{\xi}\right\rangle\right) \geq \sum_r \sigma\left(\left\langle \mathbf{w}_{y,r}^{(t)}, y\boldsymbol{\varphi}\right\rangle\right)\right) \\
=&\mathbb{P}_{(\mathbf{x},y)\sim\mathcal{R}}\left(g(\boldsymbol{\xi}) - \mathbb{E}g(\boldsymbol{\xi}) \geq 1/(P-1)\sum_r \sigma\left(\left\langle \mathbf{w}_{y,r}^{(t)}, y\boldsymbol{\varphi}\right\rangle\right) - \frac{\sigma_p}{\sqrt{2\pi}}\sum_{r=1}^m \left\|\mathbf{w}_{-y,r}^{(t)}\right\|_2\right) \\
\leq &\exp\left[-\frac{c\left(1/(P-1)\sum_r \sigma\left(\left\langle \mathbf{w}_{y,r}^{(t)}, y\boldsymbol{\varphi}\right\rangle\right) - \left(\sigma_p/\sqrt{2\pi}\right)\sum_{r=1}^m \left\|\mathbf{w}_{-y,r}^{(t)}\right\|_2\right)^2}{\sigma_p^2\left(\sum_{r=1}^m \left\|\mathbf{w}_{-y,r}^{(t)}\right\|_2\right)^2}\right] \\
= &\exp\left[-c\left(\frac{\sum_r \sigma\left(\left\langle \mathbf{w}_{y,r}^{(t)}, y\boldsymbol{\varphi}\right\rangle\right)}{(P-1)\sigma_p\sum_{r=1}^m \left\|\mathbf{w}_{-y,r}^{(t)}\right\|_2} - 1/\sqrt{2\pi}\right)^2\right] \\
\leq &\exp(c/2\pi)\exp\left(-0.5c\left(\frac{\sum_r \sigma\left(\left\langle \mathbf{w}_{y,r}^{(t)}, y\boldsymbol{\varphi}\right\rangle\right)}{(P-1)\sigma_p\sum_{r=1}^m \left\|\mathbf{w}_{-y,r}^{(t)}\right\|_2}\right)^2\right).
\end{aligned} \tag{49}$$

The second inequality is by Eq. 48 and plugging $\|g\|_{\mathrm{Lip}} \leq \sum_{r=1}^m \|\mathbf{w}_{-y,r}^{(t)}\|_2$ into Eq. 15, the third inequality is because $(s-t)^2 \geq s^2/2 - t^2, \forall s,t \geq 0$. And we can obtain

$$\begin{aligned}
\mathbb{P}_{(\mathbf{x},y)\sim\mathcal{R}}\left(yf\left(\mathbf{W}^{(t)},\mathbf{x}\right)\leq 0\right) &\leq \exp(c/2\pi)\exp\left(-0.5c\left(\frac{\sum_r \sigma\left(\left\langle \mathbf{w}_{y,r}^{(t)}, y\boldsymbol{\varphi}\right\rangle\right)}{(P-1)\sigma_p\sum_{r=1}^m \left\|\mathbf{w}_{-y,r}^{(t)}\right\|_2}\right)^2\right) \\
&\leq \exp\left(\frac{c}{2\pi} - C\min\left\{\sigma_0^{-2}d^{-1}, P\sigma_p^2 d n^{-1}\alpha^{-2}\right\}\right) \\
&\leq \exp\left(-0.5C\min\left\{\sigma_0^{-2}d^{-1}, P\sigma_p^2 d n^{-1}\alpha^{-2}\right\}\right) = \epsilon,
\end{aligned} \tag{50}$$

where $C = O(1)$, the last inequality holds since $\sigma_0^2 \leq 0.5Cd^{-1}\log(1/\epsilon)$ and $d \geq 2C^{-1}P^{-1}\sigma_p^{-2}n\alpha^2\log(1/\epsilon)$. Now we upper bound the test error $\mathcal{L}^{\text{test}}(\mathbf{W}^{T_2}, \mathcal{D})$. Depending on the strength of the unified signal vector $\boldsymbol{\varphi}$, the unlearning of $\mathcal{F}$ can exhibit either benign or harmful overfitting following SGD's characterization, dividing error bounds into two cases:

1. If $\|\boldsymbol{\varphi}\|_2 \geq C_1 d^{1/4} n^{-1/4} P \sigma_p$, we have benign overfitting on both $\mathcal{R}$ and $\mathcal{F}$. Thus,

$$\begin{aligned}
&\mathcal{L}^{\text{test}}(\mathbf{W}^{T_2}, \mathcal{D}) = \mathbb{P}_{(\mathbf{x},y)\sim\mathcal{D}}\left(y \neq \operatorname{sign}\left(f\left(\mathbf{W}^{T_2}, \mathbf{x}\right)\right)\right) \\
=&\beta \cdot \underbrace{\mathbb{P}_{(\mathbf{x},y)\sim\mathcal{R}}\left(yf\left(\mathbf{W}^{T_2}, \mathbf{x}\right) \leq 0\right)}_{\leq \epsilon_{\mathcal{R}}} + (1-\beta) \cdot \left(1 - \underbrace{\mathbb{P}_{(\mathbf{x},y)\sim\mathcal{F}}\left(yf\left(\mathbf{W}^{T_2}, \mathbf{x}\right) > 0\right)}_{\leq \epsilon_{\mathcal{F}}}\right) \\
\Longrightarrow &\lim_{\beta\to 1} \mathcal{L}^{\text{test}}(\mathbf{W}^{T_2}, \mathcal{D}) \leq \epsilon_{\mathcal{R}} = \epsilon.
\end{aligned} \tag{51}$$

   As $\beta \to 1$, $|\mathcal{F}|/n$ decreases so the model can better maintain its performance; as $\beta \to 0.5$, $|\mathcal{F}|/n$ increases and more samples are to be unlearned, making the model performance reduce to a minimally PAC-learnable guarantee. Hence, when $\beta \to 0.5$, we have $\lim_{\beta\to 0.5} \mathcal{L}^{\text{test}}(\mathbf{W}^{T_2}, \mathcal{D}) \leq 0.5 + 0.5\epsilon_{\mathcal{R}} - 0.5\epsilon_{\mathcal{F}} = \epsilon$.

2. If $\Omega(1) \leq \|\boldsymbol{\varphi}\|_2 \leq C_1 d^{1/4} n^{-1/4} P \sigma_p$, we have benign overfitting on $\mathcal{R}$ and harmful overfitting on $\mathcal{F}$. Thus,

$$\begin{aligned}
&\mathcal{L}^{\text{test}}(\mathbf{W}^{T_2}, \mathcal{D}) = \mathbb{P}_{(\mathbf{x},y)\sim\mathcal{D}}\left(y \neq \operatorname{sign}\left(f\left(\mathbf{W}^{(t)}, \mathbf{x}\right)\right)\right) \\
=&\beta \cdot \underbrace{\mathbb{P}_{(\mathbf{x},y)\sim\mathcal{R}}\left(yf\left(\mathbf{W}^{(t)}, \mathbf{x}\right) \leq 0\right)}_{\leq \epsilon_{\mathcal{R}}} + (1-\beta) \cdot \left(1 - \underbrace{\mathbb{P}_{(\mathbf{x},y)\sim\mathcal{F}}\left(yf\left(\mathbf{W}^{(t)}, \mathbf{x}\right) > 0\right)}_{\geq 0.1}\right) \\
\Longrightarrow &\lim_{\beta\to 1} \mathcal{L}^{\text{test}}(\mathbf{W}^{T_2}, \mathcal{D}) \leq \epsilon_{\mathcal{R}} = \epsilon.
\end{aligned} \tag{52}$$

   Similarly, we have $\lim_{\beta\to 0.5} \mathcal{L}^{\text{test}}(\mathbf{W}^{T_2}, \mathcal{D}) \leq 0.5\epsilon_{\mathcal{R}} + 0.45 = \epsilon$.

Remark D.6 *(β-dependence of the ϵ-bound). The overall test error*

$$\mathcal{L}^{\text{test}}(\mathbf{W}^{T_2}, \mathcal{D}) = \beta \cdot \mathbb{P}_{(\mathbf{x},y)\sim\mathcal{R}}\left(yf\left(\mathbf{W}^{(t)}, \mathbf{x}\right) \leq 0\right) + (1-\beta) \cdot \left(1 - \mathbb{P}_{(\mathbf{x},y)\sim\mathcal{F}}\left(yf\left(\mathbf{W}^{(t)}, \mathbf{x}\right) > 0\right)\right)$$

can be considered as an affine function of the mixing factor β, and so its achievable range runs from the best-case retain error $\epsilon_{\mathcal{R}}$ (as $\beta \to 1$) up to asymptotically 0.5 (as $\beta \to 0.5$)—the trivial PAC-learnability threshold. Concretely, by choosing β sufficiently close to 1, one drives $\mathcal{L}^{\text{test}}(\mathbf{W}^{T_2}, \mathcal{D})$ arbitrarily close to the small "benign" error level ϵ, whereas if β remains near 0.5 then $\mathcal{L}^{\text{test}}(\mathbf{W}^{T_2}, \mathcal{D})$ can approach 0.5, the worst-case "minimally learnable" error. Thus, all our bounds interpolate smoothly between these two extremes via the single parameter β, and we report the most informative bounds in Theorem 3.2 and Theorem 3.3.

D.3 Proof to Corollary 3.3.1

Recall the update rule for $\kappa_{j,r}$. For each epoch, the interference between retain and forget signals can be measured as

$$\sum_{b}^{|\mathcal{R}|/B} \alpha \sum_{i\in\mathcal{I}_{t,b}^{\mathcal{R}}} \ell_i'^{(t,b)} \sigma'(\langle \mathbf{w}_{j,r}^{(t,b)}, y_i\boldsymbol{\varphi}\rangle) - \sum_{b}^{|\mathcal{F}|/B} (1-\alpha)\frac{|\mathcal{R}|}{|\mathcal{F}|} \sum_{i\in\mathcal{I}_{t,b}^{\mathcal{F}}} \ell_i'^{(t,b)} \sigma'(\langle \mathbf{w}_{j,r}^{(t,b)}, y_i\boldsymbol{\varphi}\rangle). \tag{53}$$

Similar to Lemma 3.1, the expected gradient values between retain and forget samples should not differ. Since we cycle the forget set to synchronously train with the retain set, updates from $\mathcal{F}$ has been scaled up by $\frac{|\mathcal{R}|}{|\mathcal{F}|}$. Hence,

$$\mathbb{E}\left[\sum_{b}^{|\mathcal{R}|/B} \sum_{i\in\mathcal{I}_{t,b}^{\mathcal{R}}} \ell_i'^{(t,b)} \sigma'(\langle \mathbf{w}_{j,r}^{(t,b)}, y_i\boldsymbol{\varphi}\rangle)\right] = \mathbb{E}\left[\sum_{b}^{|\mathcal{F}|/B} \sum_{i\in\mathcal{I}_{t,b}^{\mathcal{F}}} \ell_i'^{(t,b)} \sigma'(\langle \mathbf{w}_{j,r}^{(t,b)}, y_i\boldsymbol{\varphi}\rangle)\right] \tag{54}$$

Combining together, to expect $\kappa_{j,r}$ to increase monotonically every epoch, we want

$$\mathbb{E}\left[\sum_{b}^{|\mathcal{R}|/B}\alpha\sum_{i\in\mathcal{I}_{t,b}^{\mathcal{R}}}\ell_i'^{(t,b)}\sigma'(\langle\mathbf{w}_{j,r}^{(t,b)},y_i\boldsymbol{\varphi}\rangle)-\sum_{b}^{|\mathcal{F}|/B}(1-\alpha)\frac{|\mathcal{R}|}{|\mathcal{F}|}\sum_{i\in\mathcal{I}_{t,b}^{\mathcal{F}}}\ell_i'^{(t,b)}\sigma'(\langle\mathbf{w}_{j,r}^{(t,b)},y_i\boldsymbol{\varphi}\rangle)\right]\geq 0$$
$$\implies \alpha-(1-\alpha)\frac{|\mathcal{R}|}{|\mathcal{F}|}\geq 0\implies\alpha\geq\frac{|\mathcal{R}|}{|\mathcal{F}|+|\mathcal{R}|}. \tag{55}$$

D.4 Proof to Lemma 3.4

By Theorem 3.3, SAM turns off noise memorization prevention mechanism when fitting $\mathcal{F}$, which leads to the same requirement on signal strength as SGD. The only difference between SAM and SGD under NegGrad is the more effective learning on $\mathcal{R}$. From Eq. 7 we have the per-batch update of $\kappa_{j,r}$ on $\mathcal{R}$ as

$$\Delta\kappa_{j,r}=\frac{\eta\|\boldsymbol{\varphi}\|_2^2}{Bm}\alpha\sum_{i\in\mathcal{I}_{t,b}^{\mathcal{R}}}\ell_i'^{(t,b)}\sigma'(\langle\mathbf{w}_{j,r}^{(t,b)},y_i\boldsymbol{\varphi}\rangle). \tag{56}$$

Let g denote the batch-average magnitude of $\ell_i'^{(t,b)}\sigma'(\langle\mathbf{w}_{j,r}^{(t,b)},y_i\boldsymbol{\varphi}\rangle)$ for convenience. We can then express per-epoch κ update as

$$\Delta_{\text{epoch}}\kappa_{j,r}=\frac{\eta\|\boldsymbol{\varphi}\|_2^2}{m}\alpha|\mathcal{R}|g. \tag{57}$$

Now, consider achieving benign overfitting on $\mathcal{R}$ only, where SGD requires $\|\boldsymbol{\varphi}\|_2=\Omega(d^{1/4}|\mathcal{R}|^{-1/4}P\sigma_p)$ while SAM only requires $\|\boldsymbol{\varphi}\|_2=\Omega(1)$. That being said, given a fixed universal $\boldsymbol{\varphi}$ for $\mathcal{D}$ and a choice of α, we have SAM learning the retain signals faster than SGD:

$$\frac{\Delta_{\text{epoch}}\kappa_{j,r}^{\text{SAM}}}{\Delta_{\text{epoch}}\kappa_{j,r}^{\text{SGD}}}=\Theta(d^{1/2}|\mathcal{R}|^{-1/2}P^2\sigma_p^2)=\Theta(\|\boldsymbol{\varphi}\|_2^2). \tag{58}$$

Hence, in order to achieve the same signal learning performance as SAM on $\mathcal{R}$, SGD needs to scale up α^{SGD}. Thus,

$$\frac{\alpha^{\text{SGD}}}{\alpha^{\text{SAM}}}=\Theta(d^{1/2}|\mathcal{R}|^{-1/2}P^2\sigma_p^2)=\Theta(\|\boldsymbol{\varphi}\|_2^2),\text{ or }\alpha^{\text{SGD}}-\alpha^{\text{SAM}}=\Theta(\|\boldsymbol{\varphi}\|_2^2). \tag{59}$$

In general, since $|\mathcal{R}|=\Theta(n)$, we can characterize the gap between α^{SGD} and α^{SAM} by $O(\sqrt{d/n})$.

E Implementation Details

E.1 Experiment Setup

We conduct major experiments on CIFAR-100 (Krizhevsky et al., 2009) and ImageNet-1K (Russakovsky et al., 2015) using ResNet-50 (He et al., 2016). We adopt pre-computed memorization scores for these two datasets from Feldman & Zhang (2020) to generate $\mathcal{F}$ of different memorization levels with $|\mathcal{F}|\approx 5\%|\mathcal{S}|$. We have $|\mathcal{F}|=3000$ for CIFAR-100 and $|\mathcal{F}|=60000$ for ImageNet. We sample high-memorization forget set $\mathcal{F}_{\text{high}}$ by choosing $|\mathcal{F}|$ samples of highest memorization scores from $\mathcal{S}$, $\mathcal{F}_{\text{low}}$ by choosing $|\mathcal{F}|$ samples of lowest memorization scores, and $\mathcal{F}_{\text{mid}}$ by choosing $|\mathcal{F}|$ samples whose memorization scores are closest to 0.5. We also run experiments with randomly sampled $\mathcal{F}_{\text{rand}}$ on Tiny-ImageNet and CIFAR-10 in App. G. We use $\mathrm{RandomResizedCrop}$ and $\mathrm{RandomHorizontalFlip}$ as train transforms.

Pretraining and retraining. We pretrain on $\mathcal{S}$ and retrain on $\mathcal{R}$ with the same settings. For CIFAR-100, we train for $T_1=200$ epochs, use batch size 256, learning rate $\eta_0=0.1$ with cosine annealing, SGD with momentum 0.9 and weight decay 5×10^{-4}. For ImageNet, we train for $T_1=150$ epochs, use batch size 512, learning rate $\eta_0=0.25$ with cosine annealing and 5 warm-up epochs, SGD with momentum 0.9 and weight decay 2×10^{-5}. For CIFAR-10, we train ResNet-18 for $T_1=50$ epochs, use batch size 256, learning rate $\eta_0=0.1$ with cosine annealing, SGD with momentum 0.9 and weight decay 5×10^{-4}. We summarize the settings, test performance of different pretrained models, as well as accuracies of retrain models in Tab. 6.

Table 6: Pretraining settings and test accuracies using different $\mathcal{A}$ (top), as well as performance of retrained models w.r.t different $\mathcal{F}$ (bottom) for CIFAR-100 and ImageNet-1K.

Dataset, Model	lr+warmup	Batch B	Epoch T	W. Decay	SGD	ASAM 0.1	ASAM 1.0	SAM 0.1
CIFAR100, Res50	0.1+0	256	200	5e-4	77.23	76.0	78.05	77.85
ImageNet, Res50	0.25+5	512	150	2e-5	75.04	74.94	76.53	76.18

Retrain	High Mem			Mid Mem			Low Mem		
Dataset, Model	Retain	Forget	Test	Retain	Forget	Test	Retain	Forget	Test
CIFAR100, Res50	99.964	3.3	74.96	99.981	57.5	74.14	99.956	100.0	75.81
ImageNet, Res50	97.134	13.828	74.826	97.388	52.27	74.832	96.671	99.858	75.018

Table 7: Ablation on weight mask cutoff choice for Sharp MinMax on CIFAR-100 with ResNet50. We report ToWs across different $\mathcal{F}$ and the averages. We observe that all choices work well: 10% works as well as 30%, while a larger $\mathbf{W}_{\mathcal{F}}$ as 50% can further improve the performance.

	$\mathcal{A}$=SGD				$\mathcal{A}$=ASAM 1.0			
Cutoff	$\mathcal{F}_{\text{high}}$	$\mathcal{F}_{\text{mid}}$	$\mathcal{F}_{\text{low}}$	AVG	$\mathcal{F}_{\text{high}}$	$\mathcal{F}_{\text{mid}}$	$\mathcal{F}_{\text{low}}$	AVG
10%	82.675	92.495	87.636	87.602	83.916	90.27	81.362	85.183
30%	82.27	94.913	86.504	87.896	84.521	87.761	84.381	85.554
50%	82.798	98.177	87.806	**89.594**	83.567	95.516	90.096	**89.726**

Unlearning. We conduct all unlearning methods for $T_2 = 10$ epochs with the same batch size and optimizer settings. For NegGrad and Sharp MinMax, we unlearn with constant learning rate 0.02. We use $\alpha = 0.99$ for CIFAR-100 and $\alpha = 0.989$ for ImageNet accounting for its slightly smaller $|\mathcal{F}|/|\mathcal{S}|$ ratio. For model splitting, we empirically find that a small ratio for forget model benefits ImageNet such as 5%, while CIFAR-100 suits a larger ratio such as 30%. For both pretraining and unlearning, we wrap SGD with vanilla SAM (Foret et al., 2020) with $\rho = 0.1$, and Adaptive SAM (ASAM) (Kwon et al., 2021) with $\rho = [0.1, 1.0]$, while keep other hyper-parameters the same for fair comparison.

E.2 Sharp MinMax Implementation

Inspired by SalUn (Fan et al., 2023), we split the model into retain, forget models $\mathbf{W}_{\mathcal{R}}, \mathbf{W}_{\mathcal{F}}$ and update using two separate optimizers: SAM on $\mathbf{W}_{\mathcal{R}}$ and sharpness maximization on $\mathbf{W}_{\mathcal{F}}$. We split the model by ranking the parameters that are important to $\mathcal{F}$ based on the magnitude of the gradient of the parameters after one pass on $\mathcal{F}$, and choose the highest percentage where we have 5% for ImageNet and 30% for CIFAR-100. The cutoff choice is based on the over-parameterization scheme: since ResNet50 w/ CIFAR-100 is much more over-parameterized than w/ ImageNet, there is less overlap between retain and forget parameters and more freedom to increase size of $\mathbf{W}_{\mathcal{F}}$ for more aggressive unlearning. We have also experimented with 10% and 50% and notice a slight better performance of using 50% cutoff in Tab. 7. Unlike SalUn, which essentially performs RL unlearning on the selected parameters, we update both models using opposite optimization. SalUn also requires a larger part of the model to fine-tune with noisy, label flipped $\mathcal{F}$ (50%). We have summarized our implementation for weight masking in Alg. 1, and Sharp MinMax in Alg. 2.

E.3 Unlearning Setup for Previous Work

We compare with state-of-the-art unlearning methods with optimized hyper-parameter settings. To our best knowledge, several previous methods are evaluated on ImageNet for the first time. We apply SGD and ASAM 1.0 on each $\mathcal{U}$ and compare the performance between SGD and SAM. For L1-Sparse (Jia et al., 2023), we use unlearn lr$= 0.02$ and $\alpha = 1\times10^{-4}$. For SCRUB (Kurmanji et al., 2023), we use unlearn lr$= 0.004$, msteps$= 8$, kd_T$= 4$, $\beta = 0.01$, and $\gamma = 0.99$. For RL (Graves et al., 2021), we use unlearn lr$= 0.06$ on CIFAR-100 and 0.02 on ImageNet. For SalUn (Fan et al., 2023), we use the unlearn lr$= 0.06$, 50% weight to finetune on CIFAR-100, and unlearn lr$= 0.04$, 30% weight to finetune on ImageNet.

Algorithm 1 WeightMask

Require: forget_loader, model, criterion, percent
for all (name, param) in model parameters **do**
    gradients[name] $\leftarrow$ zeros_like(param)
end for
for all (image, target) in forget_loader **do**
    loss $\leftarrow$ criterion(model(image), target)
    optimizer.zero_grad(); loss.backward()
    accumulate parameter gradients into gradients
end for
for all name in gradients **do**
    gradients[name] $\leftarrow$ |gradients[name]|
end for
all_vals $\leftarrow$ cat $\big(\{\text{flatten}(v) \mid v \in \text{gradients.values}()\}\big)$
cutoff $\leftarrow$ quantile(all_vals, percent) ▷ e.g., 0.1 = bottom 10%
return $\{$ name $\mapsto$ (grad $<$ cutoff) $\mid$ (name, grad) $\in$ gradients$\}$

Algorithm 2 SharpMinMax

Require: x_retain, y_retain, x_forget, y_forget, model, criterion, mask, alpha, optimizer_retain, optimizer_forget
$r\_loss1 \leftarrow \alpha \cdot \text{criterion}(\text{model}(\text{x\_retain}),\ \text{y\_retain})$
r_loss1.backward()
optimizer_retain.first_step(zero_grad=True) ▷ SAM first step
$r\_loss2 \leftarrow \alpha \cdot \text{criterion}(\text{model}(\text{x\_retain}),\ \text{y\_retain})$
r_loss2.backward()
for all (name, p) in model parameters **do**
    if p.grad **then**
        p.grad $\leftarrow p$.grad $\odot \big(1 - \text{mask[name]}\big)$ ▷ mask out forget grads
    end if
end for
optimizer_retain.second_step(zero_grad=True) ▷ sharp min
$f\_loss1 \leftarrow -(1-\alpha) \cdot \text{criterion}(\text{model}(\text{x\_forget}),\ \text{y\_forget})$
f_loss1.backward()
optimizer_forget.first_step(zero_grad=True) ▷ SAM first step
$f\_loss2 \leftarrow -(1-\alpha) \cdot \text{criterion}(\text{model}(\text{x\_forget}),\ \text{y\_forget})$
f_loss2.backward()
for all (name, p) in model parameters **do**
    if p.grad **then**
        p.grad $\leftarrow p$.grad $\odot$ mask[name] ▷ update forget params only
    end if
end for
optimizer_forget.second_step(zero_grad=True) ▷ sharp max

E.4 Evaluation Details

Membership inference attack. We adopted a MIA based evaluation from Jia et al. (2023). We train a binary classifier using the retain set $\mathcal{R}$ and the test set $\mathcal{D}_{\text{test}}$ to distinguish whether a data sample was involved in the training stage, based on the softmaxed outputs from the unlearned model. Then, we feed the forget set $\mathcal{F}$ to the classifier to evaluate this unlearned model. We expect forget samples to be classified as "non-training" data, and we evaluate the unlearning effectiveness based on MIA correctness. A lower correctness (close to 0.5) indicates difficulty to distinguish and thus better unlearning. This evaluation examines an unlearned model from a privacy perspective.

Entanglement computation. We compute both entanglement scores based on normalized embeddings of retain and forget sets from the penultimate layer of the model. We compute pair-wise entanglement between each retain and forget embedding, either globally or within a class. For variance-based entanglement E_{Var}, we directly follow Zhao et al. (2024) for implementation, and

then rescale the raw scores to $[0, 1]$ based on the value range across global and class-wise scores. For Wasserstein entanglement E_{W_p}, we randomly sample an equal number of embeddings from retain and forget embeddings and build two uniform proxy-distributions. We then use existing optimal transport library to compute the transport distance (cost), outputting entanglement scores as $1 -$ distance. No clipping is needed as we observe all scores lie within $[0, 1]$.

F Detailed Empirical Results

F.1 Statistical Significance

We demonstrate the statistical significance of our main empirical results by running each unlearning experiment three times with different seeds. In Fig. 5 and Fig. 4, we report the 95% confidence intervals ($\mu \pm 2\sigma$) of all unlearning methods on ImageNet and CIFAR-100, which correspond to Tab. 1 and Tab. 3. Each single bar represents the mean over runs and has the mean ToW scores marked on top of its error bar plotted by $\pm 2\sigma$. We observe that SAM consistently improves all unlearning methods with more noticeable results on CIFAR-100. For "All methods" subplots, we highlight the largest improvement by applying SAM to each $\mathcal{U}$. On CIFAR-100, we observe a general larger variance of SGD based unlearning, especially for SCRUB. Despite that $\mathcal{A}$=SAM 0.1 seems to provide a weaker pretrained model, Adaptive SAM settings can improve unlearning performance more steadily with lower variance, which demonstrate that SAM unlearning is more robust. Tab. 8 also records the means and variances of the "All methods" subplots for ImageNet and CIFAR-100. These additional insights further strengthen our findings.

Table 8: Verifying statistical significance ($\mu \pm \sigma$) of main experiments on ImageNet and CIFAR-100. Given various pretrained model with different $\mathcal{A}$, we observe that SAM consistently improve base unlearn methods $\mathcal{U}$ with higher means across multiple seeds. Moreover, we observe generally more stable performance with SAM based on smaller variance on average.

ImageNet	RL		SalUn		NG		MinMax	
Method	SGD	ASAM 1.0	SGD	ASAM 1.0	SGD	ASAM 1.0	SGD	ASAM 1.0
$\mathcal{A}$=SGD	82.9±0.3	83.9±0.2	70.6±0.1	71.0±0.1	83.5±0.3	84.8±0.0	80.2±0.1	87.9±0.0
$\mathcal{A}$=ASAM 0.1	82.5±0.1	83.8±0.1	70.7±0.1	71.1±0.1	83.4±0.3	84.7±0.1	79.7±0.2	87.5±0.1
$\mathcal{A}$=ASAM 1.0	83.2±0.4	83.8±0.2	71.1±0.0	71.2±0.0	84.1±0.0	84.6±0.2	80.1±0.2	88.0±0.1
$\mathcal{A}$=SAM 0.1	82.9±0.2	83.7±0.3	71.2±0.0	71.4±0.1	83.6±0.1	84.4±0.1	79.9±0.1	87.8±0.1

CIFAR100	L1 Sparse		Scrub		RL		SalUn		NG	
Method	SGD	ASAM 1.0	SGD	ASAM 1.0	SGD	ASAM 1.0	SGD	ASAM 1.0	SGD	ASAM 1.0
$\mathcal{A}$=SGD	62.1±1.4	67.3±0.1	56.5±14.1	73.6±0.4	74.2±1.0	77.2±0.2	76.1±1.5	83.8±0.9	82.8±1.1	84.0±0.9
$\mathcal{A}$=ASAM 0.1	63.6±1.7	69.3±0.6	54.3±1.8	79.3±0.8	72.1±0.9	75.8±1.3	72.9±1.6	82.5±0.4	83.9±0.8	85.5±0.6
$\mathcal{A}$=ASAM 1.0	64.2±0.7	68.7±1.7	58.4±10.5	72.0±2.1	75.7±1.5	80.3±1.2	79.0±0.3	83.3±0.2	80.2±0.5	83.9±0.2
$\mathcal{A}$=SAM 0.1	64.9±1.3	68.3±0.6	41.1±1.7	49.7±16.6	74.2±0.7	80.3±0.9	79.4±1.0	83.6±0.6	71.3±1.8	78.7±0.5

F.2 Complete Accuracies

In Tab. 9, Tab. 10, and Tab. 11, we report complete results of retain, forget, and test accuracies for all unlearning experiments, which are used to compute ToW scores in Tab. 1 and Tab. 3. As we have mentioned in the main paper, we observe that SGD often achieves lower test accuracies, motivating us to rethink the overfitting under a sample-specific unlearning scheme.

G Additional Experiments

We provide additional experiments on CIFAR-10 and Tiny-ImageNet using randomly sampled forget set $\mathcal{F}_{\text{rand}}$. To diversify our experiment settings, we use ResNet-34 with ImageNet-pretrained weights for our learning and unlearning on Tiny-ImageNet. Similar to our main setup, we pretrain and retrain using the same settings, and we have summarized basic settings and baseline performance in Tab. 12. Since Tiny-ImageNet has 100K samples, we set $|\mathcal{F}_{\text{rand}}| = 6000$ for Tiny-ImageNet. Tab. 13 records detailed accuracies and ToW scores of various unlearning and pretraining settings.

G.1 CIFAR-10

We summarize detailed unlearning settings on CIFAR-10. For L1-Sparse, we use unlearn lr= 0.02 and $\alpha = 1 \times 10^{-4}$. For SCRUB, we use unlearn lr= 0.004, msteps= 8, kd_T= 3.5, $\beta = 0.01$,

Table 9: Detailed accuracies of NegGrad on ImageNet and CIFAR-100.

ImageNet	$\mathcal{A}$ =SGD				$\mathcal{A}$ =ASAM 0.1				$\mathcal{A}$ =ASAM 1.0				$\mathcal{A}$ =SAM 0.1			
High Mem	Retain	Forget	Test	ToW	Retain	Forget	Test	ToW	Retain	Forget	Test	ToW	Retain	Forget	Test	ToW
+SGD	88.766	25.148	71.756	78.764	88.131	24.1	70.878	78.426	89.649	26.28	71.772	78.522	89.158	26.488	71.91	78.03
+ASAM 0.1	89.487	26.407	72.08	78.52	88.640	24.77	70.988	78.366	89.767	26.542	72.236	78.762	89.816	27.422	72.328	78.083
+ASAM 1.0	90.804	28.398	73.506	78.966	90.399	27.522	72.94	78.975	91.232	29.862	73.58	78.027	91.121	30.208	73.77	77.762
+SAM 0.1	91.007	29.88	73.676	77.898	90.498	28.445	73.05	78.301	91.583	30.997	73.746	77.388	91.328	31.578	73.964	76.807
Mid Mem	Retain	Forget	Test	ToW	Retain	Forget	Test	ToW	Retain	Forget	Test	ToW	Retain	Forget	Test	ToW
+SGD	88.771	56.87	71.414	84.199	89.265	57.832	71.562	83.93	89.80	58.622	71.812	83.929	89.312	58.27	72.248	84.176
+ASAM 0.1	89.56	58.502	72.154	84.113	89.276	57.698	71.576	84.07	90.087	59.08	72.378	84.267	89.945	59.263	72.482	84.062
+ASAM 1.0	90.969	61.998	73.544	83.389	91.064	62.023	73.434	83.358	91.427	62.757	73.82	83.326	91.505	63.078	74.046	83.284
+SAM 0.1	91.396	63.015	73.734	82.985	91.015	62.308	73.422	83.04	91.984	64.367	74.014	82.473	91.823	64.258	74.198	82.587
Low Mem	Retain	Forget	Test	ToW	Retain	Forget	Test	ToW	Retain	Forget	Test	ToW	Retain	Forget	Test	ToW
+SGD	87.775	99.617	71.942	88.515	86.592	99.505	71.042	86.651	88.847	99.663	72.41	89.947	87.847	99.625	72.228	88.839
+ASAM 0.1	88.251	99.643	72.198	89.188	88.296	99.635	72.044	89.098	89.293	99.7	72.658	90.579	88.553	99.69	72.776	89.973
+ASAM 1.0	89.903	99.818	73.844	92.174	89.704	99.808	73.69	91.843	90.432	99.79	73.896	92.772	90.042	99.813	74.166	92.617
+SAM 0.1	90.234	99.822	74.21	92.841	89.553	99.817	73.728	91.722	90.815	99.827	74.228	93.429	90.184	99.825	74.254	92.829

CIFAR100	$\mathcal{A}$ =SGD				$\mathcal{A}$ =ASAM 0.1				$\mathcal{A}$ =ASAM 1.0				$\mathcal{A}$ =SAM 0.1			
High Mem	Retain	Forget	Test	ToW	Retain	Forget	Test	ToW	Retain	Forget	Test	ToW	Retain	Forget	Test	ToW
+SGD	92.929	12.9	68.17	78.334	94.05	11.433	66.68	79.277	94.533	15.267	67.78	77.274	91.814	22.4	66.23	67.82
+ASAM 0.1	93.736	13.467	67.71	78.131	94.852	11.633	67.32	80.336	94.633	15.333	67.82	77.331	93.674	22.9	67.94	70.054
+ASAM 1.0	96.748	15.433	69.98	80.806	96.907	13.167	69.03	82.196	96.893	17.7	69.85	78.731	96.376	24.033	69.85	72.518
+SAM 0.1	98.552	19	72.82	81.331	99.193	17.4	72.17	82.86	99.4	26.467	72.74	74.704	99.24	36.767	73.49	65.08
Mid Mem	Retain	Forget	Test	ToW	Retain	Forget	Test	ToW	Retain	Forget	Test	ToW	Retain	Forget	Test	ToW
+SGD	93.162	60.3	66.15	83.335	95.024	58.433	65.96	86.454	95.519	69.2	67.3	78.59	93.714	72.233	66.91	74.145
+ASAM 0.1	94.055	62.633	66.97	82.846	95.005	58.133	66.85	87.539	95.524	68.133	66.75	79.074	93.838	72.367	66.95	74.158
+ASAM 1.0	96.781	69.533	69.81	81.465	97.16	65.4	68.43	84.391	97.919	72.7	69.58	79.264	97.257	76.2	69.8	75.653
+SAM 0.1	98.938	80.133	72.18	75.059	99.007	76.133	70.87	77.94	99.448	85.1	72.59	70.898	99.169	90.033	72.9	66.089
Low Mem	Retain	Forget	Test	ToW	Retain	Forget	Test	ToW	Retain	Forget	Test	ToW	Retain	Forget	Test	ToW
+SGD	91.086	97.767	65.67	83.718	95.312	98.267	67.18	88.637	93.117	98.5	66.17	85.443	85.307	96.933	62.63	76.374
+ASAM 0.1	92.736	97.767	67.3	86.78	94.676	98.5	67	87.671	94.298	97.967	67.27	88.039	86.902	96.9	62.92	78.087
+ASAM 1.0	92.824	97.8	67.53	87.052	96.267	99.1	68.94	90.502	97.883	99.533	70.59	93.249	93.517	98.7	67.35	86.759
+SAM 0.1	97.89	99.333	71.31	94.151	98.712	99.7	70.89	94.179	99.26	99.667	72.06	95.898	98.695	99.633	71.75	95.078

Table 10: Detailed accuracies of Sharp MinMax on ImageNet and CIFAR-100.

ImageNet	$\mathcal{A}$ =SGD				$\mathcal{A}$ =ASAM 0.1				$\mathcal{A}$ =ASAM 1.0				$\mathcal{A}$ =SAM 0.1			
High Mem	Retain	Forget	Test	ToW	Retain	Forget	Test	ToW	Retain	Forget	Test	ToW	Retain	Forget	Test	ToW
+SGD	87.513	29.79	71.408	73.357	86.802	28.42	70.692	73.418	88.411	31.423	72.016	73.103	87.879	30.953	71.964	73.052
+ASAM 0.1	79.741	10.555	66.334	78.066	80.84185	11.222	66.894	79.077	73.491	8.203	61.802	70.148	80.16741	11.032	66.828	78.529
+ASAM 1.0	87.993	15.903	72.224	86.658	87.748	15.605	71.638	86.166	88.563	16.453	72.452	86.915	88.435	17.083	72.498	86.272
+SAM 0.1	88.297	16.705	72.48	86.463	87.537	16.098	71.612	85.511	89.056	17.405	72.812	86.849	88.468	17.92	72.674	85.712
Mid Mem	Retain	Forget	Test	ToW	Retain	Forget	Test	ToW	Retain	Forget	Test	ToW	Retain	Forget	Test	ToW
+SGD	87.089	58.915	71.418	80.881	86.757	58.372	71.1	80.784	87.217	59.095	71.734	81.105	87.461	59.677	71.848	80.913
+ASAM 0.1	86.936	50.585	71.38	87.914	86.281	49.833	70.814	87.40	87.561	51.3	71.528	88.039	87.529	52.043	71.84	87.642
+ASAM 1.0	88.679	54.642	72.834	87.345	88.588	54.548	72.666	87.192	89.12	55.377	73.018	87.27	89.092	55.733	73.192	87.076
+SAM 0.1	89.141	56.215	73.268	86.755	88.642	55.303	72.74	86.635	89.492	56.813	73.47	86.722	89.758	57.657	73.792	86.486
Low Mem	Retain	Forget	Test	ToW	Retain	Forget	Test	ToW	Retain	Forget	Test	ToW	Retain	Forget	Test	ToW
+SGD	85.798	99.61	71.644	86.334	84.348	99.482	70.894	84.378	85.863	99.568	71.61	86.402	85.098	99.57	71.45	85.517
+ASAM 0.1	86.399	99.565	72.07	87.338	86.236	99.562	71.814	86.953	86.644	99.627	72.104	87.554	85.894	99.593	71.898	86.668
+ASAM 1.0	87.766	99.768	73.392	89.694	87.366	99.772	73.216	89.138	88.159	99.722	73.412	90.142	87.837	99.765	73.718	90.064
+SAM 0.1	87.836	99.777	73.666	90.005	87.745	99.76	73.58	89.852	88.706	99.783	73.94	91.111	87.974	99.792	73.752	90.207

CIFAR100	$\mathcal{A}$ =SGD				$\mathcal{A}$ =ASAM 0.1				$\mathcal{A}$ =ASAM 1.0				$\mathcal{A}$ =SAM 0.1			
High Mem	Retain	Forget	Test	ToW	Retain	Forget	Test	ToW	Retain	Forget	Test	ToW	Retain	Forget	Test	ToW
+SGD	92.298	20.8	67.86	70.767	95.098	22.167	68.42	72.137	92.564	25.4	66.35	65.925	87.195	25.233	63.77	60.478
+ASAM 0.1	89.574	6.133	65.57	78.895	93.819	5.333	67.37	84.968	92.095	6.3	66.52	81.825	86.969	9.233	64.03	72.897
+ASAM 1.0	92.121	6.467	67.15	82.27	88.976	5.067	63.68	77.576	93.895	6.567	67.98	84.521	90.448	10.7	65.71	76.037
+SAM 0.1	97.383	7.1	71.61	90.578	98.183	6.133	71.04	91.695	97.619	8.467	70.7	88.664	98.198	14.167	72.26	85.195
Mid Mem	Retain	Forget	Test	ToW	Retain	Forget	Test	ToW	Retain	Forget	Test	ToW	Retain	Forget	Test	ToW
+SGD	91.433	66	65.79	76.692	91.633	63.367	64.39	77.864	92.11	69.4	65.96	74.526	85.714	62.6	62.55	71.931
+ASAM 0.1	91.16	42.7	65.88	96.027	91.4	40.233	64.11	96.451	95.26	51.2	66.74	93.786	88.074	55.867	63.61	80.104
+ASAM 1.0	92.586	46.9	66.81	94.913	94.074	43.133	66.53	99.422	89.36	47.433	63.35	87.761	93.119	60.067	66.3	83.633
+SAM 0.1	97.433	60.867	70.73	90.96	97.874	55.033	69.39	95.543	98.6	64.333	70.62	88.646	98.824	76.433	71.84	78.286
Low Mem	Retain	Forget	Test	ToW	Retain	Forget	Test	ToW	Retain	Forget	Test	ToW	Retain	Forget	Test	ToW
+SGD	89.579	97.6	66.09	82.853	89.781	97.1	64.36	81.847	88.605	97.833	64.28	80.127	81.488	94.467	61.63	73.843
+ASAM 0.1	89.026	95.067	65.12	83.473	89.874	96.033	64.47	82.883	93.748	97.167	66.17	87.151	92.967	97.433	66.65	86.659
+ASAM 1.0	91.931	96.567	66.74	86.504	92.819	97.467	66.02	85.894	91.131	96.2	64.97	84.381	85.014	95.3	62.79	77.461
+SAM 0.1	96.129	98.033	70.13	92.494	96.829	98.7	69.06	91.508	97.624	98.567	69.85	93.163	96.652	99.033	68.98	90.963

and $\gamma = 0.99$. For RL and SalUn, we use unlearn lr$= 0.08$, and use 50% model parameters for SalUn. For NegGrad and Sharp MinMax, we use unlearn lr$= 0.02$ and $\alpha = 0.99$, and use 30% model parameters for unlearning on $\mathcal{F}$ and the rest for learning on $\mathcal{R}$.

From the results in Tab. 12, we observe consistent improvement by using SAM except only two cases for RL and SalUn with $\mathcal{A} = SGD$. Surprisingly, Sharp MinMax is not the best algorithm on CIFAR-10. By the nature of its design to overfit to forget signals deliberately, we hypothesize that this approach might be aggressive for small-scale unlearning. We again observe SCRUB to be an

Table 11: Detailed accuracies of previous methods on ImageNet and CIFAR-100.

ImageNet	$\mathcal{A}$ =SGD				$\mathcal{A}$ =ASAM 0.1				$\mathcal{A}$ =ASAM 1.0				$\mathcal{A}$ =SAM 0.1			
High Mem	Retain	Forget	Test	ToW	Retain	Forget	Test	ToW	Retain	Forget	Test	ToW	Retain	Forget	Test	ToW
RL	88.536	29.857	72.02	74.598	88.663	29.622	71.95	74.857	88.975	30.59	72.04	74.317	89.429	31.74	72.572	74.055
+ASAM 1.0	90.874	33.395	74.234	74.951	90.615	32.668	73.972	75.221	91.14	34.745	74.298	73.95	91.155	35.332	74.522	73.579
SalUn	93.248	67.118	75.04	44.981	93.016	65.807	74.976	46.104	93.124	66.372	75.418	45.814	92.911	66.333	75.982	46.006
+ASAM 1.0	93.123	66.217	75.496	45.998	92.963	65.058	75.28	46.938	93.134	66.472	75.712	45.856	92.855	66.032	76.172	46.358
Mid Mem	Retain	Forget	Test	ToW	Retain	Forget	Test	ToW	Retain	Forget	Test	ToW	Retain	Forget	Test	ToW
RL	88.785	54.653	71.916	86.617	88.067	53.387	71.258	86.462	89.754	56.17	72.634	86.813	88.609	54.608	72.168	86.715
+ASAM 1.0	90.597	59.53	73.836	85.581	90.457	59.337	73.654	85.473	90.993	60.35	74.078	85.393	90.902	60.402	74.348	85.494
SalUn	93.174	77.258	74.816	71.839	93.072	77.222	74.728	71.735	93.078	77.118	75.382	72.308	92.825	77.167	75.868	72.419
+ASAM 1.0	93.098	77.983	75.47	71.554	92.969	77.947	75.154	71.268	93.143	78.058	75.724	71.695	92.797	77.805	76.222	72.034
Low Mem	Retain	Forget	Test	ToW	Retain	Forget	Test	ToW	Retain	Forget	Test	ToW	Retain	Forget	Test	ToW
RL	85.745	98.603	71.162	86.714	85.451	98.463	70.768	86.192	86.472	98.74	71.522	87.63	86.865	98.95	72.36	88.594
+ASAM 1.0	88.517	99.408	73.728	91.069	88.218	99.377	73.32	90.425	88.985	99.457	73.758	91.516	88.963	99.507	74.072	91.74
SalUn	91.991	99.778	74.612	95.008	91.743	99.77	74.488	94.652	91.696	99.818	75.074	95.116	91.412	99.85	75.514	95.218
+ASAM 1.0	92.095	99.85	75.224	95.628	91.882	99.818	74.992	95.224	91.967	99.857	75.676	95.924	91.579	99.873	75.964	95.791

CIFAR100	$\mathcal{A}$ =SGD				$\mathcal{A}$ =ASAM 0.1				$\mathcal{A}$ =ASAM 1.0				$\mathcal{A}$ =SAM 0.1			
High Mem	Retain	Forget	Test	ToW	Retain	Forget	Test	ToW	Retain	Forget	Test	ToW	Retain	Forget	Test	ToW
L1-Sparse	74.76	5.267	61.49	63.448	75.426	5.067	60.89	63.699	73.969	6.167	60.17	61.252	77.429	7.133	62.56	65.258
+ASAM 1.0	77.86	5.733	62.99	66.903	77.648	5.7	62.29	66.213	77.126	6.367	62.02	65.117	75.583	6.2	60.83	63.051
SCRUB	99.867	44.567	74.52	58.418	99.793	35.267	73.85	67.163	99.902	45.233	74.59	57.816	99.971	60.7	76.47	43.246
+ASAM 1.0	99.962	53.533	76.06	50.313	99.955	42.633	74.72	60.515	99.969	55.3	76.14	48.569	99.971	85.567	77.23	18.137
RL	82.681	9.233	62.95	68.464	79.229	8.367	60.7	64.518	82.99	10.933	61.92	66.689	81.069	10.833	60.82	64.391
+ASAM 1.0	84.012	9.7	63.88	69.952	81.519	8.4	61.41	66.909	86.195	12	63.53	69.73	89.324	13.7	65.99	72.884
SalUn	89.624	16.567	64.88	69.926	86.298	15.467	62.71	66.541	91.207	20.7	64.33	67.355	90.593	18.533	65.65	69.671
+ASAM 1.0	94.557	20.9	68.96	73.268	92.326	18.3	65.94	71.426	94.519	25.033	66.46	67.715	95.636	24.367	68.89	70.933
Mid Mem	Retain	Forget	Test	ToW	Retain	Forget	Test	ToW	Retain	Forget	Test	ToW	Retain	Forget	Test	ToW
L1-Sparse	67.864	36.8	57.97	68.686	71.305	38.633	59.98	72.775	68.264	37.933	57.67	68.197	71.495	39.967	59.73	71.941
+ASAM 1.0	74.148	41.5	61.96	75.554	75.836	42.7	62.7	77.119	74.267	43.967	61.59	73.754	73.857	40.667	60.52	74.556
SCRUB	99.864	81.4	74.29	76.125	99.876	76.9	72.37	79.09	99.91	83.867	73.59	73.176	99.974	90.167	75.78	68.433
+ASAM 1.0	99.974	85.133	75.51	73.353	99.969	77.367	74.24	80.204	99.981	85.433	75.56	73.09	99.974	97.667	77.13	61.618
RL	79.262	37.067	62.53	84.395	75.757	31.733	58.31	80.215	81.955	36.433	61.21	86.411	81.905	38.033	61.48	85.481
+ASAM 1.0	81.688	38.7	63.54	86.779	81.686	37.333	62.3	86.557	85.674	38.7	63.65	91.124	84.914	40.167	63.08	88.633
SalUn	82.383	40.733	60.46	83.056	82.4	40.9	60.9	83.377	89.581	45.333	63.46	89.768	90.205	46.867	64.8	90.495
+ASAM 1.0	91.579	48.167	66.23	92.225	88.71	45.833	64.15	89.182	94.217	50.5	66.77	93.401	94.2	52.333	67.91	92.914
Low Mem	Retain	Forget	Test	ToW	Retain	Forget	Test	ToW	Retain	Forget	Test	ToW	Retain	Forget	Test	ToW
L1-Sparse	62.41	91.367	55.39	53.991	68.667	96	60.25	60.34	68.421	94.2	60.67	61.47	67.229	94.967	59.33	59.014
+ASAM 1.0	66.95	94.5	59.24	58.967	73.457	96.4	63.4	66.697	70.207	96.1	61.46	62.517	72.355	96.2	62.46	65.117
SCRUB	17.81	32.6	18.33	12.708	15.698	28.367	15.87	10.823	66.324	90.167	56.04	58.483	23.038	43.7	23.95	17.368
+ASAM 1.0	99.683	99.9	73.61	97.631	99.869	99.833	73.24	97.508	99.64	99.8	73.7	97.776	99.729	99.8	73.77	97.933
RL	76.376	89.233	61.34	72.4	73.283	86.5	59.57	69.711	73.495	84.2	57.63	69.677	76.79	91.733	60.62	70.55
+ASAM 1.0	78.286	90.533	62.59	74.409	73.881	87.3	59.08	69.375	82.695	89.333	63.53	80.321	83.483	94.167	64.12	78.066
SalUn	78.867	92.667	60.5	71.73	77.748	88.833	59.01	71.95	83.921	91.2	62.39	79.095	82.221	93.133	61.44	75.281
+ASAM 1.0	91.205	95.5	68.28	88.175	90.043	93.367	65.47	86.13	93.812	95.8	67.11	89.289	91.848	95.933	66.24	86.477

Table 12: Differed settings of pretrained models and their test accuracies using different $\mathcal{A}$, as well as performance of retrained models w.r.t $\mathcal{F}_{\text{rand}}$ for CIFAR-10 and Tiny-ImageNet.

Dataset, Model	lr+warmup	Batch B	Epoch T	W. Decay	SGD	ASAM 0.1	ASAM 1.0	SAM 0.1	Retain	Forget	Test
CIFAR10, Res18	0.1+0	256	50	5e-4	93.02	93.26	93.7	93.38	99.943	92.567	92.49
TinyImgNt, Res34	0.003+0	256	200	1e-3	62.1	62.77	62.74	63.87	99.985	59.383	61.69

unstable algorithm which collapses when unlearning with SGD given $\mathcal{A} = SAM0.1$, while SAM helps reduce variance and stabilizes SCRUB unlearning given various pretrained models.

G.2 TINY-IMAGENET

We summarize detailed unlearning settings on Tiny-ImageNet. For L1-Sparse, we use unlearn lr$=0.002$ and $\alpha = 1 \times 10^{-4}$. For SCRUB, we use unlearn lr$=0.002$, msteps$=8$, kd_T$=3.5$, $\beta = 0.01$, and $\gamma = 0.99$. For RL and SalUn, we use unlearn lr$=0.015$, and use 30% model parameters for SalUn. For NegGrad and Sharp MinMax, we use unlearn lr$=0.005$ and $\alpha = 0.99$, and use 10% model parameters for unlearning on $\mathcal{F}$ and the rest for learning on $\mathcal{R}$.

From the results in Tab. 12, we observe consistent improvement by using SAM except few cases. SCRUB performs more steadily than on CIFAR-10. While RL and SalUn perform well on other datasets, they do not appear to be effective on Tiny-ImageNet.

Table 13: Detailed accuracies of previous methods on Tiny-ImageNet and CIFAR-10.

TinyImageNet	$\mathcal{A}$ =SGD				$\mathcal{A}$ =ASAM 0.1				$\mathcal{A}$ =ASAM 1.0				$\mathcal{A}$ =SAM 0.1			
Random $\mathcal{F}_{\text{rand}}$	Retain	Forget	Test	ToW	Retain	Forget	Test	ToW	Retain	Forget	Test	ToW	Retain	Forget	Test	ToW
L1-Sparse	79.247	52.233	49.61	74.669	82.722	54.217	50.81	77.545	84.63	59.583	53.01	77.143	76.005	63.017	49.56	64.372
+ASAM 1.0	89.379	59.5	54.37	**82.753**	90.81	60.933	54.35	**82.853**	92.005	63.517	53.7	**81.168**	94.674	74.333	55.25	**75.347**
SCRUB	92.112	58.117	53.65	85.793	94.315	60.75	54.58	86.425	96.268	66.5	55.01	83.457	99.801	88.233	58.99	**69.101**
+ASAM 1.0	97.965	57.717	56.94	**94.881**	98.941	61.833	58.13	**93.095**	99.521	68.333	57.66	**86.975**	99.962	97.267	61.05	61.704
RL	64.504	63.233	46.59	52.668	67.506	66.433	47.49	53.849	70.309	69.883	48.16	54.424	75.016	73.5	49.21	56.397
+ASAM 1.0	69.356	68.733	49.22	**55.043**	73.517	72.033	50.97	**57.345**	75.88	75.617	50.38	**56.384**	81.006	79.683	50.94	**57.632**
SalUn	69.39	68.45	50	55.735	70.087	68.767	49.54	55.806	73.207	71.783	50.12	56.721	82.877	81.467	53.36	**59.206**
+ASAM 1.0	75.013	74.333	52.65	**58.042**	77.101	75.917	53.16	**58.876**	81.039	79.233	52.89	**59.248**	88.021	87.417	54.81	58.998
NegGrad	84.286	47.867	50.51	83.499	87.031	48.467	51.45	86.662	86.575	52.2	51.28	83.148	99.979	99.167	62.51	60.706
+ASAM 1.0	90.907	50.45	54.47	**91.894**	93.681	51.35	53.66	**93.094**	96.343	54.167	54.31	**93.902**	98.031	62.767	55.21	**88.59**
MinMax	81.8	52.833	51.14	77.977	82.115	54.017	50.91	77.209	81.418	55.433	50.32	75.025	68.67	54.217	46.99	61.615
+ASAM 1.0	87.654	43.183	53.4	**93.426**	88.273	43.083	52.86	**93.613**	91.947	43.6	53.37	**97.617**	94.517	48.5	53.72	**96.466**

CIFAR10	$\mathcal{A}$ =SGD				$\mathcal{A}$ =ASAM 0.1				$\mathcal{A}$ =ASAM 1.0				$\mathcal{A}$ =SAM 0.1			
Random $\mathcal{F}_{\text{rand}}$	Retain	Forget	Test	ToW	Retain	Forget	Test	ToW	Retain	Forget	Test	ToW	Retain	Forget	Test	ToW
L1-Sparse	86.467	82.967	82.25	85.12	89.06	85.567	84.45	87.688	86.683	83.467	82.11	84.811	89.462	87.133	84.82	87.144
+ASAM 1.0	91.438	88.333	87.23	**90.352**	91.674	87.767	87.24	**91.087**	90.938	88.7	86.94	**89.268**	90.886	88.633	86.43	**88.792**
SCRUB	90.767	86.033	86.27	90.739	68.205	67.367	66.75	63.466	80.193	78.933	77.97	77.95	15.11	14.2	15	6.089
+ASAM 1.0	99.6	95.167	92.65	**97.2**	99.621	96.5	93.15	**96.39**	99.807	98.2	93.38	**95.078**	99.631	98.467	93.16	**94.435**
RL	92.774	86.6	87.22	**93.186**	90.569	84.2	85.17	91.02	91.445	84.133	85.81	92.591	88.736	82.533	84.12	89.524
+ASAM 1.0	93.295	87.733	87.66	93.138	93.262	87.233	88.31	**94.187**	95.098	89.033	89.44	**95.512**	92.588	86.567	87.4	**93.206**
SalUn	96.94	88.8	89.95	**98.095**	95.726	87.6	89.02	97.052	95.99	88.733	89.35	96.598	96.612	89.867	89.86	96.668
+ASAM 1.0	97.771	91.8	90.55	96.666	98.24	91.867	91.41	**97.917**	98.029	91.6	91.2	**97.757**	98.055	92.833	91.37	**96.755**
NegGrad	97.724	93.933	90.46	94.487	98.35	94.967	91.33	94.931	98.024	94.267	90.92	94.9	96.405	93.4	89.72	93.009
+ASAM 1.0	99.074	95.8	92.39	**95.83**	99.248	96.133	92.04	**95.332**	99.219	96.2	92.42	**95.602**	98.579	94.767	91.97	**95.964**
MinMax	96.85	94.133	90.29	93.291	97.652	94.933	90.6	93.594	97.881	95.1	90.5	93.558	96.498	93.533	90.22	93.451
+ASAM 1.0	98.781	94.133	91.82	**96.638**	98.602	94	91.79	**96.565**	98.755	94.4	91.65	**96.186**	97.981	93.367	91.17	**95.97**

G.3 Unlearning with Structured Noise

We consider a noisy unlearning case where only a corrupted version of $\mathcal{S}$ is available, following corruptions in ImageNet-C (Hendrycks & Dietterich, 2019) to apply glass blur and snow effect to CIFAR-100 with medium severity for additional empirical verification, and report ToWs in Tab. 14: We observe that SAM continues to improve base unlearning methods with even more clear margins.

Table 14: Unlearning with ImageNet-C corruptions on CIFAR-100.

Glass Blur	$\mathcal{A}$=SGD				$\mathcal{A}$=ASAM			
Method	High	Mid	Low	AVG	High	Mid	Low	AVG
NG	67.760	78.824	75.931	74.172	76.152	85.534	82.556	81.414
+ASAM	73.565	80.253	84.086	**79.301**	74.993	86.567	86.296	**82.619**
SharpMinMax	66.110	76.852	73.387	72.116	66.837	79.023	78.435	74.765
+ASAM	75.327	89.859	79.104	**81.430**	74.089	92.737	84.921	**83.916**
Snow	$\mathcal{A}$=SGD				$\mathcal{A}$=ASAM			
Method	High	Mid	Low	AVG	High	Mid	Low	AVG
NG	77.394	83.328	83.196	81.306	75.041	86.424	86.838	82.768
+ASAM	76.759	84.168	86.053	**82.327**	76.520	83.774	89.343	**83.212**
SharpMinMax	70.880	78.806	77.652	75.779	69.650	79.139	81.344	76.711
+ASAM	77.188	90.997	83.933	**84.039**	80.533	93.383	87.779	**87.232**

This is because that structured noise applying to the images affects the dataset's signal and noise vectors (φ and $\boldsymbol{\xi}_i$), causing a corrupted dataset with worse initial signal-noise ratio, but it does not affect update dynamics and the gained results under our theoretical framework, as corrupted images are still visually recognizable, and SGD still overfits more to the added noise.

G.4 SAM with Adam and ViT

We also verify that our observations generalize to different base optimizers and architectures. We experiment CIFAR-100 unlearning using ViT-Small (Dosovitskiy et al., 2020) and AdamW (Loshchilov & Hutter, 2017), and summarize our priliminary results in Tab. 15. For pretraining, we use AdamW with starting lr 0.0001, weight decay 0.05, and set patch size to 4 for ViT-Small on CIFAR-100. Other experiment settings are unchanged. For unlearning, we have unlearn lr 0.0006 for NegGrad and for Sharp MinMax. Adam demands much smaller lr than SGD and

Table 15: Unlearning with ViT-Small and AdamW on CIFAR-100.

	$\mathcal{A}$=SGD				$\mathcal{A}$=ASAM			
	High	Mid	Low	AVG	High	Mid	Low	AVG
NG	80.445	82.854	84.385	82.561	78.750	82.223	86.767	82.580
+ASAM	82.880	83.084	83.402	**83.122**	82.839	81.354	87.507	**83.900**
SharpMinMax	14.794	42.055	95.222	50.690	14.279	42.017	94.833	50.376
+ASAM	76.343	95.573	103.372	**91.763**	76.664	93.966	105.868	**92.166**

is more sensitive to unlearn lr tuning. ViTs perform worse than ResNets on smaller datasets (test accuracies of pretrained models are 57%).

G.5 Relearning Attacks

We present relearning attack experiments in Tab. 16 to demonstrate SAM's unlearning robustness below. We take the unlearned models to relearn the whole $\mathcal{F}$ for one epoch with a small relearning lr, and measure the increase in forget accuracies. Reported are the averaged increase across $\mathcal{F}_{\text{high}}, \mathcal{F}_{\text{mid}}, \mathcal{F}_{\text{low}}$. We observe that SAM enhanced $\mathcal{U}$ are more resilient to relearning attacks with smaller increases. We note that these experiments highlight the robustness of our approach and hope that this encourages future works for deeper investigation into the role of loss landscape geometry for robust unlearning.

Table 16: Average increase of forget accuracies after relearning 1 epoch on $\mathcal{F}$ on CIFAR-100 and ResNet50. We observe that SAM enhanced unlearning is consistently more resilient to relearning attacks with less increase on forget accuracy.

	Relearn lr=0.002		Relearn lr=0.003		Relearn lr=0.004	
	$\mathcal{A}$=SGD	$\mathcal{A}$=ASAM	$\mathcal{A}$=SGD	$\mathcal{A}$=ASAM	$\mathcal{A}$=SGD	$\mathcal{A}$=ASAM
NG	8.644	10.333	11.167	13.256	12.789	14.7
+ASAM	**8.533**	**9.289**	**11.033**	**11.533**	13.022	**13.389**
SharpMinMax	13.1	15.067	15.589	17.5	16.144	18.511
+ASAM	**8.333**	**8.8**	**10.667**	**11.2**	**12.711**	**12.667**
RL	7.122	8.556	8.5	9.589	9.622	10.989
+ASAM	**6.222**	**7.378**	**7.444**	**8.489**	**8.367**	**9.467**

G.6 Runtime and Efficient SAMs

We implement momentum SAM (MSAM) for unlearning on CIFAR-100. As shown in Tab. 17, MSAM not only outperforms vanilla SAM by much less computation overhead but can also outperform by average ToWs for some unlearning methods. This is plausible, as recent efficient SAMs reduce computation with more informative perturbation directions than stochastic by momentum buffer, sparsity, prior gradients, sharpness-sensitive data, etc. But there is no clear theoretical justification of MSAM rather than trying to stabilize the noise and reduce overhead of SAM. This warrants a deeper study beyond our scope – our focus is to show superiority of loss landscape based methods for unlearning without worrying about speed (just like the original SAM paper), and we leave deeper theoretical/algorithmic improvements and empirical evaluations for speedups for future work. We notice that while outperforming SGD with much less computation overhead than vanilla SAM, MSAM does not outperform ASAM on SharpMinMax and SalUn. As we also observe that MSAM behaves differently from ASAM on different forget sets, further and deeper investigation is needed to study the interactions between MSAM and weight masking to improve the performance. Our results have effectively demonstrated an example of a faster SAM variant that predictably benefits unlearning with less overhead.

G.7 KLoM Scores

We follow (Georgiev et al., 2024) to compute KLoM of NegGrad with SGD and SAM and report the KL measures on $\mathcal{F}, \mathcal{R}, \mathcal{D}_{\text{test}}$ across $\mathcal{F}$ of different difficulties, report means and 95%-percentiles in Tab. 18. Given a pretrained model, we observe that SAM in unlearning also helps close the gap

Table 17: ToWs of MSAM across different $\mathcal{F}$ in addition to reported results of baseline and SAM-enhanced unlearning on CIFAR-100. We observe that MSAM not only costs much less computation overhead than SAM but can also outperform by ToW for some settings, since it leverages a smarter perturbation based on momentum buffer.

	$\mathcal{A}$=SGD				$\mathcal{A}$=ASAM 1.0				Runtime
	$\mathcal{F}_{\text{high}}$	$\mathcal{F}_{\text{mid}}$	$\mathcal{F}_{\text{low}}$	AVG	$\mathcal{F}_{\text{high}}$	$\mathcal{F}_{\text{mid}}$	$\mathcal{F}_{\text{low}}$	AVG	
L1-Sparse	63.448	68.686	53.991	62.042	61.252	68.197	61.47	63.64	165.3
+ASAM	66.903	75.554	58.967	67.141	65.117	73.754	62.517	67.129	323.6
+MSAM	68.768	76.378	64.932	70.026	70.885	76.342	65.068	70.765	201.3
NG	78.334	83.335	83.718	81.796	77.274	78.59	85.443	80.436	309.5
+ASAM	80.806	81.465	87.052	83.108	78.731	79.264	93.249	83.748	610.3
+MSAM	81.811	85.568	91.176	86.185	73.291	77.43	91.691	80.804	352.4
SharpMinMax	70.767	76.692	82.853	76.771	65.925	74.526	80.127	73.526	317
+ASAM	82.27	94.913	86.504	87.896	84.521	87.761	84.381	85.554	631
+MSAM	79.079	73.057	88.157	80.098	77.034	72.944	93.819	81.266	398.1
RL	68.464	84.395	72.4	75.086	66.689	86.411	69.677	74.259	173.3
+ASAM	69.952	86.779	74.409	77.047	69.73	91.124	80.321	80.392	344.1
+MSAM	73.032	87.608	76.537	79.059	72.656	90.675	81.027	81.453	216
SalUn	69.926	83.056	71.73	74.904	67.355	89.768	79.095	78.739	172.8
+ASAM	73.268	92.225	88.175	84.556	67.715	93.401	89.289	83.468	340.9
+MSAM	70.011	89.214	81.069	80.098	68.548	92.289	82.757	81.198	213.6

between unlearned models and retrained models, even when the standard way to retrain models with SGD does not favor SAM as they adopt different optimization dynamics. We observe similar trends as measuring performance closeness with ToWs: while SAM does not improve KL closeness on $\mathcal{F}$, it reduces the KL divergence on $\mathcal{R}$ and $\mathcal{D}_{\text{test}}$ and often halves KL on $\mathcal{R}$. Adding SAM (vs. SGD) reduces the distance to the retrained reference across memorization levels; e.g., with SGD-retrained reference the average distance drops from 0.0973 w/ SGD to 0.0827 w/ SAM. The reported KL at 95%-percentiles in the second table also show that SAM reduces KL even at tails (smaller variances). We use $N = 10$ with 10 bins for our KLoM measurements (pretraining 10 models and retraining 30 models for each $\mathcal{F}$, and unlearning 120 models for all settings).

Table 18: Mean and 95%-percentile KLoM on CIFAR-100 and ResNet50 after NegGrad unlearning. [SGD, SAM] denotes SGD-pretrained and SAM-unlearned. We observe that SAM enhanced unlearning consistently improves KLoM across different $\mathcal{F}$. Similar to what we observe with ToWs, SAM performs better on retain and testset. Based on 95%-percentile KLoM scores, we observe that SAM enhanced unlearning consistently improves KLoM on tails too, which also indicates the better stability of SAM unlearning.

KLoM Mean	$\mathcal{A}$=SGD			$\mathcal{A}$=SGD			$\mathcal{A}$=SGD			AVG
$\mathcal{A},\mathcal{U}$	Forget	Retain	Test	Forget	Retain	Test	Forget	Retain	Test	
SGD, SGD	0.1294	0.0721	0.1293	0.1221	0.0669	0.1259	0.0284	0.0747	0.1271	0.0973
SGD, SAM	0.1384	**0.0411**	**0.1076**	0.1589	**0.0331**	**0.0983**	**0.0163**	**0.0411**	**0.1093**	**0.0827**
SAM, SGD	0.1549	0.0676	0.126	0.1513	0.066	0.1246	0.025	0.0658	0.1248	0.1007
SAM, SAM	0.1714	**0.0264**	**0.095**	0.2457	**0.0253**	**0.0913**	**0.015**	**0.0311**	**0.1008**	**0.0891**
KLoM 95%	$\mathcal{A}$=SGD			$\mathcal{A}$=SGD			$\mathcal{A}$=SGD			AVG
$\mathcal{A},\mathcal{U}$	Forget	Retain	Test	Forget	Retain	Test	Forget	Retain	Test	
SGD, SGD	0.3397	0.2097	0.5212	0.4959	0.2097	0.4901	0.0956	0.2097	0.4959	0.3408
SGD, SAM	**0.3397**	**0.2097**	**0.4901**	0.5681	**0.0956**	**0.3723**	**0.0956**	**0.2097**	**0.4901**	**0.319**
SAM, SGD	0.4901	0.2097	0.5212	0.5371	0.2097	0.4959	0.0956	0.2097	0.5212	0.3656
SAM, SAM	**0.4901**	**0.0956**	**0.3723**	0.8111	**0.0956**	**0.3397**	**0.0956**	**0.0956**	**0.4901**	**0.3206**

H COMPLETE VISUALIZATIONS

In this section, we provide complete visualizations of feature space and loss landscapes of pretrained models, NegGrad unlearned models, and Sharp MinMax unlearned models, comparing SGD with SAM across all memorization levels. The observations are generally consistent across memorization levels, with $\mathcal{F}_{\text{high}}$ being more noticeable.

H.1 LOSS LANDSCAPE

Inspired by Wu et al. (2017), we quantify the flatness by basin ratio, which is the percentage of perturbed losses whose deviation from original loss $\leq 0.5 \cdot$ stddev. Fig. 6 shows loss landscapes of SAM and SGD before and after unlearning on $\mathcal{D}_{\text{test}}$ and $\mathcal{F}_{\text{high}}$. We observe SAM has higher basin ratios (flatter landscape) than SGD for pretrained model and MinMax unlearned model as expected. Surprisingly, SGD can become flatter after unlearning. We conjecture that the gradient ascent might be implicitly regularizing SGD which had more overfitting than SAM during pretraining. We leave the further characterization of loss landscapes to future work.

H.2 FEATURE VISUALIZATION

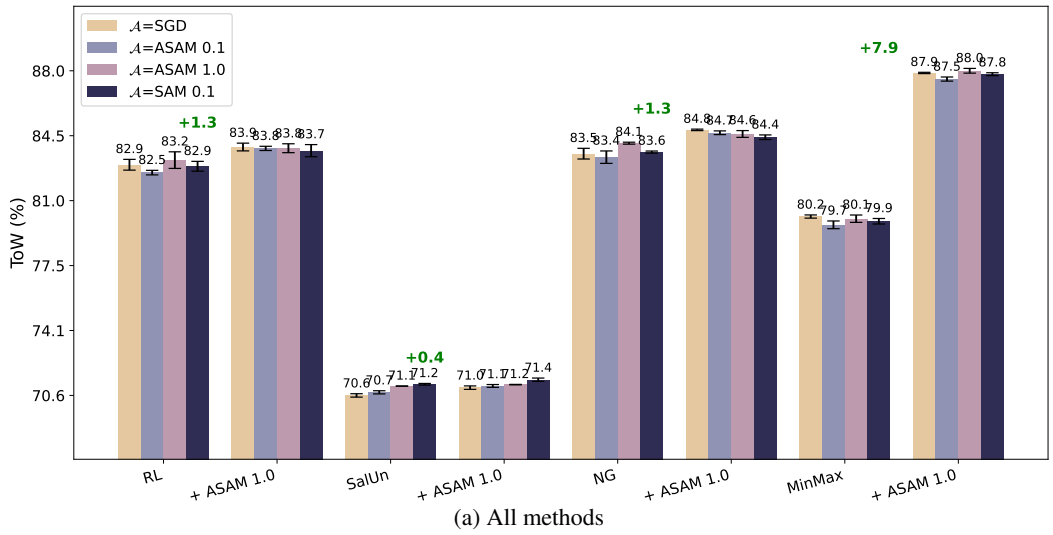

(a) All methods

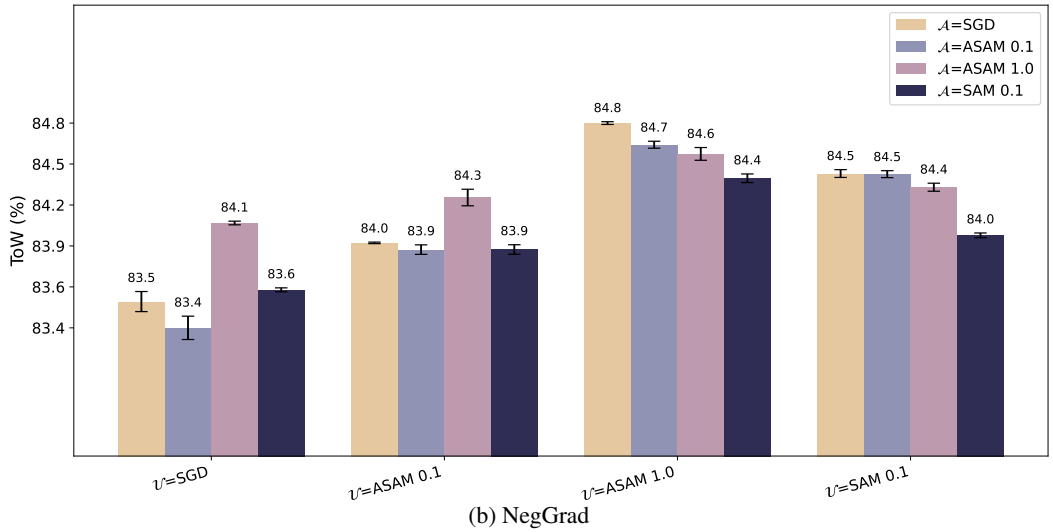

(b) NegGrad

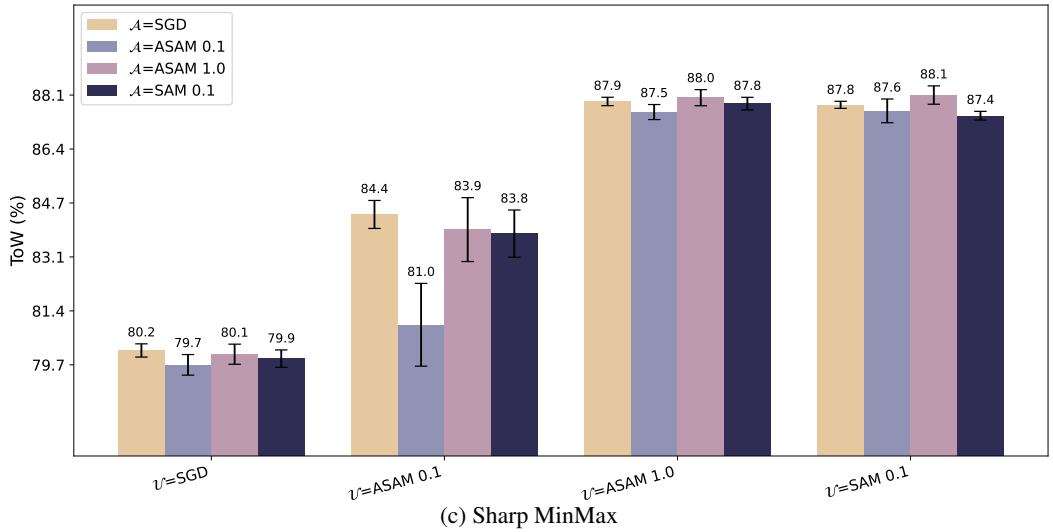

(c) Sharp MinMax

Figure 4: 95% confidence intervals ($\mu \pm 2\sigma$) of unlearning methods on ImageNet, in accordance to Tab. 1 and Tab. 3. We run each setting three times with different seeds and compute the statistical significance. SAM consistently improves base $\mathcal{U}$, and we observe ASAM 1.0 to bring largest improvement steadily.

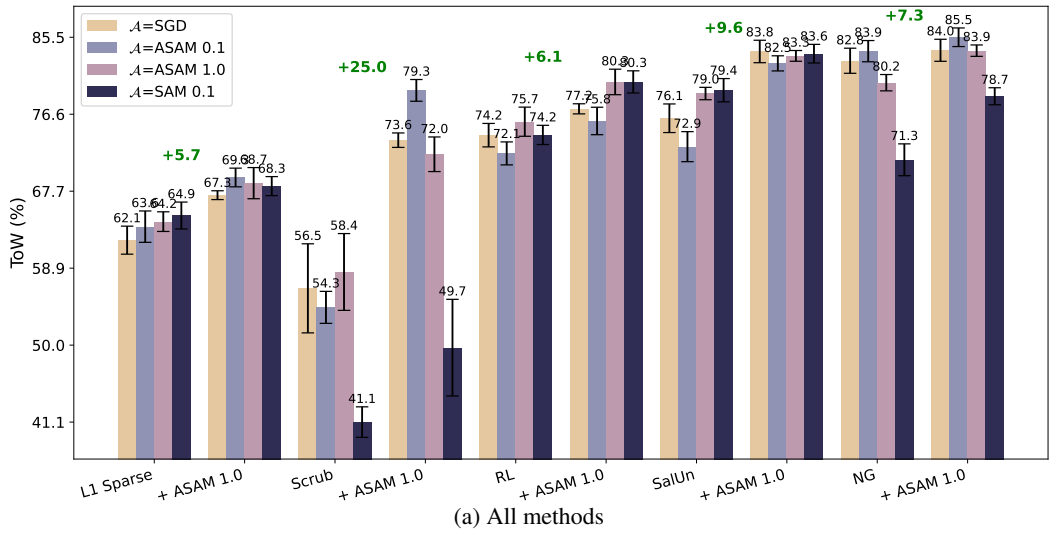

(a) All methods

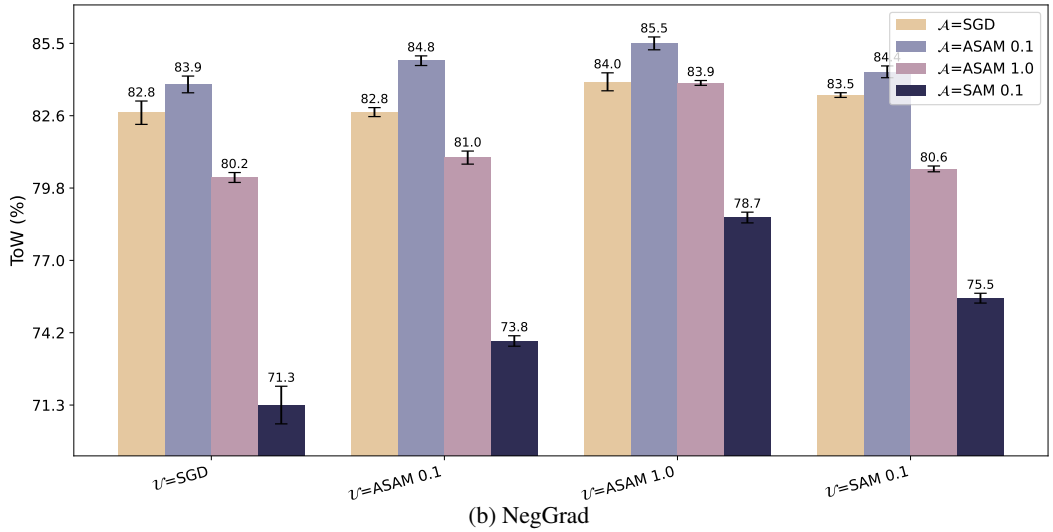

(b) NegGrad

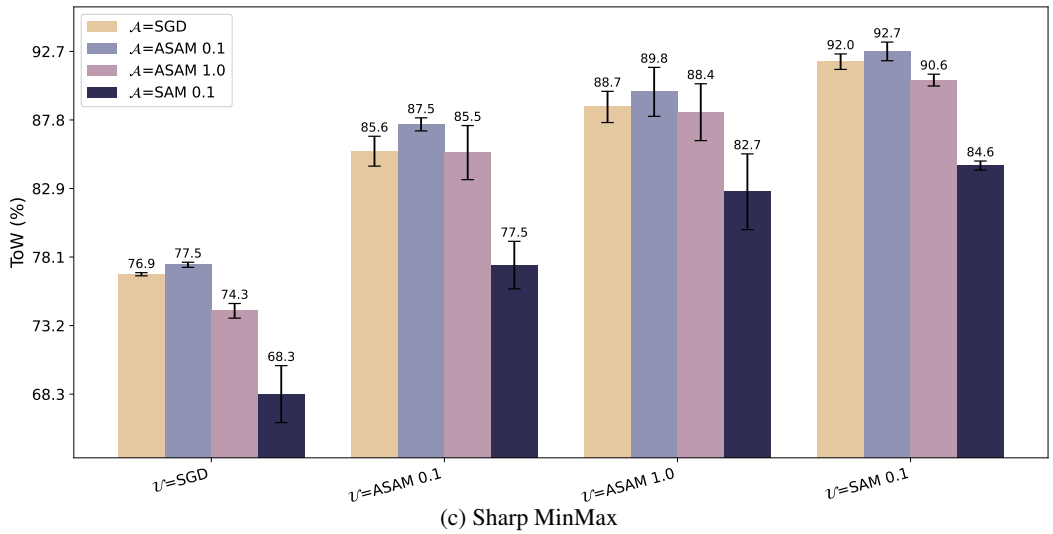

(c) Sharp MinMax

Figure 5: 95% confidence intervals ($\mu \pm 2\sigma$) of unlearning methods on CIFAR-100, in accordance to Tab. 1 and Tab. 3. We run each setting three times with different seeds and compute the statistical significance. SAM not only improves ToW of the based methods, but also more robust against variance than SGD.

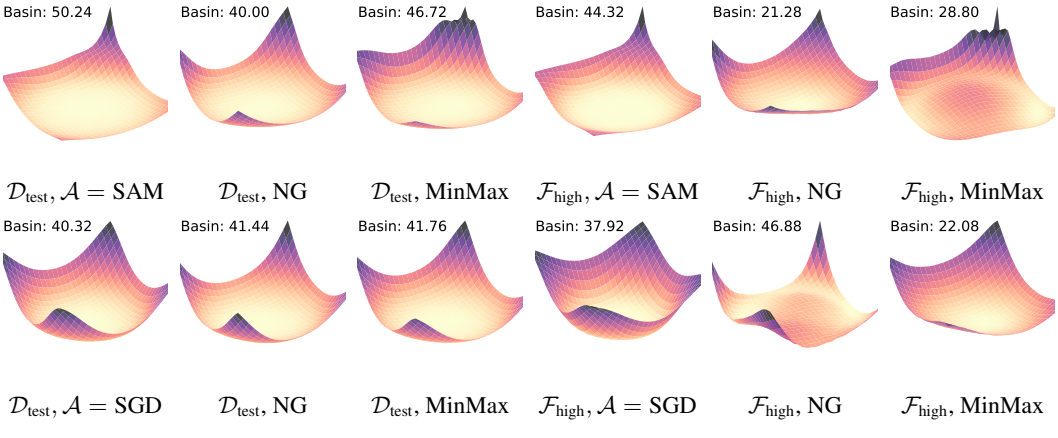

(a) High Mem $\mathcal{F}_{\text{high}}$.

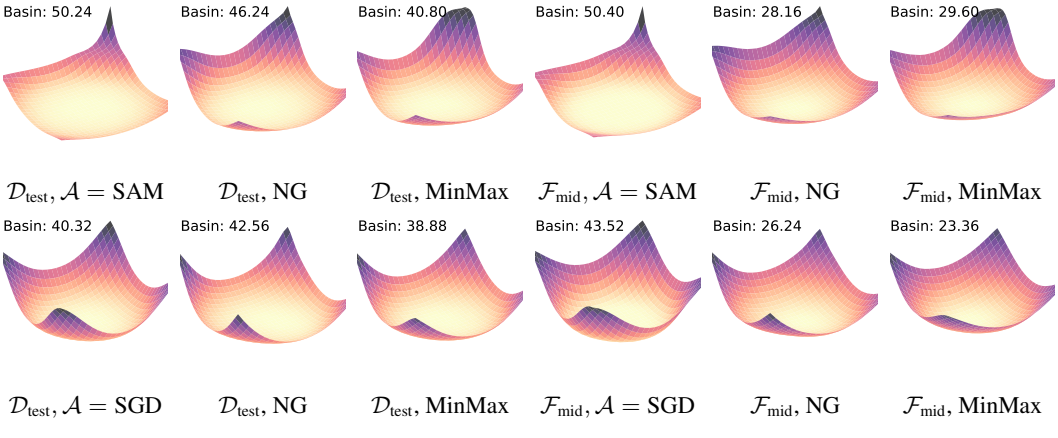

(b) Mid Mem $\mathcal{F}_{\text{mid}}$.

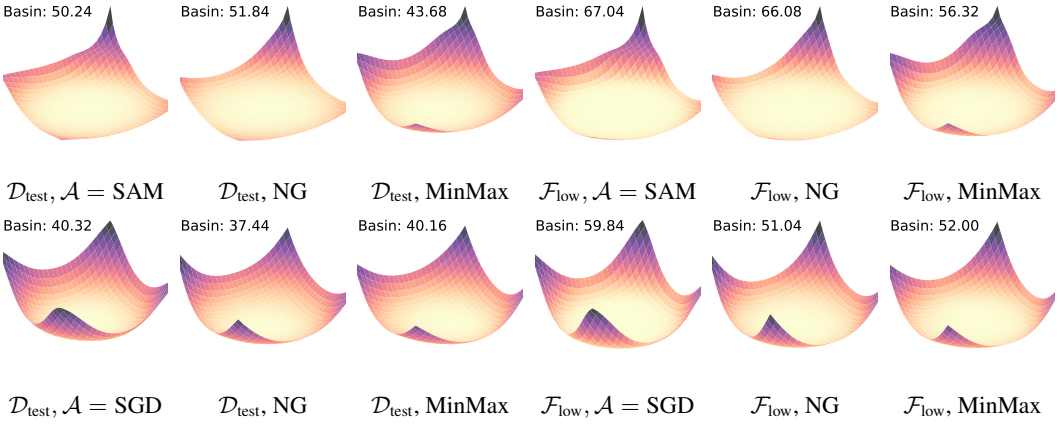

(c) Low Mem $\mathcal{F}_{\text{low}}$.

Figure 6: Loss landscapes of SAM and SGD on $\mathcal{D}_{\text{test}}$ and all $\mathcal{F}$. As memorization level goes down, $\mathcal{F}$ becomes easier to unlearn and SGD shows less to no "regularizing" effect as we have discussed on $\mathcal{F}_{\text{high}}$. The general trend preserves with decreasing memorization levels and SAM is generally flatter before and after unlearning.

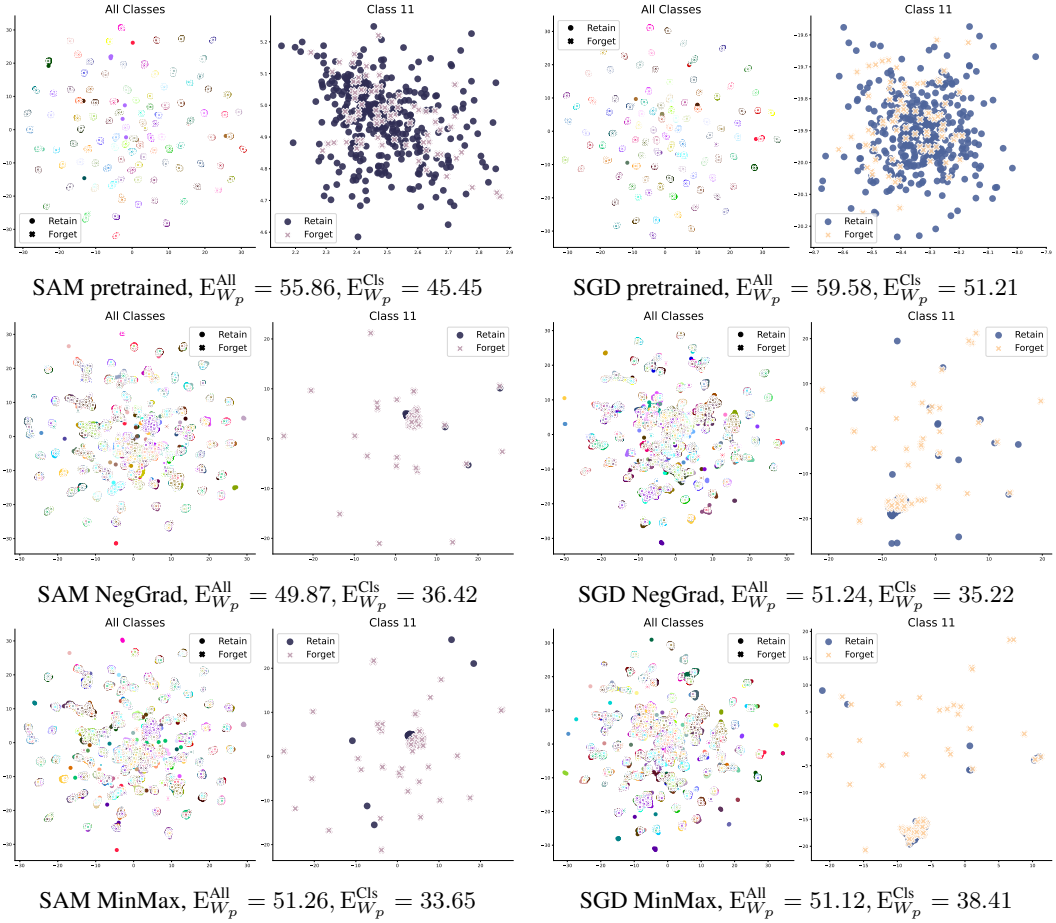

SAM pretrained, $\mathrm{E}^{\mathrm{All}}_{W_p} = 55.86, \mathrm{E}^{\mathrm{Cls}}_{W_p} = 45.45$

SGD pretrained, $\mathrm{E}^{\mathrm{All}}_{W_p} = 59.58, \mathrm{E}^{\mathrm{Cls}}_{W_p} = 51.21$

SAM NegGrad, $\mathrm{E}^{\mathrm{All}}_{W_p} = 49.87, \mathrm{E}^{\mathrm{Cls}}_{W_p} = 36.42$

SGD NegGrad, $\mathrm{E}^{\mathrm{All}}_{W_p} = 51.24, \mathrm{E}^{\mathrm{Cls}}_{W_p} = 35.22$

SAM MinMax, $\mathrm{E}^{\mathrm{All}}_{W_p} = 51.26, \mathrm{E}^{\mathrm{Cls}}_{W_p} = 33.65$

SGD MinMax, $\mathrm{E}^{\mathrm{All}}_{W_p} = 51.12, \mathrm{E}^{\mathrm{Cls}}_{W_p} = 38.41$

Figure 7: UMAP (McInnes et al., 2018) feature analysis on High Mem $\mathcal{F}_{\text{high}}$. We observe SGD unlearning forms a more obvious clump in all-classes panels while SAM unlearning better maintains class clusters. From classwise panels, we observe that SAM effectively pushes forget samples away while gathering retain samples to a dense cluster, while SGD also scatters retain samples during unlearning, suggesting overfitting.

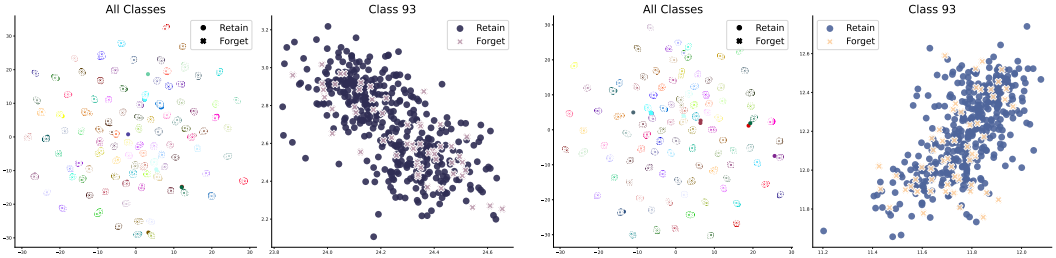

SAM pretrained, $\mathrm{E}^{\mathrm{All}}_{W_p} = 61.74, \mathrm{E}^{\mathrm{Cls}}_{W_p} = 49.88$

SGD pretrained, $\mathrm{E}^{\mathrm{All}}_{W_p} = 66.3, \mathrm{E}^{\mathrm{Cls}}_{W_p} = 57.11$

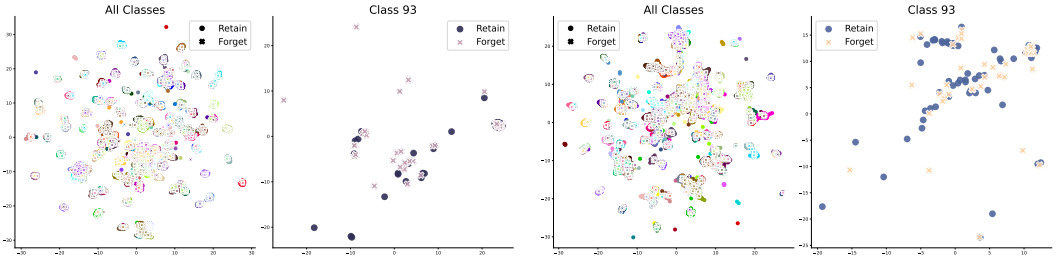

SAM NegGrad, $\mathrm{E}^{\mathrm{All}}_{W_p} = 52.36, \mathrm{E}^{\mathrm{Cls}}_{W_p} = 44.71$

SGD NegGrad, $\mathrm{E}^{\mathrm{All}}_{W_p} = 52.99, \mathrm{E}^{\mathrm{Cls}}_{W_p} = 46.91$

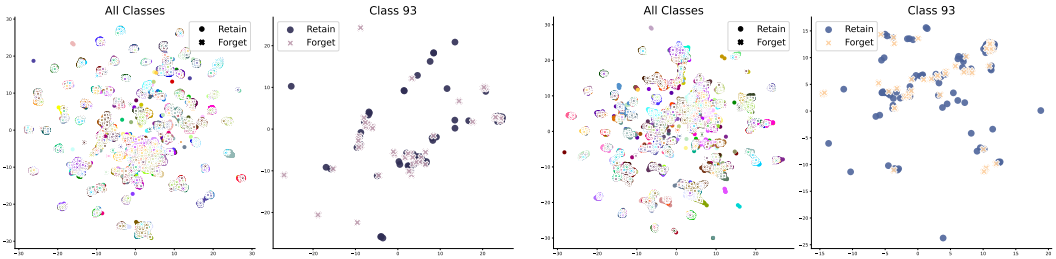

SAM MinMax, $\mathrm{E}^{\mathrm{All}}_{W_p} = 51.8, \mathrm{E}^{\mathrm{Cls}}_{W_p} = 44.56$

SGD MinMax, $\mathrm{E}^{\mathrm{All}}_{W_p} = 53.7, \mathrm{E}^{\mathrm{Cls}}_{W_p} = 49.57$

Figure 8: UMAP (McInnes et al., 2018) feature analysis on Mid Mem $\mathcal{F}_{\text{mid}}$. At all-class level, we observe that SAM better maintains class clusters after unlearning while SGD is forming a more evident clump of features; at classwise level, we observe that while both push away forget features, SGD also scatters retain features further, suggesting overfitting. This also explains the larger clump of SGD at all-class level.

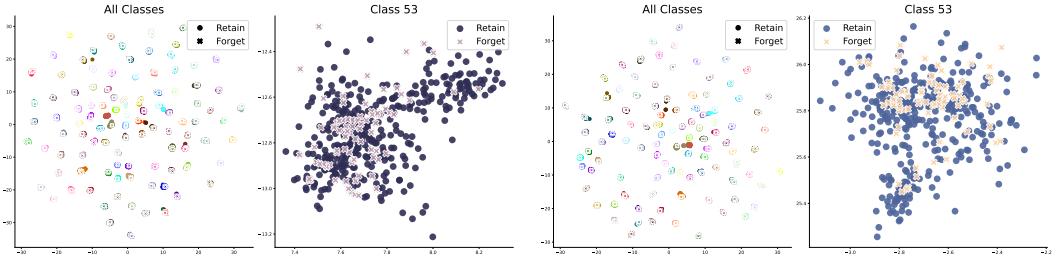

SAM pretrained, $\mathrm{E}^{\mathrm{All}}_{W_p} = 59.84, \mathrm{E}^{\mathrm{Cls}}_{W_p} = 52.46$

SGD pretrained, $\mathrm{E}^{\mathrm{All}}_{W_p} = 63.13, \mathrm{E}^{\mathrm{Cls}}_{W_p} = 59.64$

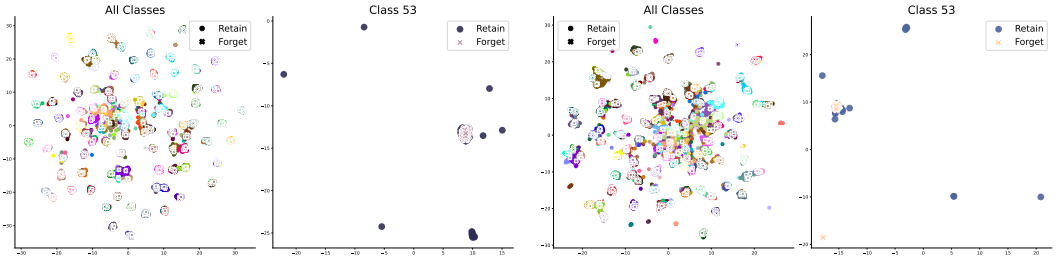

SAM NegGrad, $\mathrm{E}^{\mathrm{All}}_{W_p} = 54.93, \mathrm{E}^{\mathrm{Cls}}_{W_p} = 50.83$

SGD NegGrad, $\mathrm{E}^{\mathrm{All}}_{W_p} = 56.12, \mathrm{E}^{\mathrm{Cls}}_{W_p} = 55.93$

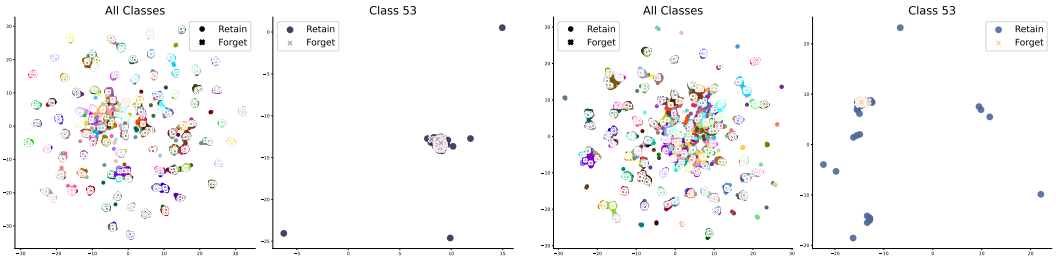

SAM MinMax, $\mathrm{E}^{\mathrm{All}}_{W_p} = 55.08, \mathrm{E}^{\mathrm{Cls}}_{W_p} = 52.55$

SGD MinMax, $\mathrm{E}^{\mathrm{All}}_{W_p} = 56.77, \mathrm{E}^{\mathrm{Cls}}_{W_p} = 57.15$

Figure 9: UMAP (McInnes et al., 2018) feature analysis on Low Mem $\mathcal{F}_{\text{low}}$. We observe SGD unlearning forms a more obvious clump in all-classes panels while SAM unlearning better maintains class clusters. From classwise panels, as $\mathcal{F}_{\text{low}}$ requires less unlearning and the model can generalize to $\mathcal{F}_{\text{low}}$, forget samples do not move much as expected. But on SGD MinMax we still observe that SGD scatters more retain samples away.